ANIMAL MODEL AND VACCINE CANDIDATE DEVELOPMENT FOR *BURKHOLDERIA MALLEI*

by

SHAWN MARIE ZIMMERMAN

(Under the Direction of Eric R. Lafontaine)

ABSTRACT

Burkholderia pseudomallei, the etiologic agent of melioidosis, is a saprophytic bacterium that is commonly found in the soil and stagnant waters of tropical countries bordering the equator. *Burkholderia mallei* is a host-adapted clone of *B. pseudomallei,* which does not readily persist outside of its equine reservoir and causes the zoonotic disease known as glanders. Infection by these organisms occurs primarily via percutaneous inoculation or inhalation of contaminated aerosols. Acute infection with *B. pseudomallei* and *B. mallei* manifest as severe pneumonia that can lead to fatal septicemia. Not only are melioidosis and glanders difficult to diagnose and problematic to treat, but there is also no vaccine to protect against these pathogens; thus, there is significant concern that these pathogens could be used as biological warfare agents. For these reasons, the Federal Select Agent Program (SAP) has classified *B. pseudomallei* and *B. mallei* as Tier 1 Select Agents, and the United States Defense Threat Reduction Agency (DTRA) has prioritized the development of medical countermeasures (MCM) to

protect against *B. mallei* and *B. pseudomallei*. To further our understanding of the pathogenesis of *B. mallei* and to aid in the development of MCM against *B. mallei,* improved large animal models are required. We validate the common marmoset as a suitable large animal model for studying intranasal infection with *B. mallei.* Additionally, we report on the characterization of two novel autotransporter (AT) proteins, BpaB and BatA, which we determined to be important virulence factors in the pathogenesis of *B. mallei* and potential vaccine candidates to protect against infection with *B. mallei.* Specifically, we identified BpaB to be an oligomeric AT that functions as a novel biofilm factor, and we characterized BatA to be a conventional AT that contributes to the intracellular survival of *B. mallei* in host macrophages and also functions as an acetylesterase. Furthermore, we also identify and characterize a novel live-attenuated strain of *B. mallei* ATCC 23344, which results in the production of a robust humoral immune response that protects against aerosol infection with *B. mallei* and *B. pseudomallei.*

INDEX WORDS: *Burkholderia mallei*, *Burkholderia pseudomallei*, autotransporters, Type V Secretion System, BpaB, BatA, biofilm factor, intracellular survival, live attenuated strain, virulence, pathogenesis, vaccines, animal models, marmosets, mice

ANIMAL MODEL AND VACCINE CANDIDATE DEVELOPMENT FOR *BURKHOLDERIA MALLEI*

by

SHAWN MARIE ZIMMERMAN

BS, Lyon College, Batesville, Arkansas, 2004

DVM, Louisiana State University, Baton Rouge, Louisiana, 2008

A Dissertation Submitted to the Graduate Faculty of The University of Georgia in Partial Fulfillment of the Requirements for the Degree

DOCTOR OF PHILOSOPHY

ATHENS, GEORGIA

2015

ANIMAL MODEL AND VACCINE CANDIDATE DEVELOPMENT FOR

BURKHOLDERIA MALLEI

by

SHAWN MARIE ZIMMERMAN

Major Professor:	Eric R. Lafontaine
Committee:	Robert J. Hogan
	Frederick D. Quinn
	Kaori Sakamoto
	Vincent J. Starai

Electronic Version Approved:

Suzanne Barbour
Dean of the Graduate School
The University of Georgia
August 2015

DEDICATION

This dissertation is dedicated to my parents and sister, Denny Zimmerman, Stacy Zimmerman, and Sheri Ozment, for their excellent guidance, constant encouragement, and undying support. We all sacrificed to support each other in our educational pursuits, but your patience and understanding throughout my fifteen year journey went above and beyond the call of duty! I love you, and I owe all my successes to you.

ACKNOWLEDGEMENTS

Many thanks to the numerous people who have contributed to my research and professional development over the last four years! In particular…

- My deepest thanks to my mentor, Dr. Eric Lafontaine, for taking a gamble and teaching hypothesis-driven molecular biology research to a molecularly-challenged veterinarian! You have been a mentor in every sense of the word. From you I have learned how to be a self-sufficient, conscientious, and critically-thinking scientist, how to be a thoughtful, engaging, and patient teacher, and how to be an overall kind and generous human being. Your sage wisdom these last four years has been indispensable. I am extremely fortunate to have been your student, and I could not have accomplished this without you!
- Sincere thanks to the members of my dissertation committee, Drs. Robert "Jeff" Hogan, Frederick Quinn, Kaori Sakamoto, and Vincent Starai, for your constructive criticism and astute advice, all of which contributed tremendously to my scientific growth and professional maturity.
- Many thanks to Frank Michel, Dr. Tomislav Jelesijevic, Xuidan Gao, Deb Carter, and Dr. Elizabeth Howerth for providing reagents and their expert guidance.
- My heartfelt thanks to my many talented friends in the Lafontaine, Hondalus, Hogan, Starai, and Quinn laboratories. I am truly grateful for your constant support and entertainment, both at work and in life!

- Lastly, my infinite gratitude to Zoetis, The Morris Animal Foundation, and The University of Georgia for awarding me a Veterinary Fellowship for Advanced Study (D12ZO-902) to financially support me in the pursuit of this work.

TABLE OF CONTENTS

LIST OF TABLES

Page

LIST OF FIGURES

Page

CHAPTER 1

INTRODUCTION

Glanders and melioidosis are fatal, highly contagious, zoonotic diseases of many veterinary species. Specifically, the causative agent of glanders (*Burkholderia mallei*) affects humans and most veterinary species; however, solipeds (horses, ponies, donkeys, and mules) are particularly susceptible to infection. In contrast, the causative agent of melioidosis (*Burkholderia pseudomallei*) readily infects most vertebrate animals, including but not limited to humans, livestock, companion animals, and a large variety of exotic species (e.g. dolphins, primates, fish, etc). Infection by *B. mallei* and *B. pseudomallei* typically occurs via the respiratory or percutaneous route, and the most common manifestations are life-threatening bacterial pneumonia and sepsis. Both diseases are highly infectious, difficult to diagnose, and require prolonged antibiotic therapy with low success rates. There is no vaccine to protect against infection with either bacterial organism. Today, naturally occurring cases of glanders and melioidosis can be found in endemic regions like Southeast Asia, Africa, the Middle East, South America, and Australia (*B. pseudomallei* only). These diseases are closely monitored by the World Organization for Animal Health (OIE) and the Federal Select Agent Program (SAP) as they are considered a serious safety and biosecurity threat. Furthermore, in non-endemic regions like the United States, animals must be screened prior to importation, and if infected, the animals are culled (1-11).

In this dissertation, we report on validation of the common marmoset as a suitable large animal model of intranasal infection with *B. mallei* (12), and we also report on the identification and characterization of two novel virulence factors with vaccinogenic potential. Previous studies indicated that the genomes of *B. mallei* and *B. pseudomallei* contain eight genes specifying autotransporter (AT) proteins, which are important virulence factors of Gram-negative bacteria (13). We characterized two of these AT, namely *Burkholderia* autotransporter A (BatA) and *Burkholderia pseudomallei* autotransporter B (BpaB), and we identified these AT as potential vaccine candidates to protect against infection with *B. mallei* and *B. pseudomallei* (14). Furthermore, we also report the discovery of a novel live-attenuated strain of *B. mallei* ATCC 23344, which results in the production of a robust humoral immune response that protects against infection with *B. mallei* and *B. pseudomallei* (Zimmerman *et al*., manuscript in progress). Given the limited diagnostic capabilities for *B. mallei* and *B. pseudomallei* and their poor response to treatment, the development of an efficacious vaccine against these bacteria are critical for improving human and equine health in endemic areas of the world. The identification of potential *B. mallei* and *B. pseudomallei* vaccine targets is the vital first step in developing novel medical countermeasures (MCM), like an efficacious vaccine against glanders and melioidosis. Such vaccines could be used not only to improve equine health in endemic areas of the world, but also to prevent the introduction of this disease to humans and animals in the United States.

CHAPTER 2

LITERATURE REVIEW

2.1 Microbiology of *B. mallei* and *B. pseudomallei*

2.1.1. Taxonomy

B. pseudomallei and *B. mallei* are betaproteobacteria of the Order *Burkholderiales* and Family *Burkholderiacea*. Over the years, these organisms have been renamed several times. Prior to 1992, most infectious *Burkholderia spp.* were identified as *Pseudomonas spp.* Thanks to improved genetic tools, these organisms have been reclassified and approximately 44 different species of *Burkholderia* have been identified. It is important to note that the vast majority of *Burkholderia spp.* are non-pathogenic. In fact, of the 15 infectious *Burkholderia spp.* only 6 have ever been found associated with vertebrate infections. The other 9 *Burkholderia sp.* are primary plant pathogens. To date, *B. pseudomallei* and *B. mallei* are the only primary human and animal (zoonotic or cross-over) pathogens. The remaining *Burkholderia spp.* (namely *B. cenocepacia, B. cepacia, B. fungorium,* and B. *gladioli*) have merely acted as opportunistic pathogens in immune-compromised hosts (15-17).

2.1.2 Organisms

B. pseudomallei is a gram-negative, encapsulated, motile, non-spore-forming, facultative intracellular bacillus (1, 3, 18). The genome of *B.*

pseudomallei K96243 has been published and consists of two chromosomes (4.1 and 3.2 Mbp, respectively). While larger than the genome of *B. mallei*, the majority of the genes found in *B. pseudomallei* are 99% identical to those of *B. mallei*. (19).

B. mallei is a Gram-negative, encapsulated, non-motile, non-spore-forming, host-adapted bacillus (1-3, 18, 20, 21). The genome of *B. mallei* ATCC23344 has also been published. It too consists of two chromosomes, but the genome of *B. mallei* is smaller than the genome of *B. pseudomallei* (3.5 and 2.3 Mbp, respectively). Interestingly, the genome of *B. mallei* ATCC23344 contains a large number of mobile DNA elements, which may have caused extensive genetic deletions and rearrangements (5).

2.2 Epidemiology of *B. mallei* and *B. pseudomallei*

2.2.1 Environmental Niche and Geographic Distribution

Given *B. pseudomallei* is a saprophytic organism, it can be found in the warm water and wet soils of endemic areas bordering the equator (between latitudes 20° North and South). Specifically, this organism is found in Southeast Asia and Northern Australia (Figure 2.1). Primary reservoirs include any stagnant water sources (e.g. rice patties, swamps, ponds). While it prefers soil with a water content of 15% and rotting organic matter, it can persist for long periods of time with minimal nutrients. Experimentally, it has even been cultured from distilled water 10 years after initial inoculation (1, 3, 11, 18, 22).

Unlike *B. pseudomallei*, *B. mallei* is host-adapted, meaning it is unable to persist outside of its host (equine) reservoir. It is highly endemic in Asia, Africa,

the Middle East, and South America (Figure 2.2) (2, 3, 20, 21, 23). This organism is now considered exotic in North America and Europe; however, it was once endemic on these continents. *B. mallei* was first introduced to North America via horses brought with early European settlers. By the 1850s, this disease reached epizootic proportions due to its transmittance by cavalry horses during the Civil War. Eventually, *B. mallei* was eradicated by implementation of a strict culling program that provided financial compensation to horse owners. Great Britain was the first to eradicate *B. mallei* in 1928. North America followed (the United States in 1934 and Canada in 1938), and by 1965, most European countries had also eradicated the organism (24-26).

2.2.2 Hosts

B. pseudomallei has a very broad host range, infecting most vertebrates. While it is considered a primary human pathogen, it infects a variety of veterinary species, including but not limited to, livestock (horses, cattle, pigs, sheep, and goats), domestic pets (dogs and cats), and exotic species (fish, birds, exotic hoof stock, primates, and dolphins) (6-9).

B. mallei primarily affects solipeds (horses, donkeys, mules). That being said, most mammals are susceptible to infection, and though rare, natural infections have been reported in dogs, cats, camels, goats, and sheep. In many zoos, *B. mallei* is emerging as a pathogen of concern for wild carnivores that consume contaminated horse meat. More importantly, *B. mallei* is considered a serious zoonotic agent, as it can infect humans. Humans are considered accidental hosts, as *B. mallei* primarily only infects individuals who work in close proximity

to infected animals (e.g. veterinarians, animal care takers) or with live cultures and/or infected tissue (laboratory personnel). (2, 9, 10).

2.2.3 Diagnosis

The genetic identity shared by *B. pseudomallei* and *B. mallei* make them very difficult to distinguish them from each other in a diagnostic setting. These two organisms cross-react on both serologic and hypersensitivity (mallein) tests. They also produce similar lesions, making them impossible to distinguish during post mortem examination and on histopathology. In non-endemic regions, distinguishing between these two agents is less of a concern because the goal is to merely prevent introduction of the disease. For these reasons, the mallein test and complement fixation are still routinely used to screen imported animals, particularly equids. However, confirmatory tests are always required as serologic tests can produce false-positive results. In endemic regions, these tests lack the sensitivity and specificity required to make a definitive diagnosis. As such, culture of lesions, respiratory secretions, and wound exudates remains the gold standard. Unfortunately, this test is not performed routinely due to the inherent risk is poses to laboratory personnel. Recent advancements in molecular diagnostics have led to the development of confirmatory diagnostic tests that can distinguish between *B. pseudomallei* and *B. mallei* (e.g. PCR, microarrays, pulsed-field gel electrophoresis, 16s rRNA sequencing, variable number tandem repeat polymorphism, multilocus sequence typing, and immunohistochemistry). However, few of these new diagnostic modalities are employed in the clinical setting due to cost and lack of wide-spread commercial availability (2, 27-34).

2.2.4 Treatment and Prevention

The treatment of animals infected with either *B. mallei* or *B. pseudomallei* in non-endemic countries is prohibited, and a strict quarantine and cull reportable disease program is enforced by the United States Department of Agriculture (USDA) and the World Organization for Animal Health (OIE). Carcasses and bedding from infected animals must be disposed of in accordance with USDA and state regulations (typically, incineration or burial), and the environment and all equipment must be appropriately disinfected. *B. mallei* is susceptible to UV irradiation, heat (55°C for 10 min), and most common disinfectants, including benzalkonium chloride, 1% sodium hypoclorite (bleach), 70% ethanol, 2% glutaraldehyde, iodine, mercuric chloride, and potassium permanganate. In countries where *B. mallei* is endemic, antimicrobial treatment can be attempted but is not advised, as the agent is zoonotic and most antimicrobial agents are ineffective. Treated animals often have disease relapses and may even remain sub-clinically infected and continue to shed the organism in the environment (2, 34-36).

In humans, *B. mallei* is susceptible to aminoglycosides, tetracyclines, doxycycline, sulfonamides, trimethoprim, imipenem, ceftazidime, and piperacillin but resistant to streptomycin, polymyxin, and penicillin. For localized lesions, surgical drainage and debridement, along with prolonged (60-150 days) oral administration of amoxicillin-clavulanate potassium, doxycycline, or trimethoprim-sulfamethoxazole is recommended. Intravenous ceftazidime along with supportive therapy has been suggested for generalized, septic disease (2).

In contrast to *B. mallei*, *B. pseudomallei* is much more resistant to antimicrobials, and therefore, even more difficult to treat. *B. pseudomallei* possesses antibiotic efflux pumps, enzymatic inactivators, a nearly impermeable capsule, and numerous mutations in target sites that render it inherently resistant to β-lactam antibiotics (e.g. penicillin and ampicillin), first-generation and second generation cephalosporins, gentamicin, tobramycin, streptomycin, and polymyxin. Some treatment efficacy has been seen with carbapenems, third generation cephalosporins (ceftazidime), doxycycline, amoxicillin-clavulanate, and trimethoprim-sulfamethoxazole. Typically, these antibiotics are given in combination over a prolonged period of time (17, 37).

Disease prevention in humans, unlike animals, is more reactionary. To date, there is no evidence of human to human transmission of *B. pseudomallei* through respiratory secretions. Persons traveling to endemic regions (tourists, troops, missionaries, etc), especially if immune-compromised, should be warned about the risk of contracting melioidosis, but no active surveillance program is available in the United States. Unfortunately, no vaccine is available for animals or humans (2, 17, 37).

2.2.5 Disease Significance

B. mallei and *B. pseudomallei* are ancient infectious organisms, having first been described by Hippocrates in 400 B.C. and Aristotle in 330 B.C. In fact, melioidosis (the disease caused by *B. pseudomallei)*, is derived from the Greek word, "melis" and translates to "a condition similar to the distemper of asses (e.g. Glanders, the disease caused by *B. mallei*)." During the Enlightenment, it was the

horsemanship and medical work of Claude Bourgelat that prompted Louis XV to grant a royal charter for the first veterinary school at Lyons, France in 1762. While Bourgelat was not the first to study *B. mallei*, his example spurned others to take interest in the disease and animal health, which ultimately led to the development of present-day veterinary medicine (26).

Although *B. pseudomallei* has never been documented to occur naturally in North America, and *B. mallei* has been eradicated, outbreaks do occur in other countries, so continued vigilance is essential. While the risk of accidental introduction into the United States is low, importation of animals with *B. mallei* remains a potential concern (2, 34).

Even more concerning, there is also the potential for *B. pseudomallei* or *B. mallei* to be introduced intentionally via bioterrorism. These organisms are efficiently transmitted, highly contagious, often fatal, difficult to diagnose, resistant to treatment, and lack preventative measures. If either organism was concentrated and delivered as an aerosol, they could have significant repercussions on not just human and animal health but also the food industry. Such fears are particularly concerning given *B. mallei* has historically been used in warfare, most notably during World War I by Germany and during World War II by Japan. Though *B. pseudomallei* has never been utilized in war, it has been investigated by both the United States and Russia as a potential bioweapon (38-40). Given these threats to national security, the Federal Select Agent Program (SAP) has classified *B. mallei* and *B. pseudomallei* as Tier 1 Select Agents, and

the United States has made the development of therapeutic and preventative measures against these pathogens a priority (2, 26, 38, 40, 41).

2.3 Host-Pathogen Interactions

2.3.1 Disease Pathogenesis

The known pathogenesis of *B. mallei* and *B. pseudomallei*, while limited, is virtually the same. Infection primarily occurs via inhalation or percutaneous inoculation, though it can also be contracted if ingested. In general, the bacteria first invade and colonize either an epithelial or mucosal surface. Next, these organisms can either disseminate directly into the blood stream or indirectly via phagocytosis by macrophages and dendritic cells, which then traffic to regional lymphoid tissues (draining lymph nodes and mucosal-associated lymphoid tissues). Pyogranulomatous inflammation ensues in these lymphoid tissues, and these organisms then continue to travel systemically by draining into the thoracic duct for redistribution via either leukocytes trafficking in lymph or bacteremia in the blood. Ultimately, host cell death and widespread tissue destruction are caused primarily by the host's inflammatory response. To date, all of the target cells and ligand-receptor interactions in this infectious process remain undetermined.

B. mallei causes the respiratory and cutaneous diseases known as glanders or farcy (respectively), while *B. pseudomallei* causes melioidosis. Each can have either acute or chronic disease manifestations. Typical clinical signs consist of mucopurulent nasal discharge, mucosal ulcers, increased respiratory effort and sounds, skin nodules on the limbs or abdomen, and/or swollen and painful joints.

B. mallei and *B. pseudomallei* primarily affect the skin, lymphatic organs, respiratory tract, spleen, and liver. Lesions typically predominate at the site of initial infection and radiate out (e.g. cutaneous form [farcy] if inoculated versus pulmonary nodules [glanders] if inhaled).

Gross lesions of the acute form of either disease consist of petechial hemorrhages, catarrhal bronchopneumonia, and enlarged lymph nodes. Gross lesions of the chronic form include: pulmonary nodules with either caseous/calcified centers surrounded by zones of inflammation, mucosal ulcers in the nose, trachea, larynx, and bronchi, pustules and nodules in the skin, and stellate scars on healing ulcers on the nasal turbinates and septum.

Histopathologic lesions of the acute form include pyogranulomatous lesions in the nasal cavity with a central core of degenerate neutrophils covered by fibrinohemorrhagic exudate. Mature histopathologic lesions of the chronic form consist of liquefactive or caseous necrosis, surrounded by epithelioid macrophages, multinucleated giant cells, lymphocytes, and lastly granulation tissue. Fibrosis and re-epithelialization eventually results in scar formation.

Given the similarity of *B. mallei* lesions to *B. pseudomallei* lesions, and the similarity of either of these lesions to other bacterial and fungal infections, it is often difficult to definitively identify these diseases. Cutaneous *Burkholderia* infections can be confused with infection with *Histoplasma farciminosus, Corynebacteria pseudotuberculosis, Sporothrix schenkii,* and *Pythium insidiosum.* Pulmonary forms of *Burkholderia* infections are often misidentified as other types

of chronic bacterial pneumonia (*Mycobacteria spp, Streptococcus equi*, and *Rhodococci equi)* (42, 43).

2.3.2 Virulence Traits

B. mallei and *B. pseudomallei* have developed a variety of mechanisms for exploiting their hosts. These traits include adhesion, intracellular invasion, intracellular survival within macrophages, evasion of autophagy, cytotoxicity, serum resistance, biofilm formation, and latency. For many of these traits, virulence factors have been identified. However, in most cases the exact mechanism of their action on the host remains unclear.

Initial attachment of *B. mallei* and *B. pseudomallei* appears to be mediated by a thin, polysaccharide capsule covering their outer membrane (18, 44). Firm attachment is primarily mediated by several protein adhesins and type IV pili (PilA), much like those utilized by *Pseudomonas aeruginosa* (18, 45, 46). Type III Secretion Systems (BopE and BipD), actin polymerization of the host cell (BimA), and a two-component regulatory system (*irlRS*) allow for and promote the intracellular invasion and spread of *B. mallei* and *B. pseudomallei* within host cells (18, 47-50). Furthermore, initial escape from host vacuoles is mediated largely by the action of Type III Secretion Systems (T3SS), which are critical for evasion of killing by the host cell via autophagy (BopA) (18, 51).

Yet another way *B. pseudomallei* evades host cell killing is by inhibiting inducible nitric oxide synthase (iNOS). iNOS is just one of the enzymes utilized by host cells to produce reactive oxygen intermediates for pathogen destruction. *B. pseudomallei* achieves this through an unclear mechanism that ultimately

activates host cell suppressors like cytokine signaling 3 (SOCS3) and cytokine-inducible src homology 2-containing protein (CIS), both of which are iNOS inhibitors (18, 52, 53).

The dissemination of *B. mallei* and *B. pseudomallei* is mediated by several different virulence traits. Macrophage cytotoxicity may seem counterintuitive, but it is actually utilized by *B. mallei* and *B. pseudomallei* as a means of escaping for dissemination. In *B. pseudomallei*, macrophage cytotoxicity and multinucleate giant cell formation may be dependent on RNA polymerase σ factor (RpoS) expression (18, 54, 55). Secondary spread may be mediated in the spleen by a conventional autotransporter (Bca1) (18). Successful dissemination of *B. mallei* and *B. pseudomallei* via the hematogenous route (e.g. septicemia) can also be attributed to serum resistance. Serum resistance is achieved via several virulence factors; namely, the bacterial capsule, lipopolysaccharide (LPS), and serine proteases, which help these organisms resist complement-mediated killing and resistance to cationic peptides and defensins (18, 56-58).

Biofilms consist of a confluent layer of bacteria encased in a carbohydrate-based fibrous matrix, which is most often composed of complex polysaccharides. While biofilm formation has not been demonstrated to be essential for virulence in *B. mallei* and *B. pseudomallei*, it may be that this trait enables these organisms to survive in unfavorable environmental conditions (18, 59).

2.3.3 Type 5 Secretion System

Gram-negative bacterial organisms secrete target proteins through a variety of different secretion systems, which are designated as Types I-IX. The type V secretion system (T5SS) in Gram-negative bacteria is composed of two major types of protein systems, namely the autotransporters (AT) and the two-partner secretion (TPS) system. More specifically, the T5SS is further divided into 5 subtypes: T5aSS (AT1, Va, classical autotransporters), T5bSS (TPS, Vb, two-partner secretion system), T5cSS (AT2, Vc, trimeric autotransporters), T5dSS (AT3, hybrid autotransporters), and T5eSS (AT4, inverted autotransporters) (13, 60-63). For the purposes of this dissertation, we will focus on just autotransporters.

AT have 3 functional domains: an amino (N)-terminal passenger domain attached to a signal peptide, an internal linker domain, and a carboxyl (C) terminal translocator domain. The N-terminal domain varies widely amongst AT and specifies the biologic function of the AT once it is secreted. The C-terminal domain tethers the AT to the outer membrane (OM) and is used to characterize the AT into subtypes. The C-terminal domain of the classical/conventional AT is a large monomer composed of 12 β-strands arranged antiparallel to each other to form a large β-barrel. The oligomeric/trimeric AT, as the name implies, assemble their β-barrels into trimers, with each protomer being composed of four antiparallel β-strands. The translocator domain of the hybrid ATs is located on the C-terminus as in classical AT; however, this domain shows sequence similarity to the translocator domains of the TPS system, rather than the AT

system. Finally, the inverted AT merely have an inverted orientation, meaning the passenger domain follows the translocator domain in the primary structure (13, 62, 64-68).

AT genes are transcribed in the cytoplasm to mRNA, with AT transcriptional regulation in most organisms being diverse, complex, and poorly understood. AT mRNA is then translated by ribosomes into the aforementioned single polypeptide AT precursor. Likewise, it is known that many AT are post-translationally modified; however, the mechanisms governing this post-translational control is also poorly understood.

After synthesis, ATs travel to and are translocated across the inner membrane (IM) and into the periplasm via the Sec translocase pathway. The Sec translocase system is composed of four main components: the signal sequence (leader peptide), a chaperone protein, a membrane-bound protein channel (SecYEG), and a cytoplasmic ATPase (SecA) that is bound to and drives SecYEG. More specifically, SecY and Sec E form the protein-conducting channel (Sec translocon), while SecG stimulates the transport. The combined structures of SecYEG and SecA are often referred to as the Sec translocase.

The major chaperone protein in Gram-negative bacteria is SecB. It binds the AT precursor as it exits the ribosome and functions to keep the AT precursor from prematurely folding into an aggregate that cannot be translocated across the IM. SecB also directs the AT precursor to the IM, ultimately delivering the AT precursor to SecA.

The signal peptide has 3 regions: a basic (positively charged) N-terminal domain, a central hydrophobic core called the H-domain, and an uncharged C-terminal domain. In conjunction with SecB, the N-domain of the signal peptide directs the AT precursor to the IM and mediates its attachment to the cytosolic side of the IM. Next, the H-domain inserts itself into the IM. Finally, the C-domain displays a peptidase recognition site, which allows a specific periplasmic peptidase to cleave the signal peptide from the AT precursor once it crosses the IM into the periplasmic space.

Interestingly, 10% of all AT precursors possess a signal peptide with an extended signal peptide region (ESPR). While the exact role of the ESPR remains under investigation, it is speculated that they may interact with YidC (IM protein integrase) to slow the translocation of AT across the IM in order to prevent the accumulation of misfolded AT precursors in the periplasm. Additionally, some AT precursors possess a lipoprotein motif in their signal peptide. This motif targets the AT precursor to an acyltransferase within the periplasm, after which the AT is then directed to a lipoprotein-specific signal peptidase (Lsp) for cleavage and eventually the attachment of a lipid moiety.

The exact secretion mechanisms employed by AT once they reach the periplasmic side of the OM is still greatly debated. In general, two main models are proposed. The first is the hairpin model, which states that the AT secretes itself by inserting its C-terminal translocator domain into the OM, after which it forms a β-barrel pore to secrete its own internal passenger domain (Figure 2.3). The second (Bam) model argues that the β-barrel pore is too narrow to

accommodate a large, completely folded protein. It contends that the AT either hijack or work cooperatively with existing secretion machinery (e.g. Bam or Lol complexes) to secrete themselves. (13, 60-62, 64-78).

To date, AT proteins (those identified in *Burkholderia* are noted) appear to be involved in many critical virulence traits, including adherence (BoaA) (79), invasion, serum resistance, phospholipolysis, cytotoxicity, intracellular survival, actin-based intracellular motility (BimA) (48, 80), dissemination (Bca1) (81), and biofilm formation (BbfA) (82). Additionally, several AT-based vaccines have been demonstrated to be effective at eliciting a protective immune response, the most notable being pertactin. Pertactin is an AT adhesin and a component of the licensed vaccine in the United States used to vaccinate adults and children against *Bordetella pertussis* (83). Since AT are surface-exposed virulence determinants that have been shown to be effective vaccines, it stands to reason AT targets shared by *B. mallei* and *B. pseudomallei* may be exceptional vaccine candidates (13, 48, 79-81, 84-86).

2.3.4 Protective Immune Responses

Engagement of both the innate and adaptive immune system is critical for clearing bacterial infections, particularly *B. pseudomallei* and *B. mallei*. Upregulation of numerous pattern recognition receptors (PRRs) have been documented in human melioidosis patients. In particular, the upregulation of CD14, MD2, TLR1, TLR2, TLR3, TLR4, TLR5, and TLR10 has been noted (87-90). Additionally, TLR signaling adaptor and amplifying proteins, like MyD88 and TREM-1, and the major inflammasome receptors, IL-1R and IL-18R, are

critically involved in neutrophil recruitment and inflammatory cytokine production during *B. pseudomallei* infection (87, 89, 91-93). Interestingly, *B. pseudomallei* has been demonstrated to activate NF-κB in both TLR-dependent and independent fashions, which ultimately leads to production of TNF-α, IL-1, IL-6, and IL-12. These pro-inflammatory cytokines not only fuel the host inflammatory response against *B. pseudomallei* but also activate complement, the coagulation cascade, autophagy, and induce apoptosis (94-101). Neutrophil and macrophage-depleted mice have demonstrated accelerated mortality when challenged with *B. pseudomallei* (102, 103). Additionally, human patients treated with granulocyte colony stimulating factor (G-CSF) had slightly longer survival times than their placebo counterparts (104). All of these findings confirm that the initial response by the innate immune system is indeed important to combating acute and possibly even chronic infection with *B. pseudomallei* and *B. mallei.*

While innate immunity is important for initial microbial killing, cell-mediated immunity seems the most critical for adequate bacterial clearance and resistance to acute infection with *B. pseudomallei* and *B. mallei*. Cell-mediated immunity is governed by IFN-γ-producing T-lymphocytes ($CD4^+$ and $CD8^+$ T-cells) classically-activated macrophages (Th1 response). This arm of the adaptive immune system is responsible for inducing the formation of classically-activated macrophages, which are primed for microbial killing. Studies have shown that IFN-γ production protects BALB/c mice from acute infection; however, these mice still develop chronic disease (105-107). Also, one report suggests that seropositive individuals with strong cell-mediated responses are more likely to

remain asymptomatic rather than develop the symptoms of chronic melioidosis (106, 108). However, no study to date has demonstrated complete, sterilizing immunity with cell-mediated immunity alone.

Humoral immunity via antibody production and alternatively-activated macrophages (Th2 response) is also important for protection against *B. pseudomallei* and *B. mallei*. This arm of the adaptive immune response uses antibodies to opsonize antigen and promote killing by polymorphonuclear leukocytes. It has been shown that antibody titers often correlate with disease severity in both humans and animal models (95). Studies with diabetic rats and BALB/c mice have demonstrated that the passive transfer of protective polyclonal or monoclonal antibodies can protect against acute infection with *B. pseudomallei.* However, sterilizing immunity with antibody alone has yet to be successful in completely protecting against infection with *B. pseudomallei* and *B. mallei* (106, 109, 110). It would seem the ideal, sterilizing vaccine must be able to not only adequately stimulate the innate immune system, but also engage both arms of the adaptive immune response.

Attempts to protect mice against acute infection with *B. pseudomallei* have been made with a number of live attenuated vaccines. To date, none have demonstrated sterilizing immunity. Additionally, the ability of *B. pseudomallei* and *B. mallei* to establish persistent infections in their hosts is always a concern when using live attenuated vaccines, which makes the development of an effective live attenuated vaccine with federal approval quite difficult (106, 111-113).

Vaccination with several heat-inactivated whole cell *B. pseudomallei* antigens have been found to provide some protection in mice. However, in other studies, no protection was noted (106, 114, 115). These conflicting results are difficult to interpret but suggest that while protective, killed vaccines alone are likely not sufficient for inducing sterilizing immunity against *B. pseudomallei.*

Purified *B. pseudomallei* and *B. mallei* antigens, both with and without adjuvant, are also being explored as possible vaccine strategies. Some mouse and horse studies using capsular polysaccharide, LPS, outer membrane proteins (OmpA), and lipoprotein-releasing transmembrane protein (LolC) have shown promise at protecting against acute infection. However, most survivors remain persistently infected with bacterial colonization in the spleen [(106, 109, 116) and Lafontaine *et al*, unpublished work]. It is unlikely that a single component vaccine will completely protect against infection with *B. pseudomallei* and *B. mallei;* however, a multivalent subunit vaccine may prove effective, especially if combined with the right adjuvant. Additional subunit vaccine delivery avenues being explored include polysaccharide-protein glycoconjugate vaccines and naked DNA vaccines [(106, 110, 117) and Lafontaine *et al*, unpublished work].

2.4 Animal Models of Infection

2.4.1 Rodents

Several rodent species have been used in experimental models of glanders and melioidosis. Guinea pigs, hamsters, diabetic rats, and BALB/c mice are particularly susceptible to acute infection via either percutaneous or aerosol routes (3, 118, 119). BALB/c mice are immunologically-biased towards a Th2 immune

response, in which antibody production is stimulated and macrophages become alternatively activated (120, 121). Similarly, it has also been demonstrated that IFN-γ R2/2 knock-out mice, which lack the IFN-γ receptor, are also highly susceptible to infection with *B. pseudomallei* and present with acute infection (3, 106, 122). In contrast, C57BL/6 mice are Th1 biased, meaning cell-mediated immunity predominates, and macrophages are classically-activated for antigen killing (120, 121). As such, these mice have been shown to be resistant to acute infection and have become an established model for the chronic disease manifestations of *B. mallei* and *B. pseudomallei* (2, 20, 43, 106, 122-129). In contrast to these reports, recent experiments by our group have demonstrated that C57BL/6 mice aerosol challenged with *B. mallei* ATCC 23344 or *B. pseudomallei* 1026b are just as susceptible as BALB/c mice to developing acute infection (Lafontaine *et al*, unpublished work). These earlier studies performed with C57BL/6 mice were conducted using either intranasal or intraperitoneal methods of infection, which raises the question if different clinical signs and disease progression can manifest both within and amongst these different rodent models by merely varying the route of inoculation.

2.4.2 Domestic Animals

Solipeds (horses, donkeys, and mules) are likely the best and most readily-available large animal model for studying both acute and chronic infection, as they are not only the natural reservoir for *B. mallei* but also highly susceptible to infection with *B. pseudomallei.* To date, a miniature horse model of glanders (130) and a horse model of both glanders and melioidosis [Lafontaine et al,

unpublished work] have been used successfully to study acute infection. Cats, dogs, sheep, and goats are susceptible to infection with *B. pseudomallei* and *B. mallei* (2, 43, 131), and recently, goats were established to be a large animal model for studying chronic infection caused by *B. mallei* and *B. pseudomallei* (131). Interestingly, cattle, pigs, and birds are more resistant to natural disease and make poor experimental models of infection (2, 43, 118, 130).

2.4.3 Non-Human Primates

While often cost-prohibitive, non-human primates (NHPs) are occasionally used for studying *B. pseudomallei*, as humans and primates are the primary hosts. Yeager *et al* recently published work on the disease progression of melioidosis in both rhesus macaques and African green monkeys (132). Additionally, the common marmoset has been identified as a primate model for studying acute subcutaneous infection with *B. mallei* and aerosol infections with *B. pseudomallei* (133, 134). While these NHP models are not necessarily the best infection model because a range of susceptibility can be observed (118), they are often sought by those interested in developing FDA-approved therapeutic and preventative countermeasures, as their anatomy and physiology is very similar to that of humans (132).

2.4.4 Surrogate Hosts

Due to the physical and financial constraints of working with mammalian models, some are investigating relevant surrogate hosts as potential models for studying some aspects of *B. mallei* and *B. pseudomallei* interactions in eukaryotic cells. *Caenorhabditis elegans* (non-parasitic nematode), *Galleria mellonella*

(greater wax moth larvae), *Acanthamoeba sp.* (protozoan), and *Gromphadorhina portentosa* (Madagascar hissing cockroach) have been used with success to study certain virulence traits (e.g. endotoxin, phagocytosis evasion, T6SS activity) (3, 135-140). While these model systems are certainly useful for *in vivo* studies, any findings regarding virulence must still be confirmed with a mammalian host.

2.5 Conclusion

Burkholderia mallei and *Burkholderia pseudomallei* are zoonotic bacterial pathogens that pose significant risks to human and animal health; hence, their classification as Tier 1 Select Agents by the United States Federal Select Agent Program. Infection by either organism often results in acute bacterial pneumonia and fatal septicemia, particularly if not diagnosed early and treated appropriately. Despite the availability of antibiotic therapy, significant morbidity and mortality remain a serious concern and underscore the need for an efficacious vaccine. Currently, no commercial vaccine is available and much remains to be understood about the pathogenesis of *B. mallei* and *B. pseudomallei* in relevant animal models. The purpose of this dissertation is to determine if the common marmoset (*Callithrix jacchus*) is a suitable large animal model for studying *B. mallei* and to characterize two potential autotransporter vaccine candidates, BpaB and BatA, which are important for the virulence of *B. mallei* and *B. pseudomallei* in an established murine model of aerosol infection.

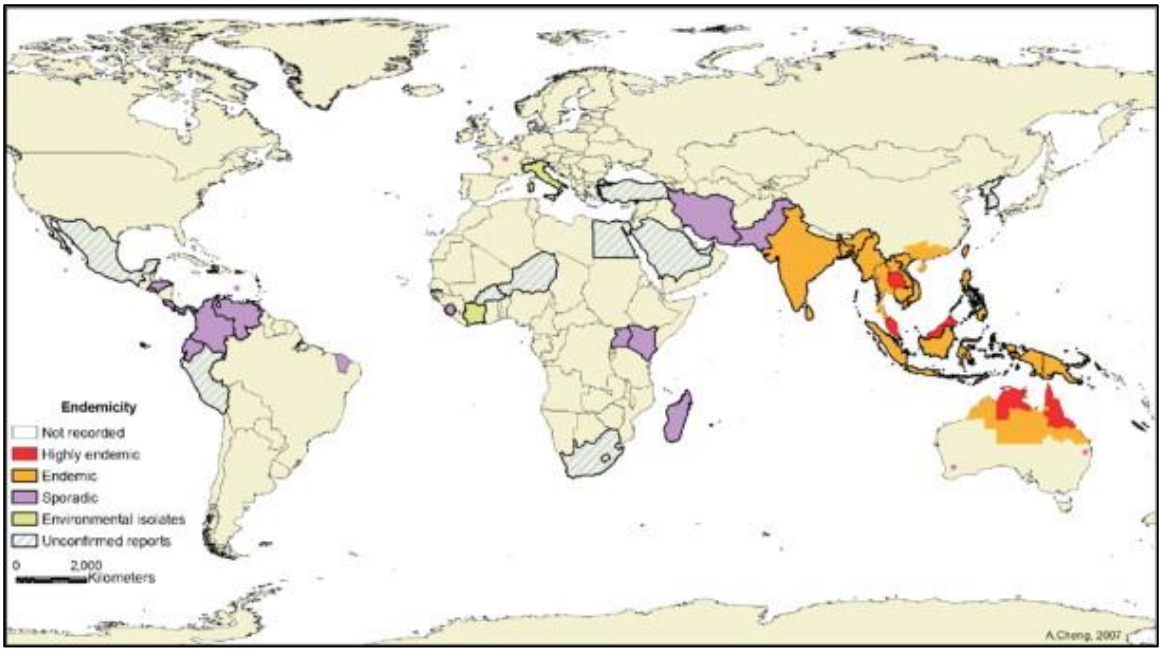

Figure 2.1. *Burkholderia pseudomallei* Geographic Distribution

Map is courtesy of Currie *et al*. 2008. Transactions of the Royal Society of Tropical Medicine and Hygiene. 102(1): S1-4.

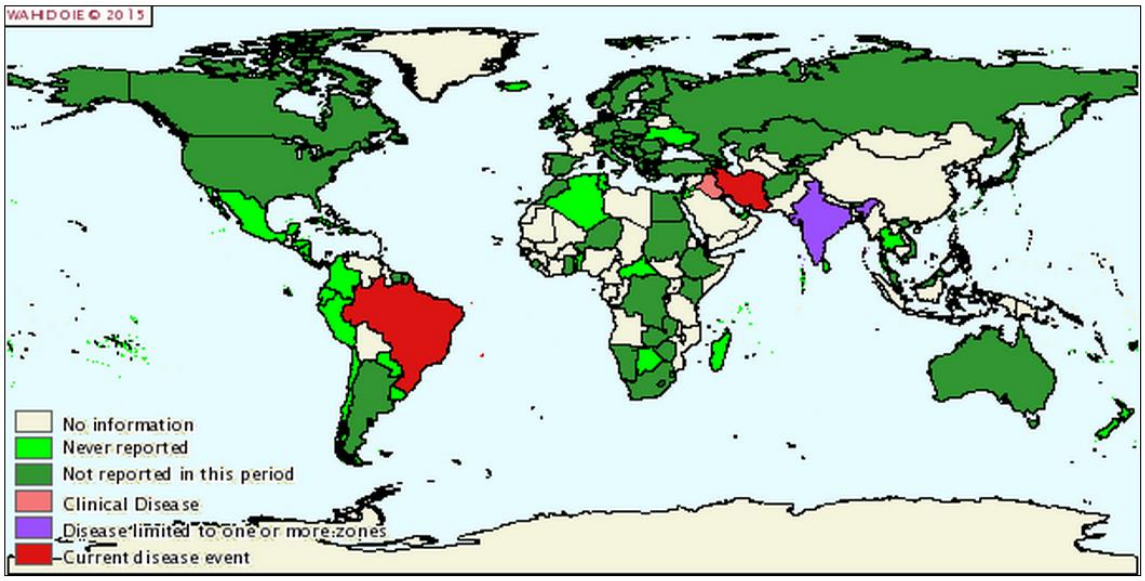

Figure 2.2. *Burkholderia mallei* Geographic Distribution

Distribution map is courtesy of the World Animal Health Information Database (WAHID) by OIE http://www.oie.int/wahis_2/public/wahid.php/Wahidhome/Home

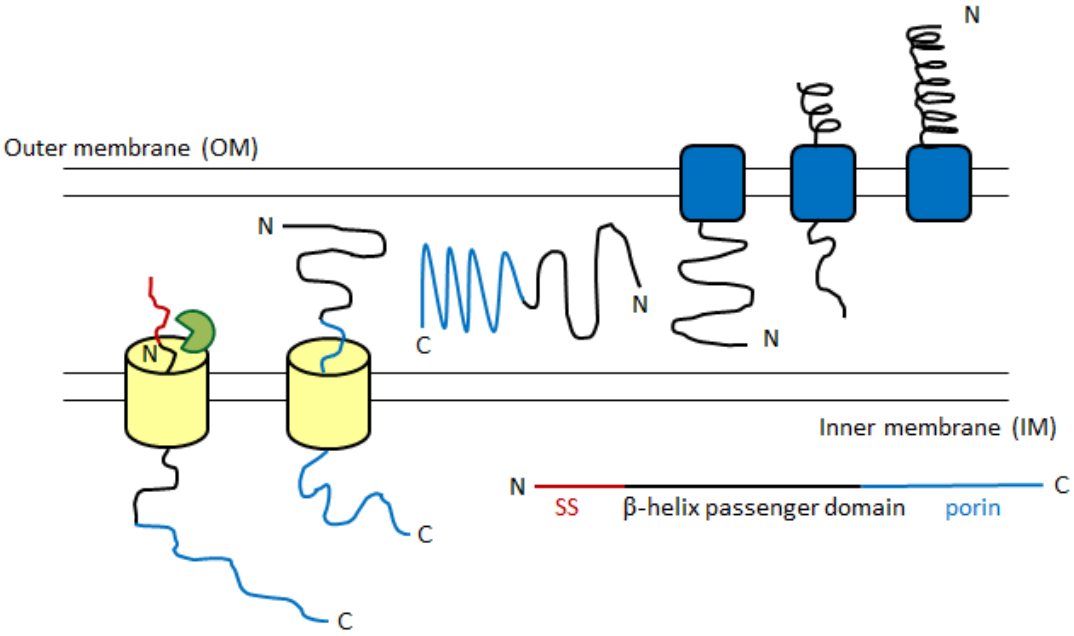

Figure 2.3. Model of autotransporter translocation across the bacterial outer membrane.

Image adapted from Junker *et al*. PNAS 2006; 103(13): 4918–4923. Current models of autotransporter secretion include passage through the inner bacterial cell membrane via an N-terminal signal sequence (shown in red). The C-terminal porin sequence (shown in blue) then inserts into the outer bacterial cell membrane and secretes the passenger domain (shown in black) through a central pore in the porin. The passenger domain then folds into its native structure outside the bacterial cell.

CHAPTER 3

USE OF THE COMMON MARMOSET TO STUDY *BURKHOLDERIA MALLEI* INFECTION [1]

[1] Zimmerman SM*, Jelesijevic T*, Harvey SB, Mead DG, Shaffer TL, Estes DM, Michel F, Quinn FD, Hogan RJ, Lafontaine ER, 2015, *PLOS ONE,* Volume 10, Issue 4, e0124181. Reprinted here with permission of the publisher. (*co-first authors)

3.1 Abstract

Burkholderia mallei is a host-adapted bacterium that does not persist outside of its equine reservoir. The organism causes the zoonosis glanders, which is endemic in Asia, Africa, the Middle East, and South America. Infection by *B. mallei* typically occurs via the respiratory or percutaneous route, and the most common manifestations are life-threatening pneumonia and bacteremia. Glanders is difficult to diagnose and requires prolonged antibiotic therapy with low success rates. There is no vaccine to protect against *B. mallei*, and there is concern regarding its use as a biothreat agent. Thus, experiments were performed to establish a non-human primate model of intranasal infection to study the organism and develop countermeasures. Groups of marmosets (*Callithrix jacchus*) were inoculated intranasally with *B. mallei* strain ATCC 23344 and monitored for clinical signs of illness for up to 13 days. We discovered that 83% of marmosets inoculated with doses of 2.5×10^4 to 2.5×10^5 bacteria developed acute lethal infection within 3-4 days. Signs of disease were severe and included lethargy, inappetence, conjunctivitis, mucopurulent and hemorrhagic nasal discharges, and increased respiratory effort with abdominal lifts. *Burkholderia mallei* was cultured from the lungs, spleen, and liver of these animals, and pathologic examination of tissues revealed lesions characteristic of glanders. Challenge experiments also revealed that 91% of animals infected with doses ranging from 25 to 2.5×10^3 bacteria exhibited mild, non-specific signs of illness and were culture negative. One marmoset inoculated with 2.5×10^3 organisms developed moderate signs of disease and reached humane end-points 8 days post infection. The liver and spleen of this animal were colonized with the agent, and pathological analysis of tissues showed nasal, splenic, and hepatic lesions. Taken

together, these data indicate that the marmoset is a suitable model to study respiratory infection by *B. mallei*.

3.2 Introduction

Burkholderia mallei is a non-motile, Gram-negative bacillus that does not persist in the environment outside of its natural equine reservoir. The organism causes the highly contagious and debilitating zoonotic disease glanders, which primarily affects horses, mules, and donkeys. Glanders is an old disease, having first been described by Aristotle in 330 B.C. Other less commonly known names that have been used throughout history to describe the disease include equinia, malleus, droes, and farcy. Though now considered exotic in North America and Europe, glanders once was endemic in these regions. Early settlers introduced the disease in the U.S. via the import of infected horses. By the 2nd half of the 19th century, glanders was widespread due to the Civil War, when it was readily transmitted to thousands of cavalry horses passing through remount stations. In response to this epidemic, industrial countries implemented vigorous eradication programs that entailed financial incentive to owners, destruction of infected animals, and disinfection of affected facilities. Great Britain was first to eradicate the disease in 1928, followed by the U.S. in 1934, Canada in 1938, and most European countries by 1965 (3, 141-148). Despite the success of eradication efforts, naturally occurring glanders is still found in parts of Asia, Africa, the Middle East, and South America. The disease is closely monitored by the World Organization for Animal Health (OIE), as it is considered a serious safety and biosecurity threat.

Humans, goats, dogs, cats, rabbits, and carnivorous predators living in the vicinity of equids with glanders, have been naturally infected. Camels have also been reported to

harbor the disease and have been linked to zoonotic transmission (3, 141-146, 149-152). In humans, infection generally occurs via the respiratory route or direct invasion of punctured skin after contact with infected animals. Disease progression and pathology in humans and horses are similar, though the presentation of any 2 cases in the same species, even if related by direct transmission, may vary. Clinical manifestations include fever, myalgia, fatigue, lymphadenopathy, pneumonia, and necrosis of the tracheobronchial tree. Pustular skin lesions and development of multiple abscess-forming nodules, known as farcy, are also common. Most patients become bacteremic, and *B. mallei* bacilli disseminate to the liver, spleen, and lymph nodes, where it rapidly causes necrotizing abscesses (3, 141-146, 149, 153-157). The disease is difficult to identify, and a conclusive diagnosis requires culturing *B. mallei* from patients. The mortality rate is high (up to 50%) despite aggressive antimicrobial therapy. *Burkholderia mallei* is resistant to many antibiotics, which limits treatment options. The recommended two-phase treatment process involves the use of ceftazidime and meropenem (intensive phase), followed by TMP-SMX and co-amoxiclav (eradication phase) for several weeks (158). Response to treatment is slow, and unless treated immediately, eradication of the agent can be difficult as patients are prone to relapses characterized by prolonged bouts of remission and recrudescence. There is currently no vaccine available to reduce the risk of infection by *B. mallei*.

Though human cases of glanders are rare, there is legitimate concern that *B. mallei* might be used as a bioweapon because it has been utilized in this manner on multiple occasions (39, 141, 144, 159-163). During World War I, Germany implemented a bold biological sabotage campaign in several countries including the U.S.,

Russia, Romania, France, and Mesopotamia. For example, horses, mules, and other livestock being shipped from the U.S. to allies were inoculated with cultures of *B. mallei*. German agents also infected thousands of mules in Mesopotamia with the organism, and a German agent was arrested in Russia with similar intentions in 1916. Between 1932 and 1945, the Japanese deliberately infected horses, civilians, and prisoners of war with glanders at the Pin Fan Institute in occupied Manchuria. More recently (1980s), the Soviet Union purportedly weaponized *B. mallei* and used it against opposition forces in Afghanistan (162). For these reasons, the U.S. Federal Select Agent Program classifies *B. mallei* as a Tier 1 agent, and the development of medical countermeasures (MCM) against the organism is highly desirable.

Several animal models have been developed to study glanders, including hamsters, mice, and horses (164-169). These models have been crucial to our current understanding of pathogenesis by *B. mallei* and provide excellent platforms for developing MCM (*i.e.* identification and characterization of targets). In contrast, there have been very few reports describing the use of non-human primates as surrogates to study glanders and validate lead MCM candidates (170-172). To address this, we performed experiments to establish a model of intranasal infection for *B. mallei* using the common marmoset. Our data indicate that this species is a suitable surrogate to study glanders.

3.3 Materials and Methods

3.3.1 Bacterial strain and growth conditions

The *B. mallei* strain ATCC 23344 (173) was used in this study. To prepare the inoculum for infection, the organism was cultured on Brucella broth

agar (BD-BBL) supplemented with 5% (vol/vol) glycerol for 42 hr at 37°C. These plate-grown bacteria were suspended in Phosphate-Buffered Saline (PBS) to an optical density of 250 Klett units using a Klett Colorimeter (Scienceware). Following this, the suspension was serially diluted, and 100 μL aliquots were immediately spread onto agar plates to determine the number of colony forming units (CFU) in the inoculum. Fifty μL of serial dilutions 10^{-2} (250,000 CFU), 10^{-3} (25,000 CFU), 10^{-4} (2,500 CFU), 10^{-5} (250 CFU), and 10^{-6} (25 CFU) were used to infect animals.

3.3.2 Experimental animals and intranasal infection procedures

Both male and female, healthy, sexually mature common marmosets (*Callithrix jacchus*) were obtained from Worldwide Primates Inc. The animals were > 36 months old and weighed 220-430 grams at the time of infection, and were acclimatized to their new surroundings for at least two weeks. Prior to inoculation, the animals were anesthetized in their nest boxes with inhalant isoflurane gas until a respiratory rate of 10-12 breaths per minute was achieved. Once anesthetized, the animals were held in supine position, and droplets of *B. mallei* suspension (5-10 μL) were delivered to the right nostril using a sterile filtered tip attached to a P200 Pipetman. The droplets were inhaled through the nasal passageways, and a total volume of 50 μL of bacterial suspension was administered.

Marmosets were housed individually in stainless steel cages (16.625" W x 18.75" D x 30.625" H, open wire bar – front and top) positioned to allow visual

and vocal communication. The animals were provided various forms of environmental enrichment including wooden perches, mirrors, teethable circular link baby toys, and Kong puzzle toys filled with forage items (dried fruits or vegetables, seeds, nuts, and miniature marshmallows). Water and food were provided *ad libitum*. The animals were fed a balanced commercial primate diet (ZuPreem) supplemented with various food items (fruit, nuts, yogurt, eggs, rice, pasta) in order to recreate their previous diet at the Worldwide Primates Inc. Therapeutic intervention with antibiotics and/or analgesics was not provided as such treatments would have affected the experimental outcomes of the study. Infected animals were monitored every 8 hr.

Humane end-points were strictly observed. Marmosets exhibiting signs of moderate to severe discomfort were euthanized. The following scoring system was used to determine if euthanasia was appropriate: 3 points: complete anorexia and/or lack of water consumption for 24 hr; 3 points: non-responsiveness to external stimuli, recumbency, marked difficulty breathing (dyspnea); 2 points: a "dull" appearance, manifested in part by a reduced responsiveness to external stimuli or lethargic movements in the cage; 2 points: failure to enter the nestbox or climb onto a resting perch; 2 points: failure to consume water for 24 hr; 1 point: mild changes in respiration, such as slightly increased difficulty or an increased respiratory rate; 1 point: inappetence for 1 day. Any animal with a point score $\geq$ 3 was humanely euthanized. This was accomplished by anesthetizing marmosets in their nest boxes using inhalant isoflurane gas. Once anesthetized, the animals were administered a dose of 10-20 mg/kg ketamine

intramuscularly and then euthanized by intracardiac injection of a pentobarbital dose of 240 mg/kg. This procedure is in accordance with the AVMA Guidelines for the Euthanasia of Animals. The median lethal dose (LD_{50}) value was calculated according to Reed and Muench (174), and is defined as the dose where 50% of the animals reached humane end-points.

3.3.3 Post mortem analysis

A board-certified veterinary anatomic pathologist performed post mortem examination of tissues and organs from all animals.

3.3.4 Bacteriology

Samples of lung, liver, spleen, and trachea were aseptically collected for bacterial culture prior to processing the tissues for cytology and histology. These samples were weighed, homogenized with 15-mL disposable tissue grinders (Fisherbrand), serially diluted, and plated on agar medium to calculate the number of viable *B. mallei* bacteria in tissues. To suppress growth of the marmoset normal flora, agar plates containing 8 μg/mL Polymyxin B (MP Biomedicals), 2 μg/mL Bacitracin (MP Biomedicals), and 5 μg/mL Cyclohexamide (MP Biomedicals) were utilized.

3.3.5 Cytology

Tissue imprints of lung, liver, and spleen were prepared on glass slides, air-dried for 10 min, fixed with 100% anhydrous methanol, and stained with modified Wright-Giemsa using an automated Aerospray Hematology Slide

Stainer (Wescor Biomedical Systems). Cytologic evaluation was performed by a board-certified veterinary clinical pathologist using an Olympus BX51 light microscope (Olympus Corporation). Images were captured using an Olympus DP71 camera and software (Olympus Corporation).

3.3.6 Histology

Tissues selected for histology included sagittal sections of the right nasopharynx, sections of all lobes of the lungs, trachea, submandibular and tracheobronchial lymph nodes, liver, spleen, kidneys, adrenal glands, and representative sections of the gastrointestinal tract (stomach, duodenum, jejunum, ileum, cecum, and colon). The tissues were submersed in 10% buffered formalin (Fisher Chemical) for 3 weeks, cut, placed into histology cassettes for biopsy samples (Leica BIOSYSTEMS), and fixed in 10% buffered formalin for an additional 2 days. For nasopharyngeal tissues, the animals' heads were bisected and placed into decalcification solution (Leica BIOSYSTEMS) for 5 hr prior to cutting, placing into cassettes, and submersing into 10% buffered formalin. After verifying that fixed tissues no longer contained live *B. mallei*, the samples were taken out of the BSL3 laboratory, embedded in paraffin, cut into 3 µm-thick sections, and stained with hematoxylin and eosin (H&E). Histologic evaluations were performed by a board-certified veterinary anatomic pathologist using an Olympus BX41 microscope (Olympus Corporation). Images were captured using an Olympus DP71 camera and software (Olympus Corporation).

Selected tissues were stained using a modified Gram stain method developed by the Histology Laboratory at The University of Georgia College of Veterinary Medicine, which identifies bacteria as Gram positive (purple-black) or Gram-negative (dark pink-red). Selected tissues were also concurrently processed for examination by immunofluorescence microscopy. Briefly, tissue sections were incubated in a 10 mM sodium citrate buffer (pH 6.2) for 10 min at a temperature of 120°C to unmask antigens. Following this high-temperature antigen retrieval step, the tissues were washed, permeabilized with a solution containing 0.05% Triton X-100 for 20 min at room temperature, and probed for 1 hr with convalescent serum from mice that survived acute *B. mallei* infection. The serum, which was obtained in the context of a previous study (169), was used at a dilution of 1:100. Next, the tissues were washed to remove excess primary antibodies and incubated at room temperature for 1 hr with a goat anti-mouse IgG (H+L) antibody labeled with AlexaFluor 488 (Life Technologies) at a dilution of 1:100. After washing off unbound secondary antibody, the tissues sections were treated with Prolong Gold Antifade Mountant reagent containing DAPI (Life Technologies) and examined by microscopy with a Nikon Eclipse Ti confocal microscope. Images were captured and analyzed with the Nikon NIS-Elements software. Phosphate-buffered saline (pH 7.4) supplemented with 0.05% Tween 20 and 1% normal goat serum (SIGMA-ALDRICH) was used to wash tissues and dilute antibodies.

3.3.7 Compliance and animal research ethic statement

Preparation of the inoculum for infection and processing of tissues containing live *B. mallei* bacilli were performed inside a Class II Biosafety Cabinet (BSC) in a BSL3 laboratory. Animals infected with *B. mallei* were housed in wire front and top cages within an ABSL3-Ag room, which served as primary containment (air HEPA-filtered in and out, 15 complete air changes per hour), at The University of Georgia Animal Health Research Center. The animal facility is part of the University of Georgia's program that is accredited by the Association for Assessment and Accreditation of Laboratory Animal Care, International (AAALAC-I). Post mortem examination and tissue collection were performed in a BSL3 necropsy suite equipped with a Class II BSC. All experiments were performed in compliance with the rules and regulations of the U.S. Federal Select Agent Program and were approved by The University of Georgia Institutional Biosafety Committee (IBC) and Institutional Animal Care and Use Committee (IACUC). Animal experiments were carried out in strict accordance with the recommendations in the Guide for the Care and Use of Laboratory Animals of the National Institutes of Health. All efforts were made to minimize animal suffering. Anesthesia and euthanasia procedures were performed by trained personnel including board-certified veterinarians, animal care staff, and research team members. The IACUC approval number covering this specific study is AUP A2013 01-018-Y2-A2.

3.4 Results

3.4.1 Median lethal dose determination and clinical findings

Burkholderia mallei infection generally occurs via the respiratory or percutaneous route. The respiratory route of infection and subsequent pulmonary disease are of particular concern with respect to the use of *B. mallei* as a biothreat agent because the airways are the most likely route of entry for the bacterium during a biologic attack. For these reasons, we developed a marmoset model of intranasal infection to study the organism. Five groups of animals were inoculated with increasing doses of strain ATCC 23344 and monitored for clinical signs of illness for a period of up to 13 days. Two uninfected marmosets were included as controls and were housed in the same room with the infected animals. The results are summarized in Table 3.1. Based on these data, the calculated median lethal dose for the organism is 9,953 CFU. This value is higher than that reported for other models of respiratory infection. Using a similar intranasal route of inoculation, the LD_{50} in mice has been reported to be 820 CFU (175). Nebulization of the organism into the murine lungs with a MicroSprayer device produced roughly the same value (169). The use of a mouse whole body aerosol model yielded LD_{50} doses of 1,000-1,800 CFU (167, 176, 177).

Given that the common marmoset had not been previously used to study respiratory infection by *B. mallei*, considerable effort was put into documenting the clinical presentation of disease. As expected, the severity and onset of clinical signs correlated with the bacterial dose administered. Marmosets in the low dose

groups (25 and 250 CFU) displayed mild and non-specific signs of illness. At day 7 post-infection, the animals stopped grooming, and by day 10, most exhibited withdrawn behavior (hiding, moderately reduced vocalization, limp tails), had decreased appetite and reduced activity, and developed dry and crusted nostrils. One marmoset from each group also displayed mild unilateral conjunctivitis at the end point of the study (172 and 194, Table 3.1). Animals in the medium dose group (2,500 CFU) developed a similar disease presentation. By day 10, nearly all exhibited crusted nostrils and were often observed wiping their faces against their perches or with their hands, indicating the presence of nasal discharge. One marmoset, 225, was confirmed to have a clear nasal discharge when euthanized at the end point of the study. Another marmoset was observed sneezing on multiple occasions and quickly developed unilateral conjunctivitis (D37, Table 3.1). On day 8 post-infection, this animal presented with an increased respiratory rate and was euthanized, having reached humane experimental end points.

Two marmosets in the medium-high dose group (25,000 CFU) displayed moderate symptoms of disease. By day 4, both reached humane experimental end points, as they exhibited rough coats, unilateral conjunctivitis, clear nasal discharges, inappetence, lethargy, and increased respiratory rates (109 and 755, Table 1). The third animal in this group (135, Table 3.1) only showed mild and non-specific signs of illness (reduced grooming, moderately decreased vocalization, limp tail).

Marmosets in the high dose group (250,000 CFU) rapidly developed severe signs indicative of glanders. Two days post-infection, all three animals

stopped grooming, were inappetent, and their water intake was reduced. One marmoset unexpectedly died ~60 hr post-challenge (544, Table 3.1). This animal had an increased respiratory rate and showed evidence of ocular/nasal discharge (wet face), but was mobile and responsive to stimulation 52 hr post-infection, and thus had not met the humane endpoint criteria. Another marmoset had clear ocular and nasal discharges as well as unilateral conjunctivitis 72 hr post-challenge (55B, Table 3.1). Eight hours later, this animal was euthanized, as it became moribund and exhibited hemorrhagic nasal discharge, increased respiratory effort with abdominal lifts, and a head tilt. The third marmoset in this group was euthanized on day 4 after developing overnight a mucopurulent discharge from the right nostril, unilateral conjunctivitis, lethargy, inappetence, and increased respiratory rate (F48, Table 3.1).

The two uninfected control animals exhibited mild and non-specific signs of illness attributable, presumably, to the BSL3 environment. These included brief periods of decreased appetite and mildly withdrawn behavior (limp tail, reduced vocalization), occasional soft stools, and rough unkempt coat at the end point of the study.

3.4.2 Bacteriology findings

To examine replication and dissemination of *B. mallei*, we collected tissues from infected animals at the indicated end points and determined bacterial loads in the lungs, spleen, liver, and trachea. The results are shown in the last 4 columns of Table 3.1. All trachea samples and tissues collected from the two

uninfected control marmosets (data not shown) were culture negative. The organism was not recovered from the tissues of animals in the low dose groups (25 and 250 CFU), which is consistent with their non-specific clinical presentation. Likewise, tissues from marmosets 225, 968, and D65 in the medium dose group (2,500 CFU) were culture negative. The fourth marmoset in this group, D37, was colonized with *B. mallei* in the spleen and liver, which correlates with the overt signs of illness displayed by the animal on day 8 post-infection.

The two marmosets in the medium-high dose group (25,000 CFU) exhibiting moderate symptoms of infection were colonized with *B. mallei* (109 and 755, Table 3.1). The spleen and liver of both animals were culture positive, but only one marmoset was colonized in the lungs. *Burkholderia mallei* bacilli were not recovered from tissues of the third animal in this group, 135, which is consistent with the mild and non-specific signs of illness displayed by the marmoset throughout the study. Tissues from only one animal in the high dose group (250,000 CFU) were processed for culture, and the results show colonization of the spleen, liver, and lungs (F48, Table 3.1).

3.4.3 Cytology findings

To investigate pathologic changes induced by *B. mallei* during infection, tissue imprints (liver, spleen, lungs) were prepared at the indicated end points and examined by microscopy. The cytology findings are summarized in Table 3.2 and images of representative impression smears are shown in Figure 3.1. Consistent with clinical and bacteriology findings, the tissues of animals in the low dose

groups (25 and 250 CFU) did not show cytologic evidence of infection and looked identical to the samples from uninfected controls. The liver impression smears were high in cellularity and contained clumps of well-differentiated hepatocytes (Figure 3.1 A). The splenic imprints also were high in cellularity and consisted of many lymphoid cells, minimal extramedullary hematopoiesis (*i.e.* presence of erythroid, myeloid, and megakaryocytic precursor cells), and occasional segmented neutrophils with normal morphology (Figure 3.1 D). The lung specimens were highly cellular and contained well-differentiated ciliated columnar epithelial cells (Figure 3.1 G).

The samples obtained from marmosets 225 and 968 in the medium dose group (2,500 CFU) appeared normal, correlating with their unremarkable clinical presentation and culture-negative status (Table 3.1). Interestingly, the liver and splenic impression smears from marmoset D65, which was also culture negative and exhibited non-specific signs of illness, showed lymphoid hyperplasia (Figure 3.1 B and 3.1 E). The smears contained increased numbers of medium-sized lymphocytes, plasma cells, and even rare Mott cells, suggesting antigen stimulation. Samples from the fourth marmoset in the medium dose group, D37, were clearly indicative of infection (Table 3.2). The liver imprint showed extracellular bacilli and suppurative inflammation characterized by many degenerate neutrophils intimately associated with hepatocytes. Degenerate neutrophils are essentially dying segmented neutrophils that possess swollen and pale nuclei. These cells typically form in toxic microenvironments due to the presence of bacterial endotoxin (*i.e.* LPS), which perforates the nuclear and

cellular membranes of the neutrophil and ultimately inhibits the cell's ability to control water homeostasis. The splenic sample from marmoset D37 also contained numerous degenerate neutrophils. These findings are consistent with the moderate symptoms of glanders displayed by the animal on day 8 post-challenge and colonization of its spleen and liver with *B. mallei* (Table 3.1). The lung impression smears collected from all 4 marmosets in the medium dose group were within normal limits.

The spleen samples from marmosets 109 and 755 in the medium-high dose group (25,000 CFU) exhibited suppurative inflammation. Neutrophil morphology in these samples ranged from normal to vacuolated and degranulated. Neutrophil vacuolation and degranulation typically occur during inflammation and signify the release of bactericidal molecules (degradative enzymes, antimicrobial peptides, and reactive oxygen species). The samples also showed moderate lymphoid hyperplasia as well as moderate extramedullary hematopoiesis (Table 3.2). These findings are consistent with the moderate symptoms of disease displayed by the animals on day 4 post-challenge and colonization of their spleens with *B. mallei* (Table 3.1). The liver impression smears from marmosets 109 and 755 did not show cytologic evidence of infection, which was unexpected given that *B. mallei* was cultured from these tissues. The third animal in the medium-high dose group, 135, did not show signs of illness and was culture-negative (Table 3.1). Conversely, spleen and liver imprints from this marmoset demonstrated marked lymphoid hyperplasia and moderate extramedullary hematopoiesis, which indicate antigen stimulation and

increased hematopoietic demand, respectively (Table 3.2). The lung impression smears from all 3 animals in the medium-high dose group appeared normal.

Tissue impressions from only one marmoset in the high dose group (250,000 CFU) were examined and were clearly indicative of bacterial infection (F48, Table 3.2). Representative images of the liver and spleen imprints are shown in Figures 3.1 C and 3.1 F, respectively, and demonstrate severe suppurative inflammation characterized by a large number of degenerate neutrophils intimately associated with parenchymal cells. Many extracellular, medium-sized bacilli were observed in the background of the liver sample (see inset in Figure 3.1 C). Both tissues also showed marked extramedullary hematopoiesis and severe lymphoid hyperplasia. These findings are consistent with the severe clinical signs of glanders displayed by this animal on day 4 post-challenge, and colonization of its spleen and liver with *B. mallei* (Table 3.1). Consistent with the other experimental groups, the lung impression from marmoset F48 was cytologically unremarkable.

3.4.4 Gross and histology findings

To further investigate pathologic changes induced by *B. mallei*, tissues were collected at the indicated end points, fixed with formalin, processed into thin sections, stained, and examined by microscopy. The histology findings are summarized in Table 3.3, and representative images are shown in Figures 3.2-3.6. Most pathology was observed in the lungs, liver, spleen, lymph nodes, and nasopharynx, hence only these tissues are depicted. Consistent with the clinical,

bacteriology, and cytology findings, the tissues from animals in the low dose groups (25 and 250 CFU) did not demonstrate gross or histologic evidence of infection, similar to samples from the uninfected controls. The nasopharyngeal mucosal surface was composed of histologically normal, ciliated, pseudostratified columnar epithelial cells and goblet cells, supported by underlying secretory glands and connective tissue (Figure 3.2 A). The lungs contained numerous clear alveolar spaces and were composed of histologically unremarkable bronchi, bronchioles, alveoli, and their associated blood vessels (Figure 3.3 A). The lymph nodes were surrounded by a thin capsule and organized into a prominent outer cortex of lymphoid follicles containing large numbers of lymphoid cells and an inner medullary layer composed of lymphocytes, rare plasma cells, and few macrophages (Figure 3.4 A). Liver tissues consisted of closely packed rows of hepatocytes, portal tracts, and blood vessels all radiating outward from a central vein. No prominent liver sinusoid capillaries were noted (Figure 3.5 A). The spleens were surrounded by a thin capsule and composed of an aggregated meshwork of white pulp containing large numbers of lymphoid cells, admixed with red pulp consisting of a dense meshwork of erythroid precursors, erythrocytes, and blood vessels (Figure 3.6 A).

The samples obtained from marmosets D37, 225, and D65 in the medium dose group (2,500 CFU) contained lesions indicative of infection. Marmoset D37 had severe, bilateral, mucopurulent and pyogranulomatous rhinitis, locally-extensive, fibrinopurulent perihepatitis and hepatitis, and marked splenomegaly with microabscesses and pyogranulomas. All lesions contained numerous

degenerate neutrophils, and the nasopharyngeal and liver specimens showed intralesional bacilli. These findings are consistent with the obvious symptoms of illness displayed by the animal on day 8 post-challenge (Table 3.1), colonization of its spleen and liver with *B. mallei* (Table 3.1), and the pathologic changes observed in splenic and hepatic impression smears (Table 3.2). Interestingly, the spleens of marmosets D65 and 225, which were culture-negative and exhibited non-specific signs of illness (Table 3.1), contained microabscesses with scattered degenerate neutrophils. The nasopharyngeal and liver samples from these 2 animals appeared normal. The fourth marmoset in this group, 968, did not show gross or histological evidence of infection, correlating with the animal's unremarkable clinical presentation (Table 3.1), culture-negative status (Table 3.1), and the normal appearance of liver, lungs, and spleen tissue imprints (Table 3.2). The lung and lymph node samples from all 4 marmosets in the medium dose group were within normal limits.

Examination of tissues from marmosets 109 and 755 in the medium-high dose group (25,000 CFU) revealed lesions in the nasopharynx, lungs, spleen, and liver with intralesional bacilli (Table 3.3). These findings correlate with the obvious symptoms of infection displayed by these animals on day 4 post-challenge (Table 1), colonization of their tissues with *B. mallei* (Table 3.1), and the pathologic changes observed in impression smears (Table 3.2). Both animals showed small foci of embolic pneumonia and pyogranulomatous rhinitis with marked necrosis (Table 3.3). The nasopharyngeal lesion in marmoset 109 was particularly extensive with inflammatory cells and bacilli infiltrating the

surrounding subcutis, skeletal muscle, bone marrow, lymphatics, and blood vessels (Figure 3.2 D); immunofluorescence staining of the tissue confirmed the intralesional bacilli as *B. mallei* (Figure 3.2 F). Multinucleated giant cells, which are hallmarks of infection with the organism observed both *in vitro* and *in vivo* (3, 178-180), were also present (inset in Figure 3.2 D). The livers and spleens of both marmosets (109 and 755) contained multiple microabscesses with necrotic parenchymal cells and degenerate neutrophils, but lymph nodes were within normal limits (Table 3.3). Consistent with the clinical and bacteriology findings (Table 3.1), the tissues from the third marmoset in the medium-high dose group, 135, did not demonstrate pathology.

Tissues from all three marmosets in the high dose group (250,000 CFU) were examined and showed extensive pathology in their nasal cavity, lungs, liver and spleen with intralesional bacilli and multinucleated giant cells (Table 3.3). The most prominent lesions in the nasopharynx were necrosis of the mucosa accompanied by pyogranulomatous inflammation and mucopurulent exudate within the nasal cavity. In marmoset 55B, small amounts of mucopurulent exudate with moderate numbers of degenerate neutrophils were also present in the larynx. Pulmonary lesions varied from small, scattered parenchymal necropyogranulomas in marmosets 55B and F48, to severe and massive necropurulent bronchopneumonia in marmoset 544. Panels E-H of Figure 3.3 depict a representative necropurulent granulomatous lesion and identify intralesional bacilli as *B. mallei*. Examination of liver samples from marmoset 544 revealed numerous, variably-sized, scattered foci of necrosis composed of

leukocyte nuclear debris, necrotic hepatocytes, and intralesional *B. mallei* bacilli (Figure 3.5 E-H). The liver tissues from marmosets F48 and 544 showed scattered microabscesses with minimally damaged parenchyma, and necrosis of the myeloid lineage in hepatic foci of extramedullary hematopoiesis, respectively (Table 3.3). Grossly, the spleens of all three marmosets in the high dose group were markedly enlarged and contained scattered, 1-2 mm, white lesions (data not shown). Histologically, splenic lesions varied from scattered microabscesses (F48, Table 3.3), large multifocal pyogranulomas with multinucleated giant cells (55B, Table 3.3), to multifocal and coalescing necropurulent splenitis (544, Table 3.3 and Figure 3.6 E-H). Only one marmoset in this group, 544, showed pathology in the lymph nodes. Figure 3.3 depicts sections of tracheobronchial lymph nodes from this animal containing necrotic and purulent lesions that almost entirely efface normal lymph node architecture. Taken together, these histological findings are consistent with the severe clinical signs of glanders displayed by marmosets F48, 55B and 544 on days 3 and 4 post-challenge (Table 3.1). The pathology in tissues of marmoset F48 also correlates with cytology findings (Table 3.2) and colonization of the lungs, spleen, and liver with *B. mallei* (Table 3.1).

3.5 Discussion

In this study, we demonstrate that the common marmoset is susceptible to intranasal infection with *B. mallei*. We show that this non-human primate develops an illness similar to that described in other established models for the organism, and the disease onset and progression resemble that reported for humans with glanders. We also

document the median lethal dose that causes acute disease by the intranasal route of inoculation and detail pathologic changes induced by *B. mallei* during infection.

We discovered that 91% of animals infected with doses ranging from 25 to 2.5 X 10^3 bacteria exhibited mild and non-specific signs of illness and were culture-negative for *B. mallei*. Only one marmoset inoculated with 2.5 X 10^3 organisms (D37, Table 1) developed moderate signs of disease, reached humane end-points 8 days post-infection, and was culture-positive. Challenge experiments also revealed that 83% of animals inoculated with higher doses of 2.5 X 10^4 and 2.5 X 10^5 bacteria developed acute lethal infection within 3-4 days. Only one marmoset inoculated with 2.5 X 10^4 organisms (135, Table 3.1) was culture negative and presented with mild and non-specific symptoms. Based on these results, we calculated a median lethal dose for *B. mallei* strain ATCC 23344 of 9,953 CFU. This value is higher than that reported for other models of *B. mallei* respiratory infection, but this finding is not that surprising. It is known that the choice of bacterial strain, inoculation route, and animal background can significantly affect the course of disease. For example, infection of BALB/c mice with *B. mallei* ATCC 23344 via the intranasal or intratracheal route produced LD_{50} values of ~ 800 organisms (169, 175), while the median lethal dose of the strain upon intraperitoneal inoculation is 7 X 10^5 CFU (165). In contrast, the LD_{50} for the agent via the intraperitoneal route is less than 10 bacteria in hamsters (166, 181). Our study is the first to provide a median lethal dose for *B. mallei* in marmosets; hence, no direct comparison can be made with data from other groups. A marmoset model of acute aerosol infection has been established for the closely-related bacterium *Burkholderia pseudomallei*, the causative agent of melioidosis (182). However, the authors of that study were not able to

establish an LD_{50} value as animals inoculated with as few as 2 CFU reached humane end-points 78-hr upon challenge. In those experiments, marmosets were inoculated using an aerosol chamber.

We observed that marmosets infected with higher doses of *B. mallei* develop an acute onset of clinical signs (within 24-hr) and rapidly progressive lethal disease (3-8 days), the severity of which correlates with inoculum size. Symptoms in animals infected with medium, medium-high, and high doses consisted of subdued behavior (decreased vocalizations and limp tails), lethargy, inappetence, decreased water intake, decreased grooming behavior with piloerection (rough coats), ocular and nasal discharges, conjunctivitis, tachypnea (increased respiratory rate), and dyspnea (difficulty breathing with abdominal lifts). Natural cases of glanders in humans and other animals exhibit many of these signs, namely malaise, excessive lacrimation (tearing), nasal discharge, conjunctivitis, tachypnea, and dyspnea (141, 145, 146, 151-155, 157, 183, 184). These hallmarks also have been reported in murine and equine experimental models of glanders (164, 165, 169).

Consistent with their clinical presentation, the marmosets infected with higher doses of *B. mallei* were colonized with the organism (Table 3.1). Though discrepancies between bacteriology and histology findings were noted, these were likely caused by collecting separate portions of the same tissues for analysis. For example, the lungs of marmoset 109 were culture negative (Table 3.1), but contained lesions with bacilli on histology (Table 3.3). These lesions were not grossly visible and appeared focal in distribution by histology. Hence, portions of tissues lacking lesions were presumably and inadvertently sampled to determine bacterial burden. Another possible explanation for

discrepancies between bacteriology and histology findings is that the number of organisms in tissues was below the limit of detection of our culture method. The negative culture obtained for the lungs of another marmoset that developed overt signs of illness, D37, is not surprising, since no pathologic lesions were found by cytology (Table 3.2) or histopathology (Table 3.3). This finding is counterintuitive given that lung colonization was expected after intranasal inoculation. However, glanders is notorious for its varied clinical presentations. In natural cases of infection, it is not uncommon to see localized disease, disseminated disease, or even local disease that rapidly progresses to dissemination (141, 145, 146, 151-155, 157, 183, 184). Marmoset D37 had obvious nasopharyngeal lesions (Table 3.3); thus, we suspect that bacteria disseminated directly from these lesions to the liver and spleen via the circulatory system. This trafficking mechanism is especially likely since *B. mallei* is known for having a predilection for reticuloendothelial organs (165-167, 169, 176), as these organs are highly vascularized and utilize large numbers of resident macrophages to survey and filter the blood during circulation.

To our knowledge, this is the first study in which impression smears from affected organs were examined cytologically for evidence of infection with *B. mallei*. Our laboratory developed a mouse model of intratracheal inoculation for the organism, and we reported bacteriologic and cytopathologic analyses of tissues (169). However, the samples analyzed in that particular study were from bronchoalveolar lavages (BAL). The primary pathologic change noted in the murine BAL samples was the presence of suppurative (neutrophilic) inflammation characterized by a predominance of degenerate neutrophils with both intracellular and extracellular bacilli. These changes were

identified in impression smears of the spleen and liver of marmosets infected with medium and high doses of *B. mallei* (D37 and F48, respectively). Additional findings in these samples consisted of highly vacuolated and degranulated neutrophils, band neutrophils, lymphoid hyperplasia, and increased extramedullary hematopoiesis (Table 3.2). Lymphoid hyperplasia is indicative of antigenic stimulation, which can be attributed to bacterial infection and subsequent inflammatory responses occurring in tissues. Increased and/or excessive extramedullary hematopoiesis is often seen in animals with disseminated infections, particularly those with agents eliciting excessive inflammatory responses. It should be noted that 2 marmosets, 109 and 755, showed histologic lesions (Table 3.3) and/or were colonized with *B. mallei* (Table 3.1) in the liver and spleen, but lacked pathologic changes on cytology (Table 3.2). Additionally, all lung samples obtained and evaluated by cytology appeared normal despite the presence of histologic lesions and culture positive results in some marmosets. These discrepancies are likely attributed to sampling error, as some of these lesions were not grossly visible and appeared mild and focal in their distribution by histology. Histopathology of tissues from marmosets infected with *B. mallei* consisted of necrotizing purulent to pyogranulomatous rhinitis, pneumonia, splenitis, hepatitis, and lymphadenitis. These findings are consistent with those described in other established experimental models for glanders, including mice, hamsters, and horses. Moreover, these pathologic changes are also the classic lesions documented for cases of *B. mallei* infection in humans, horses, and camels (141-146, 150, 152-157, 164, 178). We observed Gram-negative bacilli intimately associated with nearly all necrotizing lesions in marmoset tissues, and these bacilli were specifically identified as *B. mallei* by immunofluorescence staining.

While preparing this manuscript, Nelson and colleagues published a report in which the common marmoset was used to develop a subcutaneous model of infection for *B. mallei* (185). Marmosets were inoculated in the inner thigh with 10^2 CFU of strain ATCC 23344 and reached humane endpoints 7-10 days post-challenge. In contrast, the marmosets in our study did not demonstrate clinical evidence of glanders and lethality until challenged with 10^3 organisms. We determined a median lethal dose of 9,953 CFU, with animals reaching humane endpoints within 3-8 days. This difference in bacterial dosage and survival most likely reflects the different routes of inoculation used. Subcutaneous injection circumvents physical barriers employed by the immune system to combat infection and allows immediate access to host cells as well as blood and lymphatic vessels. Conversely, the intranasal route of inoculation exposes *B. mallei* to the respiratory mucosal barrier and mucociliary escalator, which the organism has to overcome in order to establish itself and cause disease. Similar to our findings, marmosets inoculated subcutaneously exhibited clinical signs (lethargy, rough coat, conjunctivitis) and histopathology (necrotizing pneumonia, small pyogranulomas in the liver and spleen) documented in other experimental models of glanders as well as in natural cases in equids and humans. Hence our findings complement those of Nelson and colleagues and underscore the usefulness and relevance of the marmoset model to study glanders and develop countermeasures.

3.6 Acknowledgements

We thank Alfredo Torres (University of Texas Medical Branch) and Elizabeth Howerth (University of Georgia) for providing reagents and advice on experimental

design. We thank William Jeffrey Martin, Wayne Jacobs, Vicki Ellis, and Renee Rhome (University of Georgia) for their technical assistance during the study.

Table 3.1. Marmoset groups, identifiers, inoculating doses, clinical presentations, and bacterial loads in selected tissues.

Identifier	Inoculating dose (CFU)	End point[¥]	Clinical presentation	Survival	Lungs[¶]	Spleen[¶]	Liver[¶]	Trachea[¶]
171	25	13	Mild, non-specific		-	-	-	-
172	25	13	Mild, non-specific	4/4	-	-	-	-
174	25	13	Mild, non-specific		-	-	-	-
186	25	13	Mild, non-specific		-	-	-	-
189	250	12	Mild, non-specific		-	-	-	-
191	250	12	Mild, non-specific	4/4	-	-	-	-
194	250	12	Mild, non-specific		-	-	-	-
196	250	12	Mild, non-specific		-	-	-	-
225	2,500	11	Mild, non-specific		-	-	-	-
968	2,500	11	Mild, non-specific	3/4	-	-	-	-
D65	2,500	11	Mild, non-specific		-	-	-	-
D37	2,500	8*	Moderate, specific		-	$2.7x10^3$	$1.3x10^3$	-
109	25,000	4*	Moderate, specific		-	$1.8x10^4$	$5.6x10^3$	-
755	25,000	4*	Moderate, specific	1/3	$1.6x10^4$	$1.9x10^4$	$2.3x10^3$	-
135	25,000	12	Mild, non-specific		-	-	-	-
F48	250,000	4*	Severe, specific		$3.6x10^4$	$7.2x10^4$	$6.1x10^3$	-
55B	250,000	3*	Severe, specific	0/3	ND	ND	ND	ND
544	250,000	3**	Severe, specific		ND	ND	ND	ND

- : *B. mallei* not recovered from tissues
ND: not determined
[¥]: days post-infection
*: animal reached humane end point and was euthanized
**: animal was unexpectedly found dead
[¶]: Bacterial burden (CFU/gr of tissues)

Table 3.2. Marmoset identifiers, groups, and cytology findings.

Identifier	Inoculating dose (CFU)	Lungs	Spleen	Liver
171	25	Normal	Normal	Normal
172	25	Normal	Normal	Normal
174	25	Normal	Normal	Normal
186	25	Normal	Normal	Normal
189	250	Normal	Normal	Normal
191	250	Normal	Normal	Normal
194	250	Normal	Normal	Normal
196	250	Normal	Normal	Normal
225	2,500	Normal	Normal	Normal
968	2,500	Normal	Normal	Normal
D65	2,500	Normal	Moderate LH	Mild-moderate LH
D37	2,500	Normal	Mild-moderate suppurative inflammation with degenerate neutrophils	Mild-moderate suppurative inflammation with degenerate neutrophils and extracellular bacilli
109	25,000	Normal	Moderate suppurative inflammation, moderate LH and EMH	Normal
755	25,000	Normal	Moderate suppurative inflammation, moderate LH and EMH	Normal
135	25,000	Normal	Moderate-marked LH and EMH	Mild-moderate EMH
F48	250,000	Normal	Severe suppurative inflammation, severe LH and EMH	Severe suppurative inflammation, severe LH and EMH, degenerate neutrophils with extracellular bacilli
55B	250,000	ND	ND	ND
544	250,000	ND	ND	ND

EMH = extramedullary hematopoiesis, LH = lymphoid hyperplasia, ND = not determined

Table 3.3. Marmoset identifiers, groups, gross pathology, and histopathology findings.

Identifier	Inoculating dose (CFU)	Lungs	Spleen	Liver	Nasopharynx	Lymph nodes
171	25	Normal	Normal	Normal	Normal	Normal
172	25	Normal	Normal	Normal	Normal	Normal
174	25	Normal	Normal	Normal	Normal	Normal
186	25	Normal	Normal	Normal	Normal	Normal
189	250	Normal	Normal	Normal	Normal	Normal
191	250	Normal	Normal	Normal	Normal	Normal
194	250	Normal	Normal	Normal	Normal	Normal
196	250	Normal	Normal	Normal	Normal	Normal
225	2,500	Normal	Microabscesses with scattered degenerate neutrophils	Normal	Normal	Normal
968	2,500	Normal	Normal	Normal	Normal	Normal
D65	2,500	Normal	Microabscesses with scattered degenerate neutrophils	Normal	Normal	Normal
D37	2,500	Normal	Splenomegaly with microabscesses, pyogranulomas, and degenerate neutrophils	Fibrinopurulent perihepatitis and hepatitis with degenerate neutrophils and ILB	Mucopurulent and pyogranulomatous rhinitis with degenerate neutrophils and ILB	Normal
109	25,000	Small foci of embolic pneumonia with ILB	Microabscesses with scattered degenerate neutrophils and ILB	Scattered microabscesses with necrotic hepatocytes and ILB	Pyogranulomatous rhinitis with marked necrosis, ILB, and MGC	Normal
755	25,000	Small foci of embolic pneumonia with ILB	Microabscesses with scattered degenerate neutrophils and ILB	Scattered microabscesses with necrotic hepatocytes and ILB	Pyogranulomatous rhinitis with marked necrosis and ILB	Normal
135	25,000	Normal	Normal	Normal	Normal	Normal
F48	250,000	Necropurulent pneumonia with ILB and MGC	Splenomegaly, microabscesses with scattered degenerate neutrophils	Scattered microabscesses and necrotic hepatocytes	Necropurulent and pyogranulomatous rhinitis	Normal
55B	250,000	Scattered necrotizing pyogranulomas with ILB and MGC	Splenomegaly, pyogranulomatous splenitis with ILB and MGC	Multifocal necrotizing hepatitis with ILB	Necropurulent rhinitis and osteomyelitis with ILB and fibrin thrombi	Normal
544	250,000	Severe coalescing necropurulent bronchopneumonia with ILB and MGC	Splenomegaly, multifocal and coalescing necropurulent splenitis with ILB	Multifocal necrotizing hepatitis with ILB	Necropurulent rhinitis with ILB and MGC	Necropurulent lymphadenitis with ILB

ILB = intralesional bacilli, MGC = multinucleated giant cells
Other tissues examined (kidneys, adrenal glands, stomach, duodenum, jejunum, ileum, cecum, colon) did not show gross or histologic evidence of infection

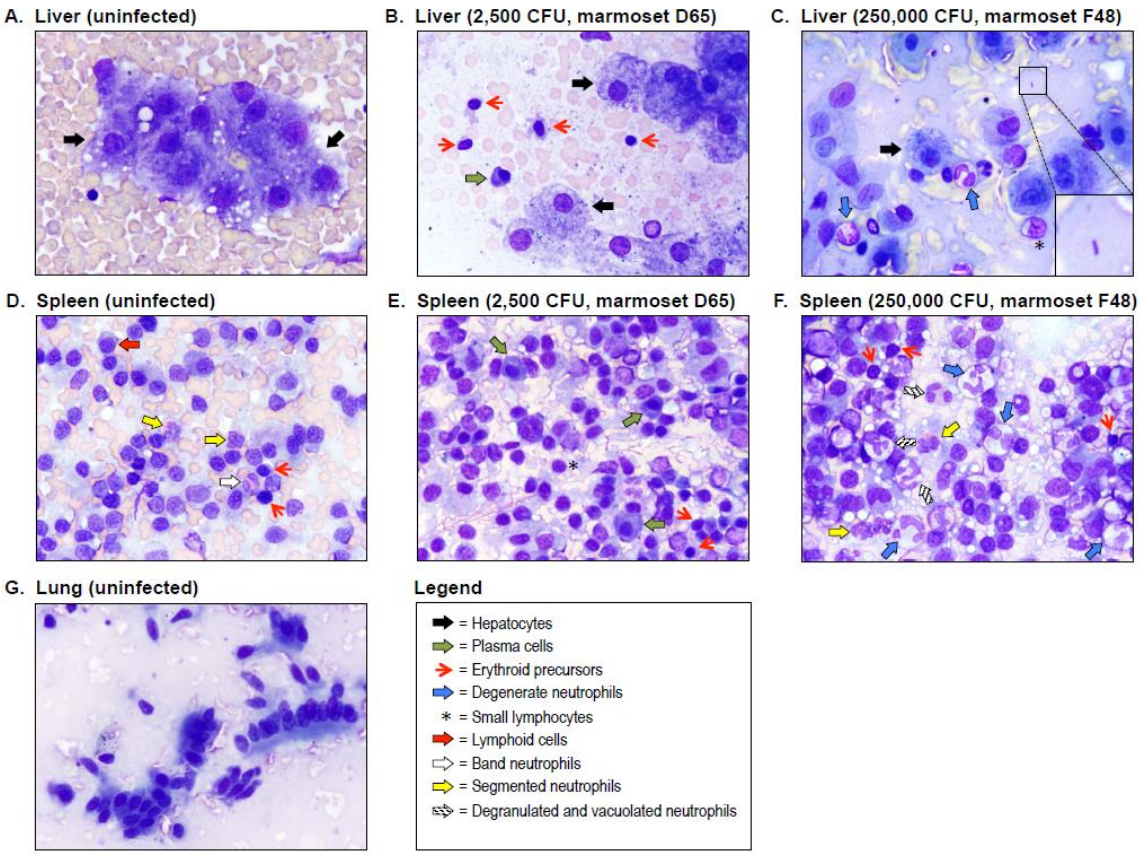

Figure 3.1. Cytologic examination of liver, lung, and spleen impression smears.

Tissue imprints from control and infected animals were made on glass slides, fixed with methanol, air-dried, stained with modified Wright-Giemsa, examined by light microscopy and photographed. Representative fields are shown. Panel A shows a liver sample from an uninfected control marmoset. The sample was high in cellularity and consisted of clumps of well-differentiated hepatocytes (black block arrows). Panel B shows a liver sample from marmoset D65, which was infected with a medium dose of *B. mallei* (2,500 CFU). The sample was high in cellularity and consisted of well-differentiated hepatocytes (black block arrows), admixed with increased numbers of small lymphocytes, plasma cells (green block arrow), and erythroid precursors (red arrows). Panel C shows a liver sample from marmoset F48, which was infected with a high dose

of *B. mallei* (250,000 CFU). It consisted primarily of large numbers of degenerate neutrophils (blue block arrows) admixed with well-differentiated hepatocytes (black block arrows), some small lymphocytes (asterisk), extracellular bacilli (inset), and disrupted cellular debris. Panel D shows a splenic sample from an uninfected control marmoset. The sample was high in cellularity and consisted primarily of lymphoid cells (red block arrow) and erythroid precursors (red arrows) admixed with occasional heavily granulated band neutrophils (white block arrow) and segmented neutrophils (yellow block arrows). Panel E shows a splenic sample from marmoset D65, which was infected with a medium dose of *B. mallei* (2,500 CFU). The sample was high in cellularity and contained plasma cells (green block arrows), small lymphocytes (asterisk), and erythroid precursors (red arrows). Panel F shows a splenic sample from marmoset F48, which was infected with a high dose of *B. mallei* (250,000 CFU). The sample was high in cellularity and consisted of many degenerate neutrophils (blue block arrows), degranulated and vacuolated neutrophils (shaded block arrows), segmented neutrophils (yellow block arrow), and an increased number of erythroid precursors (red arrows). Panel G shows a lung sample from an uninfected control marmoset. The sample was high in cellularity and consisted of both individualized and clumped, well-differentiated, ciliated, columnar epithelial cells.

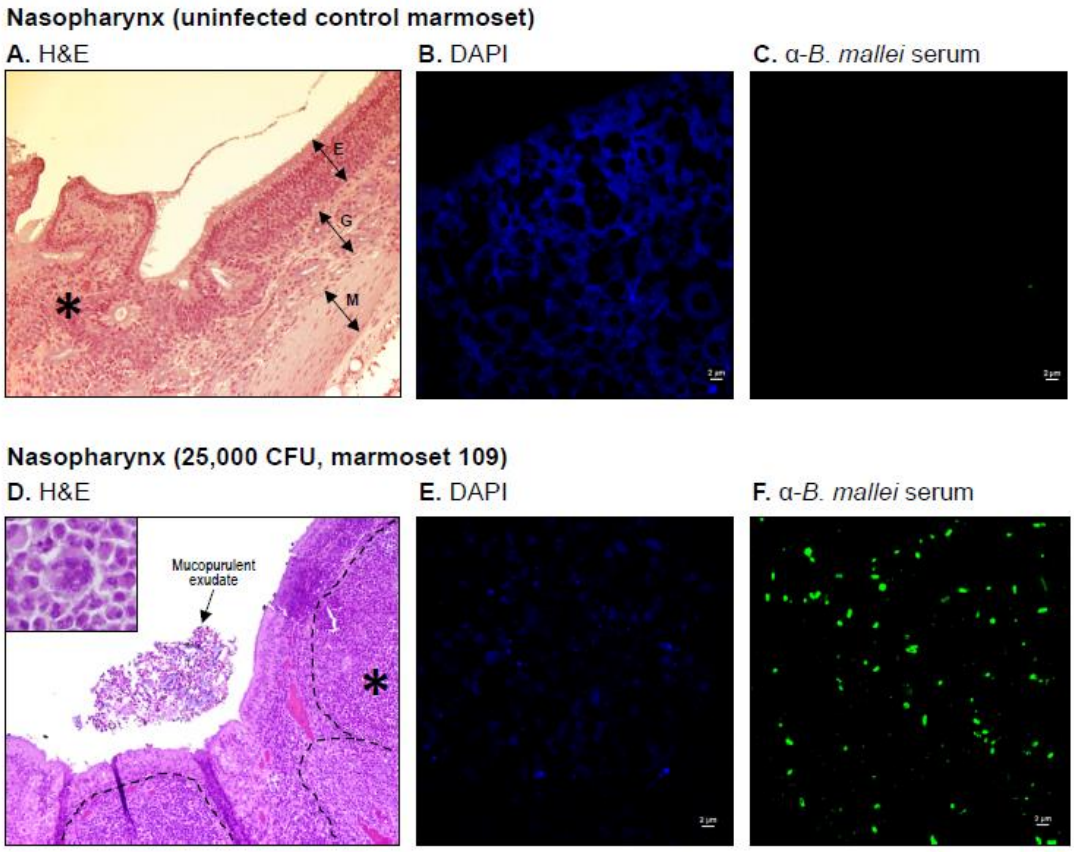

Figure 3.2. Histologic and immunofluorescence examination of nasopharyngeal tissues.

Tissue sections from control and infected animals were stained with H&E (panels A and D), DAPI (panels B and E), or convalescent serum from mice that survived acute infection with *B. mallei* and a goat anti-mouse antibody conjugated AlexaFluor 488 (panels C and F), examined by microscopy, and photographed. Representative fields are shown. Panel A shows tissue within normal limits from an uninfected control animal at a magnification of 20x. The tissue consisted of a mucosal surface composed of ciliated pseudostratified columnar epithelial cells and goblet cells (E), supported by underlying secretory glands (G) and smooth muscle (M). The asterisk indicates the area used to acquire the images shown in panels B and C. Panel B shows staining of nucleic acid from host cells (blue) at a magnification of 100x. Panel C shows the lack of reactivity of

the anti-*B. mallei* serum with tissue from the uninfected control animal at a magnification of 100x. Panel D shows tissues from marmoset 109, which was infected with a medium-high dose of *B. mallei* (25,000 CFU), at a magnification of 20x. Mucopurulent exudate was present in the nasal cavity, and the tissue exhibited extensive pyogranulomatous rhinitis with marked necrosis. The dotted lines show coalescing pyogranulomas that infiltrated and expanded the connective tissues underlying/supporting the nasal mucosa. The inset shows one of many multinucleated giant cells observed in pyogranulomas at a magnification of 100x. The asterisk indicates the area used to acquire the images shown in panels E and F. Panel E shows staining of nucleic acid from host cells and bacteria (blue) at a magnification of 100x. Panel F shows reactivity of the anti-*B. mallei* serum with intralesional bacilli (green) at a magnification of 100x.

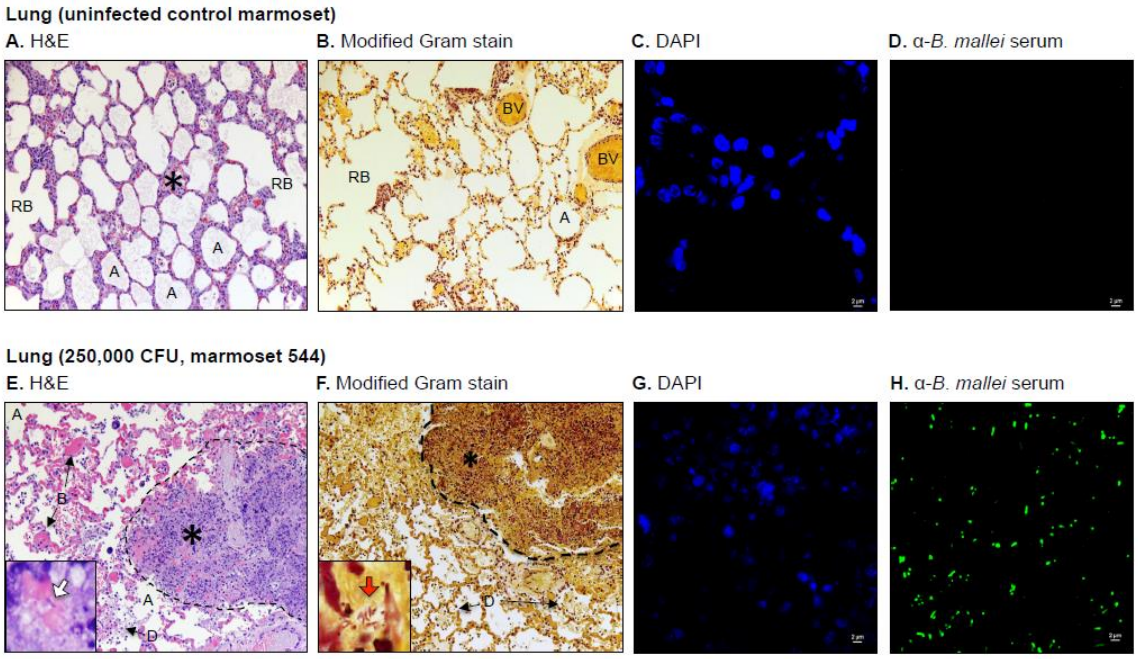

Figure 3.3. Histologic and immunofluorescence examination of lung tissues.

Tissue sections from control and infected animals were stained with H&E (panels A and E), a modified Gram stain method (panels B and F), DAPI (panels C and G), or convalescent serum from mice that survived acute infection with *B. mallei* and a goat anti-mouse antibody conjugated AlexaFluor 488 (panels D and H), examined by microscopy, and photographed. Representative fields are shown. Panel A and B show tissue within normal limits from an uninfected control animal at a magnification of 20x. The tissue contained numerous clear alveolar spaces (A), respiratory bronchioles (RB) and blood vessels (BV). The asterisk indicates the area used to acquire the images shown in panels C and D. Panel C shows staining of nucleic acid from host cells (blue) at a magnification of 100x. Panel D shows the lack of reactivity of the anti-*B. mallei* serum with tissue from the uninfected control animal at a magnification of 100x. Panel E and F shows tissues from marmoset 544, which was infected with a high dose of *B. mallei*

(250,000 CFU), at a magnification of 20x. The dotted lines delineate a severe necropurulent granuloma surrounded by clear alveolar spaces as well as alveolar spaces filled with blood (B) and/or necrotic debris (D). The inset in Panel E shows an intralesional bacillus (white block arrow) at a magnification of 100x. The inset in Panel F shows intralesional Gram-negative (dark pink-red) bacilli (red block arrow) at a magnification of 100x. The asterisk indicates the area used to acquire the images shown in panels G and H. Panel G shows staining of nucleic acid from host cells and bacteria (blue) at a magnification of 100x. Panel H shows reactivity of the anti-*B. mallei* serum with intralesional bacilli (green) at a magnification of 100x.

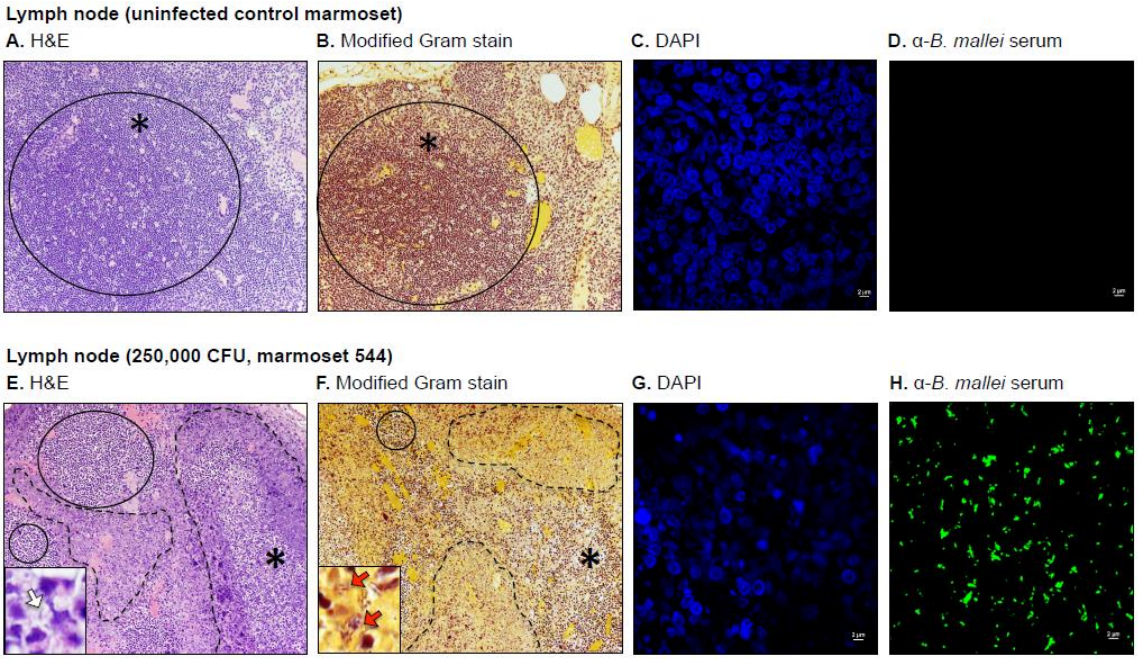

Figure 3.4. Histologic and immunofluorescence examination of lymph node tissues.

Tissue sections from control and infected animals were stained with H&E (panels A and E), a modified Gram stain method (panels B and F), DAPI (panels C and G), or convalescent serum from mice that survived acute infection with *B. mallei* and a goat anti-mouse antibody conjugated AlexaFluor 488 (panels D and H), examined by microscopy, and photographed. Representative fields are shown. Panel A and B show tissue within normal limits from an uninfected control animal at a magnification of 20x. The solid line circle indicates a normal diffuse medullary lymphoid tissue. The asterisk indicates the area used to acquire the images shown in panels C and D. Panel C shows staining of nucleic acid from host cells (blue) at a magnification of 100x. Panel D shows the lack of reactivity of the anti-*B. mallei* serum with tissue from the uninfected control animal at a magnification of 100x. Panel E and F shows tissues from marmoset 544, which was infected with a high dose of *B. mallei* (250,000 CFU), at a magnification of

20x. The tissue contained necrotic and purulent areas (dashed lines) almost entirely effacing normal lymph node architecture (solid line circles). The inset in Panel E shows an intralesional bacillus (white block arrow) at a magnification of 100x. The inset in Panel F shows intralesional Gram-negative (dark pink-red) bacilli (red block arrows) at a magnification of 100x. The asterisk indicates the area used to acquire the images shown in panels G and H. Panel G shows staining of nucleic acid from host cells and bacteria (blue) at a magnification of 100x. Panel H shows reactivity of the anti-*B. mallei* serum with intralesional bacilli (green) at a magnification of 100x.

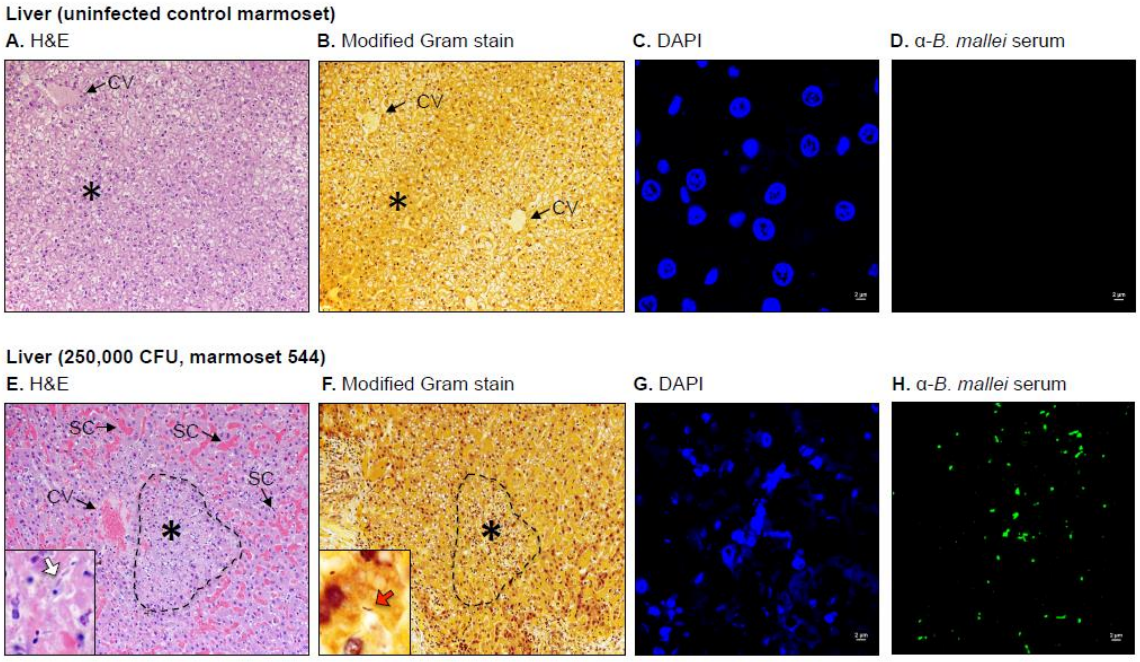

Figure 3.5. Histologic and immunofluorescence examination of liver tissues.

Tissue sections from control and infected animals were stained with H&E (panels A and E), a modified Gram stain method (panels B and F), DAPI (panels C and G), or convalescent serum from mice that survived acute infection with *B. mallei* and a goat anti-mouse antibody conjugated AlexaFluor 488 (panels D and H), examined by microscopy, and photographed. Representative fields are shown. Panel A and B show tissue within normal limits from an uninfected control animal at a magnification of 20x. The tissues consisted of closely packed rows of hepatocytes, portal tracts and blood vessels all radiating from a central vein (CV). No prominent liver sinusoid capillaries were present. The asterisk indicates the area used to acquire the images shown in panels C and D. Panel C shows staining of nucleic acid from host cells (blue) at a magnification of 100x. Panel D shows the lack of reactivity of the anti-*B. mallei* serum with tissue from the uninfected control animal at a magnification of 100x. Panel E and F

shows tissues from marmoset 544, which was infected with a high dose of *B. mallei* (250,000 CFU), at a magnification of 20x. The dashed lines indicate foci with completely disrupted liver architecture consisting of necrotic hepatocytes and leukocyte debris surrounded by an enlarged and distorted central vein (CV) as well as numerous dilated liver sinusoid capillaries (SC). The inset in Panel E shows intralesional bacilli (white block arrow) at a magnification of 100x. The inset in Panel F shows an intralesional Gram-negative (dark pink-red) bacillus (red block arrow) at a magnification of 100x. The asterisk indicates the area used to acquire the images shown in panels G and H. Panel G shows staining of nucleic acid from host cells and bacteria (blue) at a magnification of 100x. Panel H shows reactivity of the anti-*B. mallei* serum with intralesional bacilli (green) at a magnification of 100x.

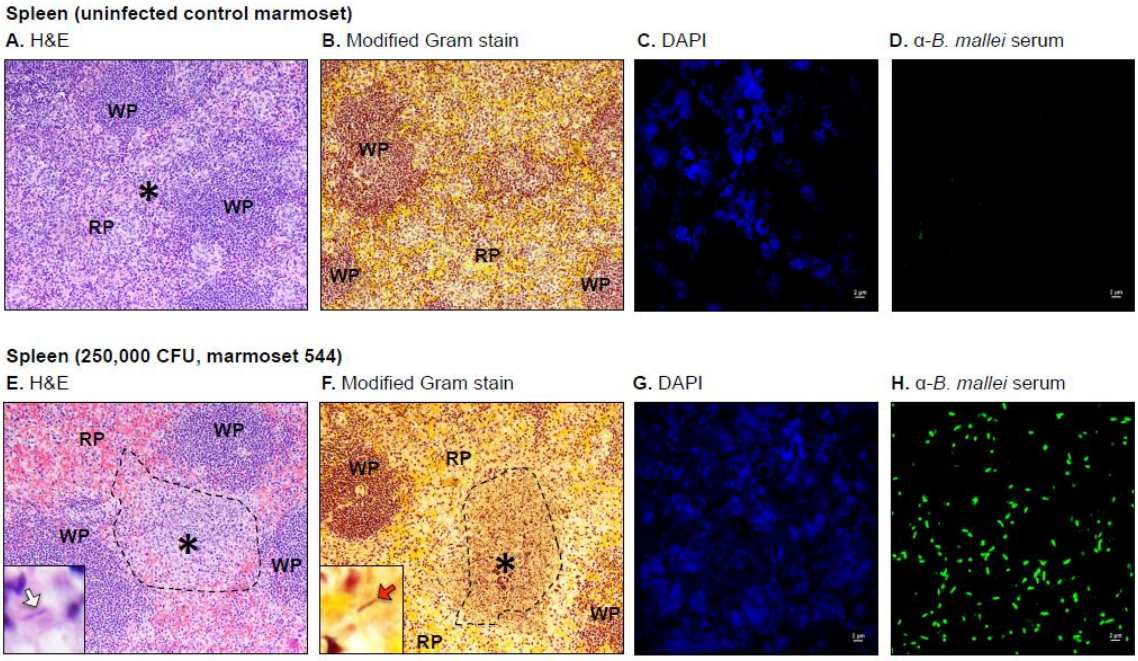

Figure 3.6. Histologic and immunofluorescence examination of spleen tissues.

Tissue sections from control and infected animals were stained with H&E (panels A and E), a modified Gram stain method (panels B and F), DAPI (panels C and G), or convalescent serum from mice that survived acute infection with *B. mallei* and a goat anti-mouse antibody conjugated AlexaFluor 488 (panels D and H), examined by microscopy, and photographed. Representative fields are shown. Panel A and B show tissue within normal limits from an uninfected control animal at a magnification of 20x. The tissues consisted of a meshwork of white pulp (WP) containing a large number of lymphoid cells admixed with red pulp (RP). The asterisk indicates the area used to acquire the images shown in panels C and D. Panel C shows staining of nucleic acid from host cells (blue) at a magnification of 100x. Panel D shows the lack of reactivity of the anti-*B. mallei* serum with tissue from the uninfected control animal at a magnification

of 100x. Panel E and F shows tissues from marmoset 544, which was infected with a high dose of *B. mallei* (250,000 CFU), at a magnification of 20x. The dashed lines indicate necropurulent areas with complete loss of normal follicular structure surrounded by normal meshworks of white and red pulp. The inset in Panel E shows an intralesional bacillus (white block arrow) at a magnification of 100x. The inset in Panel F shows an intralesional Gram-negative (dark pink-red) bacillus (red block arrow) at a magnification of 100x. The asterisk indicates the area used to acquire the images shown in panels G and H. Panel G shows staining of nucleic acid from host cells and bacteria (blue) at a magnification of 100x. Panel H shows reactivity of the anti-*B. mallei* serum with intralesional bacilli (green) at a magnification of 100x.

CHAPTER 4

THE AUTOTRANSPORTER BPAB CONTRIBUTES TO THE VIRULENCE OF *BURKHOLDERIA MALLEI* IN AN AEROSOL MODEL OF INFECTION [1]

[1] Zimmerman SM, Michel F, Hogan RJ, Lafontaine ER, 2015, *PLOS ONE*, Volume 10, Issue 5, e0126437. Reprinted here with permission of the publisher.

4.1 Abstract

Burkholderia mallei is a highly pathogenic bacterium that causes the zoonosis glanders. Previous studies indicated that the genome of the organism contains eight genes specifying autotransporter proteins, which are important virulence factors of Gram-negative bacteria. In the present study, we report the characterization of one of these autotransporters, BpaB. Database searches identified the *bpaB* gene in ten *B. mallei* isolates and the predicted proteins were 99-100% identical. Comparative sequence analyses indicate that the gene product is a trimeric autotransporter of 1,090 amino acids with a predicted molecular weight of 105-kDa. Consistent with this finding, we discovered that recombinant bacteria expressing *bpaB* produce a protein of ≥300-kDa on their surface that is reactive with a BpaB-specific monoclonal antibody. Analysis of sera from mice infected with *B. mallei* indicated that animals produce antibodies against BpaB during the course of disease, thus establishing production of the autotransporter *in vivo*. To gain insight on its role in virulence, we inactivated the *bpaB* gene of *B. mallei* strain ATCC 23344 and determined the median lethal dose of the mutant in a mouse model of aerosol infection. These experiments revealed that the *bpaB* mutation attenuates virulence 8-14 fold. Using a crystal violet-based assay, we also discovered that constitutive production of BpaB on the surface of *B. mallei* promotes biofilm formation. To our knowledge, this is the first report of a biofilm factor for this organism.

4.2 Introduction

Autotransporter proteins (AT) form one of the largest class of virulence factors in Gram-negative organisms and perform important functions in pathogenesis, including; flocculation (186, 187), formation of biofilms (188, 189), complement resistance (190,

191), host cell adhesion and entry (192-194), intracellular motility and replication (195, 196), cytotoxicity (197), and lipolytic activity (198-200). These molecules share 4 common structural characteristics: a signal sequence (leader peptide), an N-terminal passenger domain, a C-terminal transporter domain, and a helical region of ~ 40 amino acids (aa) that links the passenger and transporter domains. The passenger domain is surface-exposed and specifies the biological function of the AT, while the transporter domain consists of hydrophobic β-strands and anchors the protein to the outer membrane (OM). Depending on the structure of the transporter domain, AT are classified as conventional or oligomeric (77, 201-205). Conventional AT have a large C-terminus of ~300 aa that form 10-12 antiparallel β-strands and are produced as monomers. In contrast, oligomeric AT have a short C-terminus (~70 aa) specifying only 4 β-strands and are typically produced as trimers.

After synthesis, AT are targeted to the inner membrane (IM) via their signal sequence and are secreted into the periplasm through the Sec translocase pathway (206). Approximately 10% of AT possess a leader peptide with an Extended Signal Peptide Region (ESPR), which has been proposed to interact with the YidC IM protein integrase to slow translocation and prevent the accumulation of misfolded AT in the periplasm (206). The molecular basis by which AT are secreted and displayed on the bacterial surface once they reach the periplasmic side of the OM is still under investigation. One proposed mechanism, the hairpin model, entails that AT self-secrete by inserting the C-terminal transporter domain into the OM to form a porin-like channel that is used to secrete the N-terminal passenger domain (201, 207). Another model proposes that AT

parasitize the β-barrel assembly machinery (Bam) complex, which assembles integral membrane proteins in the OM, thus transporting the AT to the cell surface (206).

Given their function in pathogenesis and overall structure, AT are excellent targets for developing medical countermeasures (MCM) against pathogenic organisms. A significant portion of AT (passenger domain) is readily accessible for recognition by the immune system, as it is exposed on the bacterial surface. Additionally, AT perform key roles in virulence, and targeting them may interfere with disease progression. Many reports have demonstrated the efficacy of AT-based countermeasures. For instance, a vaccine containing the AT cytotoxin Pta of *Proteus mirabilis* has been shown to elicit antibodies that neutralize the cytotoxicity of Pta for bladder cells *in vitro* and reduce bacterial loads as well as pathology in a mouse model of urinary tract infection (208). Antibodies against *Haemophilus influenzae* Hap block adherence to epithelial cells *in vitro* and reduce nasopharyngeal colonization *in vivo* (209, 210). Moreover, the AT adhesins, *Bordetella pertussis* Pertactin and *Neisseria meningitidis* NadA, are components of licensed vaccines against whooping cough (Daptacel, Infanrix, Boostrix, Adacel) and meningitis (Bexsero), respectively.

Burkholderia mallei is a Gram-negative coccobacillus for which developing MCM is desirable. The organism causes the zoonosis glanders, which predominantly affects equids and is endemic to regions of Africa, South and Central America, the Middle East, and Asia (3, 4, 141, 144, 155-157, 211). Humans are generally infected with *B. mallei* through contact with tissues or body fluids of infected animals, and the clinical manifestations include myalgia, fever, fatigue, lymphadenopathy, pneumonia, and dissemination of the agent to target tissues (spleen, liver, kidney), where it forms

purulent lesions (141, 144, 145). The recommended two-phase treatment process entails the use of the β-lactams ceftazidime and meropenem (intensive phase), followed by administration of Trimethoprim-Sulfamethoxazole (TMP-SMX) and the β-lactam Amoxicillin mixed with the β-lactamase inhibitor clavulanic acid (co-amoxiclav) for several weeks (eradication phase) (158).

The genome of *B. mallei* has been reported to encode 6 oligomeric AT gene products (13). Of these, BoaA [adhesin, (212)], BimA [intracellular motility protein, (196)] and BpaC [adhesin, (213)] have been functionally characterized. The genome of the closely-related bacterium, *Burkholderia pseudomallei,* specifies these 6 AT gene products, and all were recently studied to establish their biological roles as well as contribution to virulence (214). One of these, named BpaB (locus tag number BP106B_I2046), was shown to be involved in adherence to human lung cells, which is a key step in the pathogenesis of the agent because it leads to colonization (214). In the present study, we characterized the *bpaB* ortholog of *B. mallei* and evaluated its contribution to virulence in a mouse model of aerosol infection.

4.3 Materials and Methods

4.3.1 Strains, plasmids, tissue culture cell lines, and growth conditions

Strains and plasmids are described in Table 4.1. *Burkholderia mallei* was cultured at 37°C using Brucella medium (BD) supplemented with 5% (vol/vol) glycerol. When indicated, antibiotics were added at the following concentrations: 7.5 μg/mL Polymyxin B (MP Biomedicals), 5 μg/mL kanamycin (MP Biomedicals), and 7.5 μg/mL zeocin (Life Technologies). *Burkholderia mallei*

bacteria used to inoculate mice were cultured on agar plates and suspended in PBS to the indicated concentrations, as previously reported (169). Aliquots of the bacterial suspension were immediately spread onto agar plates to determine the number of colony forming units (CFU) in the inoculum. *Escherichia coli* was cultured at 37°C using Low Salt Luria Bertani (LSLB) agar (Teknova) supplemented with 15 μg/mL chloramphenicol, 50 μg/mL kanamycin, 100 μg/mL ampicillin (Sigma-Aldrich), or 50 μg/mL zeocin, where applicable. The cell lines A549 (human type II alveolar epithelium; ATCC CCL85) and J774A.1 (murine macrophages; ATCC TIB-67) were cultured as described elsewhere (199, 212).

4.3.2 Recombinant DNA methodology

Standard molecular biology methods were performed as outlined by others (215). Genomic DNA was purified using the Easy-DNA Kit (Life Technologies). Plasmid DNA was purified using the QIAprep Spin Miniprep kit (Qiagen).

The broad host range plasmid pBHR1 was digested with *Dra*I, excised from an agarose gel, purified with the High Pure PCR Product Purification kit (Roche Applied Science), and ligated in order to delete a 339-nucleotide (nt) fragment internal to the chloramphenicol resistance marker. The resulting plasmid, designated pBHR1ΔDra, was sequenced to verify that the deletion was successfully engineered. The plasmid was also tested to confirm that it no longer confers resistance to chloramphenicol.

Platinum *Pfx* DNA Polymerase (Life Technologies) was used in all PCR experiments as per the manufacturer's recommended conditions. A DNA

fragment of 3,516-nt containing the *bpaB* gene was amplified from the genome of *B. mallei* ATCC 23344 with primers P1 (5'-GCC TCG GCA AAT AAA TTT CAA TTG-3') and P2 (5'-GTC GGA GAG CAC GTA TGC ATT GAA-3'). The amplicon was cloned in the vector pCC1 using the CopyControl PCR cloning kit (epicenter Illumina), producing plasmid pCCbpaB. The latter was digested with *BamH*I, and a 3,529-nt fragment containing the *bpaB* gene was purified from agarose gel slices, treated with the End-It DNA End Repair Kit (epicenter Illumina), and subcloned into the *Dra*I site of pBHR1ΔDra to yield plasmid pBpaB.

The plasmid pCCbpaB was digested with the enzymes *Rsr*II and *Asc*I to remove a 1,454-nt fragment internal to the *bpaB* ORF, treated with the End-It DNA End Repair Kit, and ligated with a blunt 0.4-kilobases (kb) zeocin resistance cassette to yield plasmid pCCbpaB.zeo. This plasmid was restricted with *BamH*I, and a 2.5-kb fragment corresponding to the *bpaB* ORF disrupted by the insertion of the zeocin resistance cassette was gel-purified, treated with the End-It DNA End Repair Kit, and subcloned into the *EcoR*V site of the suicide vector pKAS46, producing plasmid pKASbpaB.zeo.

A PCR product specifying aa 57 to 984 of the *bpaB* ORF was generated from *B. mallei* ATCC 23344 genomic DNA with oligonucleotides P3 (5'-CCC AAG CTT GGC ACG GAT AAC GTC TA-3'; *Hind*III site underlined) and P4 (5'-GGT TAA TTA AAG GAC CGC ATC GGT CG-3'; *Pac*I site underlined). This amplicon was purified, digested with *Hind*III and *Pac*I, and ligated in-frame with the N-terminal His-tag of vector pETcoco-1. The resulting plasmid was

designated pHisBpaB. A similar approach was used to engineer plasmid pGSTBpaB, which encodes the same portion of the *bpaB* gene product joined to an N-terminal Glutathione-*S*-Transferase (GST) tag. The DNA fragment was amplified with primers P5 (5'-CGG GAT CCG GCA CGG ATA ACG TCT A-3'; *Bam*HI site underlined) and P6 (5'-CCG CTC GAG TGA CCG CAT CGG TCG C-3'; *Xho*I site underlined) and cloned in the vector pGEX4T-2.

Plasmids were sequenced to verify that PCR did not introduce mutations resulting in aa substitutions in the *bpaB* gene product. Restriction endonucleases and T4 DNA ligase were purchased from New England BioLabs, Inc.

4.3.3 Construction of a *B. mallei* ATCC 23344 *bpaB* isogenic mutant strain

The plasmid pKASbpaB.zeo was introduced in the *E. coli* strain S17 by electroporation and subsequently transferred into *B. mallei* ATCC 23344 by conjugation, as previously reported (212, 216). Upon conjugation, *B. mallei* colonies were first selected for resistance to Polymyxin B (to prevent growth of *E. coli* S17) and zeocin (to select strains containing the disrupted copy of *bpaB* in their genome). These potential mutants were then tested for sensitivity to kanamycin to identify strains that do not contain the suicide vector pKAS46 integrated in their genome. Lastly, colonies were screened by PCR with primers P7 (5'-CGC TCG ATA CCC ACG TTT AT-3') and P8 (5'-GCG ATG CAG ATG CGT ATA GA-3'). The primers yielded a PCR product of 7.6-kb in the parent strain and a smaller amplicon of 6.6-kb in the *bpaB* KO mutant (data not shown). This 1-kb difference in size is consistent with deletion of the

aforementioned 1.4-kb *Rsr*II-*Dra*I fragment internal to the *bpaB* ORF and insertion of the 0.4-kb zeocin resistance marker in its place. The PCR product from the mutant strain was sequenced to verify proper allelic exchange and successful disruption of *bpaB*.

In order to perform complementation experiments, the plasmids pBHR1ΔDra and pBpaB were electroporated in *E. coli* S17 and subsequently transferred into the *B. mallei bpaB* KO mutant by conjugation. Conjugants were selected for resistance to zeocin (specified by the isogenic mutation in the genome of strain *bpaB* KO), kanamycin (specified by pBHR1ΔDra and pBpaB), and Polymyxin B (to prevent growth of *E. coli* S17).

4.3.4 Nucleotide sequence and bioinformatics analyses

Plasmids and purified PCR fragments were sequenced at the University of Michigan Sequencing Core (http://seqcore.brcf.med.umich.edu). Sequencher 5 (Gene Codes Corporation) was used to analyze chromatograms. Assembled contigs were analyzed with Vector NTI (Life Technologies) and online tools available at the ExPASy Bioinformatics Resource Portal (http://www.expasy.org).

4.3.5 Experiments with human lung epithelial cells and murine macrophages

Plate-grown bacteria (40-hr for *B. mallei*, 20-hr for *E. coli*) were used for all experiments. Adherence and intracellular survival assays were performed as previously reported (212, 213, 217, 218). Cells were infected with bacteria at a multiplicity of infection of 100 (adherence) and 10 (intracellular survival). Duplicate assays were performed on at least 3 occasions. Statistical analyses were

performed using the Mann-Whitney test (GraphPad Prism 6 software), and *P* values < 0.05 are reported as statistically significant.

4.3.6 Crystal violet-based biofilm assay

This procedure was modified from a protocol published by Pearson *et al* (219). Plate-grown bacteria (20-hr for both *B. mallei* and *E. coli*) were suspended in broth to a density of 10^7 CFU/mL, and 100 μL of these suspensions were seeded into quadruplicate wells of polyvinyl chloride (PVC) round bottom microplates (Corning). These plates were then incubated statically at 37°C (24-hr for *E. coli*, 48-hr for *B. mallei*). Following this, broth was removed from the wells and replaced with 200 μL of Ham's F12 medium (Cellgro) supplemented with 0.035% (wt/vol) crystal violet (Sigma-Aldrich). After 30-min at room temperature, the crystal violet staining mixture was removed, and the wells were washed with deionized water. A 200 μL volume of methanol was added to each well, and the plate was incubated for 30 min. Well contents were transferred to a new microplate, and the absorbance at a wavelength of 570 nm, which is indicative of bacteria forming biofilms on PVC and stained with crystal violet, was measured spectrophotometrically. Statistical analyses were performed using the Mann-Whitney test (GraphPad Prism 6 software), and *P* values < 0.05 are reported as statistically significant.

4.3.7 Antigen preparations and analysis

Total membrane proteins and sarkosyl-insoluble fractions containing OM proteins were obtained as described by Carlone *et al* (220). The method used to

prepare whole cell lysates and perform western blot experiments are described elsewhere (217). The plasmids pHisBpaB and pGSTBpaB were electroporated in the *E. coli* strain TUNER for the purpose of producing and purifying His- and GST-tagged BpaB proteins, respectively. Both proteins were extracted from inclusion bodies and purified under denaturing conditions as previously outlined by our laboratory (199, 221). Purified capsular polysaccharides (CPS) from the *Burkholderia pseudomallei* LPS^- mutant strain MB100 (222) were kindly provided by Donald E. Woods at the University of Calgary.

To obtain polyclonal antibodies directed against BpaB, purified His-tagged BpaB was emulsified in Freund's adjuvant (Sigma-Aldrich) and administered to female BALB/c mice (Frederick National Laboratory for Cancer Research) as reported by Lafontaine and colleagues (223). Serum antibodies were demonstrated to recognize BpaB by western blot using purified GST-tagged BpaB (data not shown). The BpaB-specific monoclonal antibody #4 (BpaB-MAb#4) was generated by fusing splenocytes from a vaccinated mouse with Sp2/mIL6 cells (ATCC CRL 2016). The fused cells were plated in methylcellulose medium containing hypoxanthine, aminopterin, and thymidine using a ClonaCell HY kit per the manufacturer's specifications (Stemcell Technologies). Hybridomas secreting antibodies specific for BpaB were identified by ELISA.

For ELISA, duplicate wells of Immulon 2HB plates (Thermo Scientific Nunc) were coated with purified antigens (CPS, GST-tagged BpaB) overnight at 4°C. Unbound antigens were removed by washing wells with 1X wash solution (KPL), and the wells were then filled with 10% BSA Diluent/Blocking solution

(KPL) diluted to 0.5% with PBS and supplemented with 3% (wt/vol) dry milk (blocking buffer). After incubation at room temperature for 1-hr, the wells were washed with 1X wash solution and probed for 1-hr at room temperature with primary antibodies (serum from mice that survived aerosol infection with *B. mallei* ATCC 23344, serum from mice immunized with His-tagged BpaB, culture supernatants from hybridomas producing monoclonal antibodies) diluted in blocking buffer. After this incubation, the wells were washed with 1X wash solution and incubated at room temperature with goat anti-mouse secondary antibodies conjugated to alkaline phosphatase diluted in blocking buffer. After washing off the excess secondary antibodies with 1X wash solution, 100 μL of *p*NPP solution (KPL) was added to wells. Color development, indicative of antibody binding to antigen, was measured by determining the absorbance of well contents at a wavelength of 405 nm.

4.3.8 Immunofluorescence labeling

Production of BpaB on the bacterial surface was visualized by immunofluorescence microscopy as outlined by Balder *et al* (212). Briefly, plate-grown bacteria (40-hr for *B. mallei*, 20-hr for *E. coli*) were fixed with 4% (wt/vol) paraformaldehyde, spotted onto glass slides, probed with α-BpaB polyclonal antibodies, and incubated with a goat α-mouse antibody labeled with Alexa Fluor 488 (Life Technologies) and the nucleic acid dye DAPI (Life Technologies). Slides were examined by microscopy using a Nikon Eclipse Ti confocal system.

A minimum of 5 random fields was assessed on at least 2 separate occasions for each strain.

Production of BpaB on the bacterial surface was measured by flow cytometry as described by Lipski and colleagues (199). Plate-grown bacteria (40-hr for *B. mallei*, 20-hr for *E. coli*) were fixed with 4% (wt/vol) paraformaldehyde, probed with α-BpaB polyclonal antibodies, and incubated with a goat α-mouse antibody labeled with Alexa Fluor 488. Labeled bacteria were analyzed using a BD LSR II flow cytometer.

4.3.9 Aerosol infection experiments

Female BALB/c mice (14-28 weeks of age at the time of infection) were purchased from Frederick National Laboratory for Cancer Research. The animals were anesthetized by injecting a dose of 250 mg/kg of 2, 2, 2 tribromoethanol (TBE, Sigma-Aldrich) intraperitoneally. Once anesthetized, mice were inoculated intratracheally with 50 μL of bacterial suspensions using a Microsprayer model I-1C (PennCentury) as previously reported by our laboratory (169, 213). Infected animals were monitored daily. Food and water were provided *ad libitum*. Humane end-points were strictly observed. Mice exhibiting signs of moderate to severe discomfort were euthanized. This was accomplished by anesthetizing the animals with TBE followed by cervical dislocation, in accordance with the AVMA Guidelines on Euthanasia. Tissues (lungs and spleen) were aseptically collected, homogenized, serially diluted, and plated on agar medium to calculate bacterial loads. Survival data were analyzed using the Kaplan-Meier method, and the LD_{50} values were calculated according to Reed and Muench (174).

4.3.10 Compliance and animal research ethics statements

All experiments with live *B. mallei* were performed inside a Class II Biosafety Cabinet in a BSL3 laboratory and in compliance with the rules and regulations of the U. S. Federal Select Agent Program. The University of Georgia's Institutional Biosafety Committee (IBC) approved the experiments.

Animal experiments were carried out in strict accordance with the recommendations in the Guide for the Care and Use of Laboratory Animals of the National Institutes of Health. The University of Georgia's Institutional Animal Care and Use Committee (IACUC) approved the experiments. All efforts were made to minimize animal suffering.

4.4 Results

4.4.1 Selected features of the *bpaB* genomic locus and gene product

Comparative sequence analyses identified a *B. pseudomallei bpaB* ortholog on chromosome I of the *B. mallei* ATCC 23344 genome (locus tag number BMA0840). The ORF is 3,270-nt in length and predicted to specify a protein of 1,090 aa with a molecular mass of 105,486 (Fig. 4.1, Table 4.2). Database searches with the NCBI Microbial Protein BLAST service also identified the *bpaB* gene in another 10 *B. mallei* (including ATCC 23344) and 29 *B. pseudomallei* strains. The predicted proteins were found to be highly-conserved among isolates of both species (99-100% identity). Interestingly, the genome of the closely-related bacterium, *Burkholderia thailandensis*, which is a non-pathogenic environmental saprophyte (224-227), does not contain the *bpaB*

gene. Potential ORFs were located upstream and downstream of *bpaB*, and these ORFs show similarities to a transcriptional regulator and the well-characterized OM protein, OmpA, respectively (Fig. 4.1 A, Table 4.2).

As depicted in Fig. 4.1 B, the *B. mallei* ATCC 23344 *bpaB* gene product possesses conserved structural features of oligomeric AT. Analysis with the PSIPRED secondary structure prediction method revealed that the last 50 aa form 4 antiparallel β-strands, each connected by short loops of 4 residues. This potential membrane-anchoring transporter domain is preceded by a helical region of 46 residues (aa 982-1,028), and a putative signal sequence cleavage site was detected at the N-terminus between aa 50 and 51 using the SignalP 4.1 server. Sequence analysis of BpaB using the Entrez Conserved Domains Database (CDD) also identified several domains commonly associated with oligomeric AT (Table 4.3).

4.4.2 Production and functional analysis of the BpaB protein in *E. coli*

The data presented in Table 3 indicate that BpaB exhibits sequence and structural similarities to the adhesins *M. catarrhalis* UspA1 (228), *Y. enterocolitica* YadA (190), and *H. influenzae* Hia (229). Hence, we hypothesized that BpaB mediates adherence to epithelial cells. In addition, previous work demonstrated that mutating the *bpaB* gene in *B. pseudomallei* reduces adherence to A549 human type II pneumocytes (214). To determine whether BpaB mediates adherence to epithelial cells, the *bpaB* gene of *B. mallei* ATCC 23344 was cloned and expressed in the recombinant background of the nonadherent *E. coli* cloning

strain EPI300. To verify protein production, whole cell lysates (WCL), total membrane proteins (TMP), and sarkosyl-insoluble fractions containing OM proteins (OMP) were prepared from *E. coli* EPI300 harboring the plasmid pBHR1ΔDra (control) or pBpaB (specifies *B. mallei* ATCC 23344 *bpaB*) and analyzed by western blot. Figure 4.2 A shows that the BpaB-specific monoclonal antibody BpaB-MAb#4 reacts with an OMP of ~300-kDa in bacteria expressing the *bpaB* gene, which closely matches the predicted trimeric molecular weight of the gene product (315-kDa).

Immunofluorescence-labeling and microscopy examination of bacteria was used to establish that BpaB is displayed on the surface of *E. coli*. As shown in Fig. 4.2 B, bacteria carrying pBpaB are stained by α-BpaB polyclonal antibodies, whereas *E. coli* carrying the control plasmid pBHR1ΔDra are not. Labeling of nucleic acids with DAPI verified that comparable numbers of bacteria were examined. Surface-display of BpaB was confirmed by flow cytometry analysis of immunofluorescently-labeled cells. Figure 4.2 C demonstrates that α-BpaB polyclonal antibodies caused a shift in fluorescence of *E. coli* carrying pBpaB, indicating that they bind to the surface of intact recombinant bacteria producing BpaB. As expected, α-BpaB antibodies did not bind to the surface of *E. coli* carrying the control plasmid. Of note, the BpaB-specific antibodies used in western blot, immunofluorescence microscopy, and flow cytometry experiments were raised against a purified recombinant His-tagged protein encompassing aa 57-984 of BpaB, which corresponds to the predicted surface-exposed passenger domain (Fig. 4.1 B).

Quantitative adherence assays revealed that bacteria producing BpaB bind to A549 cells at levels 5-fold greater than bacteria carrying pBHR1ΔDra (Fig. 4.3 A). These data show that BpaB mediates adherence to airway cells. *Burkholderia mallei* is a serum-resistant, facultative intracellular bacterium that replicates inside different types of eukaryotic cells. Furthermore, AT adhesins often perform additional functions including biofilm formation (219, 230), serum resistance (190, 228), invasion (192), and intracellular survival/replication (195). Therefore, we tested whether *E. coli* producing BpaB form biofilms using a crystal violet staining assay. We discovered that recombinant bacteria carrying plasmid pBpaB form a ring-like pellicle located at the liquid-air interface, indicative of biofilm formation, whereas *E. coli* harboring the control plasmid pBHR1ΔDra did not (Fig. 4.3 B). In additional experiments, we also discovered that BpaB production by *E. coli* does not increase serum resistance, epithelial cell entry, or phagocytosis by/survival inside J774 murine macrophages (data not shown). Taken together, our data indicate that BpaB is a multifunctional oligomeric AT that mediates adherence to human lung cells and contributes to biofilm formation.

4.4.3 Production and functional analysis of the BpaB protein in *B. mallei*

To investigate the function of the *bpaB* gene product in the native background of *B. mallei*, we constructed an isogenic mutant of strain ATCC 23344. Whole cell lysates were prepared from wild-type (WT) and mutant strains, and analyzed by western blot to verify lack of BpaB production in the mutant. However, α-BpaB antibodies did not react with protein preparations of

the parent strain (or mutant, as expected). Other detection methods such as immunofluorescence-labeling and immunoprecipitation also failed to demonstrate BpaB production. These findings indicate that the AT is not produced at detectable levels under routine *in vitro* growth conditions. To determine whether BpaB is produced *in vivo*, we used ELISA to test serum samples from mice infected via the aerosol route with *B. mallei* ATCC 23344. Panel A in Fig. 4.4 shows that mice produced antibodies against BpaB, with a reciprocal end-point titer of 400; serum from control mock-infected mice did not contain α-BpaB antibodies. As positive control, we tested serum samples for the presence of antibodies against capsular polysaccharides (CPS), which are known immunogenic molecules on the surface of *B. mallei* during infection (231). As shown in Fig. 4.4 B, the reciprocal end-point titer of α-CPS antibodies in the serum of infected mice is 3,200.

To gain insight on the role of BpaB in virulence, we determined the median lethal dose of the mutant using a mouse model of aerosol infection. In these experiments, we also collected tissues from survivors and determined bacterial burden, which is indicative of *in vivo* fitness. We discovered that the *bpaB* mutation attenuates *B. mallei* virulence 12-fold (Fig. 4.5 A and B). We also found that at equivalent inoculating doses of 10^2 CFU, bacterial loads in the lungs (Fig. 4.5 C) and spleen (Fig. 4.5 D) of survivors were comparatively reduced in mice infected with the mutant. This attenuation in virulence does not appear to be related to *in vitro* defects of the mutant in growth rate, serum resistance, epithelial

cells adherence/invasion, phagocytosis by murine macrophages, or survival inside these immune cells (data not shown).

To further investigate the functional properties of BpaB and its contribution to virulence, we introduced plasmid pBpaB in the *bpaB* KO mutant. As shown in Fig. 4.6, recombinant bacteria produced an antigen of the expected size (Panel A) on their surface (Panels B and C). Surprisingly, 2 independent experiments to determine the median lethal dose of the complemented mutant revealed that constitutive production of BpaB further attenuates virulence. The *bpaB* KO mutant carrying the control plasmid pBHR1ΔDra shows 8- and 14-fold reductions in LD_{50} values (Fig. 4.7 B and Supporting Information Fig. 4.9 B, respectively) when compared to WT *B. mallei,* which is consistent with the 12-fold attenuation in virulence measured for the mutant without the plasmid (Fig. 4.5 B). In contrast, the LD_{50} values of the mutant harboring plasmid pBpaB were 55- and 58-fold lower than those of the parent strain (Fig. 4.7 B and Supporting Information Fig. 4.9 B, respectively). At similar inoculating doses (~10^2 CFU), bacterial loads in the lungs and spleen of survivors were slightly reduced in mice infected with the mutant compared to animals inoculated with WT *B. mallei* (Panels C and D in Fig. 4.7 and Supporting Information Fig. 4.9). To verify that the reduced virulence phenotype of the *bpaB* KO strain producing BpaB is not due to an overall growth defect, we measured the replication of WT *B. mallei* alongside the *bpaB* KO mutant carrying plasmids pBHR1ΔDra and pBpaB in broth. We found that all strains grew at comparable rates (Supporting

Information Fig. 4.10). These experiments also established that in the absence of antibiotic selection, both plasmids are stably maintained (data not shown).

Because biofilm and adherence assays with recombinant *E. coli* bacteria indicate that BpaB production increases biofilm formation and adherence to A549 cells (Fig. 4.3), we compared the ability of WT *B. mallei* and the *bpaB* KO strain carrying plasmids pBHR1ΔDra and pBpaB to form biofilm and attach to epithelial cells. Consistent with the *E. coli* data, we found that BpaB production confers the mutant with the ability to form biofilms (Fig. 4.8). The mutant carrying the control plasmid pBHR1ΔDra and WT *B. mallei*, which does not express BpaB under the growth conditions used to perform experiments, did not form ring-like pellicles at the liquid-air interface. Quantitative adherence assays indicated that all 3 strains adhered to A549 cells at comparable levels (data not shown).

4.5 Discussion

This study demonstrates that BpaB is a surface-located oligomeric AT that promotes the formation of biofilms and contributes to the virulence of *B. mallei* in a model of aerosol infection. We show that BpaB is conserved among sequenced *B. mallei* isolates, is produced *in vivo*, and elicits the production of antibodies during infection. Hence, BpaB displays many properties of an excellent target for developing countermeasures.

We discovered that *B. mallei* ATCC 23344 does not produce detectable amounts of BpaB when cultured under routine laboratory conditions. This does not appear to be a strain- or species-specific phenomenon. Western blot analysis of lysates from *B. mallei*

ATCC 10399 (China 5), *B. pseudomallei* 1026b, and *B. pseudomallei* K96243 also show lack of reactivity with α-BpaB polyclonal and monoclonal antibodies (data not shown), even though the genome of these strains specify a WT *bpaB* gene (locus tag numbers BMA10399_E0436, BP106B_I2046, BPSL2063, respectively). Published microarray data for the organisms are consistent with our findings and suggest precise regulation of *bpaB*. The gene is not appreciably expressed *in vitro* by *B. mallei* isolates (232) and is not upregulated by restricting iron concentrations in the culture medium (233). In addition, *bpaB* expression is not detected in the liver of Syrian golden hamsters two days after infection with *B. mallei* ATCC 23344 (173). Ooi and colleagues recently measured expression of *B. pseudomallei* K96243 genes under 82 conditions, many of which mimicking exposures the organism encounters in the environment or in an infected host (234); *bpaB* is 1 of 468 genes that does not exhibit detectable expression under any of the conditions tested.

BpaB is the fourth *B. mallei* oligomeric AT reported as not being produced under routine laboratory growth conditions. BoaA (212) and BpaC (213), both AT adhesins for airway cells, and the intracellular motility protein BimA (235, 236) are the others. The *bimA* gene is under the control of a two-component regulatory system consisting of the sensor histidine-kinase protein VirA and the DNA response regulator VirG. The *virAG* genes are contiguous to *bimA* in the Cluster 1 Type VI Secretion System T6SS-1 on chromosome II of *B. mallei* ATCC 23344, and are up-regulated following internalization of the agent into phagocytic cells (180, 236). It has also been shown that constitutive overproduction of VirAG activates *bimA* transcription under routine *in vitro* culture conditions (236). Interestingly, a putative DNA binding response regulator of the OmpR

family is located upstream of *bpaB* (see BMA0838 in Fig. 4.1 and Table 4.2). Open reading frames specifying DNA response regulators were also identified adjacent to the *boaA* and *bpaC* genes in the *B. mallei* ATCC 23344 genome (data not shown). Based on these observations, it is tempting to speculate that *bpaB* expression is under the control of the BMA0838 gene product. The BpaB-specific antibody reagents as well as recombinant strains developed in this study will facilitate testing this hypothesis.

While not produced under routine laboratory growth conditions, BpaB is produced during the course of aerosol infection of mice as indicated by the presence of BpaB-specific antibodies in serum samples after resolution of acute infection (Fig. 4.4). Sera from horses with experimental glanders have also been shown to contain high antibody titers against BpaB (237). These results are especially compelling because horses are the natural host and reservoir for *B. mallei* and are arguably the most relevant surrogate to study glanders. Using protein microarray technology, Varga *et al* demonstrated that serum from a human patient with glanders also contain increased levels of α-BpaB antibodies (238). Our animal experiments showing that a mutation in *bpaB* attenuates virulence (Figs. 4.5 and 4.7, Supporting Information Fig. 4.9) substantiate these observations and underscore the potential usefulness of BpaB as a target for developing countermeasures. The AT is produced during infection and contributes to pathogenesis by *B. mallei*. Hence, targeting BpaB may interfere with disease progression.

The analysis of recombinant bacteria constitutively producing BpaB suggests that the AT contributes to pathogenesis by promoting biofilms. Using a crystal violet staining assay, we discovered that *E. coli* and *B. mallei* producing BpaB both form ring-like

biofilm structures on polyvinyl at the air-liquid interface of static broth cultures (Figs. 4.3 B and 4.8). To our knowledge, this is the first report of a *B. mallei* gene product directly participating in biofilm formation. Quantitative attachment assays revealed that BpaB production significantly increases adherence of *E. coli* to A549 human lung cells (Fig. 4.3 A). Conversely, we found that constitutive production of the AT does not have a measurable effect on *B. mallei* adherence (data not shown). Likewise, the mutation in the *bpaB* gene does not impair binding of strain ATCC 23344 to A549 cells. One possible explanation for this lack of effect is that other adhesins produced by the *bpaB* KO mutant provide a high background of adherence. For instance, BoaA (212) and BpaC (213) have been shown to mediate binding of *B. mallei* ATCC 23344 to A549 cells. The organism also produces a Type IV pilus (239), which is a common adherence factor of Gram-negative bacteria (240). It is also possible that the increased adherence measured when BpaB is produced in the heterologous genetic background of *E. coli* is a result of biofilm formation. Continued investigation of the molecular mechanism by which *B. mallei* regulates BpaB production and a detailed structure-function analysis of the AT will clarify its role in adherence and biofilm formation. Of note, Lazar Adler *et al.* have reported that *B. pseudomallei* also produces an AT directly involved in biofilms, BbfA (locus tag number BPSS1439) (241). The *bbfA* ortholog of *B. mallei* is BMAA0810, not BpaB, and has yet to be functionally characterized.

The most surprising result of our study is the discovery that constitutive production of BpaB by the *bpaB* KO mutant strain does not restore virulence, but instead further attenuates the organism (Fig. 4.7 and Supporting Information Fig. 4.9). While this finding seems counter-intuitive, there are precedents in the literature for such a

phenomenon. For example, constitutive production of the *Cryptococcus neoformans* adhesin Cfl1 (242), the *Salmonella enterica* flagellum (243), and the *Yersinia pestis* F1 capsule (244) have been reported to substantially attenuate the virulence of these organisms. In fact, overproduction of bacterial surface-associated molecules is an emerging technique for developing novel live attenuated vaccines dubbed Attenuating Gene Expression (AGE) (245). The molecular basis for attenuation is not fully understood and appears to vary between model systems. In the case of the *Salmonella* flagellum, overproduction of the flagellar apparatus has been shown to disrupt the structural integrity of the bacterial membranes, which in turn facilitates clearance of the agent by innate immune mechanisms. On the other hand, constitutive production of Cfl1 by *C. neoformans* appears to impact pathogenicity through increased and untimely cell adhesion. The mechanism by which constitutive production of BpaB attenuates virulence is currently being investigated.

Taken together, our data demonstrate that BpaB is a virulence factor and that precise regulation of production is central to its role in the pathogenesis of *B. mallei*. Identification of the specific signals that modulate BpaB production as well as the host-related cues influencing these pathways will provide novel insights in the complex biology and virulence of the organism, and will yield useful information for the development of MCM and diagnostics for glanders.

4.6 Acknowledgements

The authors wish to thank Dr. Tomislav Jelesijevic (University of Georgia), Jennifer Willingham (University of Georgia), Dr. Vincent Starai (University of Georgia),

and Dr. Teresa Shaffer (University of South Alabama) for their helpful comments on the manuscript.

Table 4.1. Strains and plasmids.

Strain or plasmid	Description	Source or reference
Strains		
B. mallei		
ATCC 23344	Wild-type strain; Polymyxin B resistant, zeocin and kanamycin sensitive	(173)
***bpaB* KO**	Isogenic *bpaB* mutant strain of ATCC 23344; resistant to Polymyxin B and zeocin, kanamycin sensitive	This study
E. coli		
EPI300	Cloning strain	epicenter Illumina
S17	Strain used for conjugational transfer of plasmids pBHR1ΔDra, pBpaB and pKASbpaB.zeo to *B. mallei*; sensitive to Polymyxin B	(246)
TUNER	Production strain used for purification of His- and GST-tagged BpaB proteins	EMD Millipore
Plasmids		
pBHR1	Broad host range cloning vector; contains chloramphenicol and kanamycin resistance markers	MoBiTec Molecular Biotechnology
pBHR1ΔDra	pBHR1 containing a 339-nt deletion in the chloramphenicol resistance marker; confers resistance only to kanamycin	This study
pBpaB	pBHR1ΔDra containing the *B. mallei* ATCC 23344 *bpaB* gene; kanamycin resistant	This study
pCC1	Cloning vector; contains chloramphenicol resistance marker	epicenter Illumina
pCCbpaB	pCC1 containing the *B. mallei* ATCC 23344 *bpaB* gene; chloramphenicol resistant	This study
pCCbpaB.zeo	pCCbpaB in which a 1.4-kb fragment internal to the *bpaB* ORF is replaced with a 0.4-kb zeocin resistance cassette; confers resistance to chloramphenicol and zeocin	This study
pKAS46	Mobilizable suicide plasmid; contains kanamycin resistance marker	(247)
pKASbpaB.zeo	pKAS46 containing the insert from pCCbpaB.zeo; confers resistance to kanamycin and zeocin	This study
pEM7/ZEO	Source of the zeocin resistance marker	Life Technologies
pETcoco-1	Protein production vector; chloramphenicol resistant	EMD Millipore
pHisBpaB	pETcoco-1 producing BpaB residues 57-984 joined to an N-terminal His-tag; chloramphenicol resistant	This study
pGEX4T-2	Protein production vector; ampicillin resistant	GE Healthcare Life Sciences
pGSTBpaB	pGEX4T-2 producing BpaB residues 57-984 joined to an N-terminal GST-tag; ampicillin resistant	This study

Table 4.2. Selected features of the *bpaB* genomic locus of *B. mallei* ATCC 23344.

Locus tag number	Length of gene product and predicted MW	Description
BMA0838	231 aa, 26-kDa	Putative DNA-binding response regulator of the OmpR family (CDD number 223816, E-value of 2.31e-57).
BMA0839	80 aa, 9-kDa	Hypothetical protein, no conserved domain found or similarity to other proteins.
BMA0840 (*bpaB*)	1090 aa, 105-kDa	AT, 99% identical to *B. pseudomallei* 1026b BpaB (214).
BMA0841	223 aa, 23-kDa	Putative OmpA_C-like OM protein based on the high level of sequence similarity of residues aa 110-204 to CDD domain number 143586 (E-value of 4.22e-22).
BMA0842	509 aa, 56-kDa	Hypothetical protein. Residues 81-175 show sequence similarity with TPR domain (Tetratricopeptide repeat domain, CDD number 238112, E-value of 1.94e-10). Proteins containing this domain are often involved in protein-protein interactions.

Table 4.3. Regions of BpaB with high level of sequence similarity to conserved domains in the NCBI Entrez Conserved Domain Database (CDD).

BpaB residues	E-value	CDD domain	CDD number	Description
1-24	8.25e-08	ESPR	257462	Extended Signal Peptide of Type V secretion system. Present at the N-terminus of the signal peptides of proteins belonging to the Type V secretion systems, including AT.
108-251	2.16e-3	LbR-like Superfamily	248061	Left-handed β-roll. This family contains a variety of domains with a left-handed β-roll structure including virulence factors and various other proteins such as the oligomeric AT UspA1 of *Moraxella catarrhalis* and YadA of *Yersinia enterocolitica.*
346-439	1.93e-12	LbR_YadA-like	240612	YadA-like, left-handed β-roll. This group contains the collagen-binding domain of the virulence factor and oligomeric AT YadA of *Y. enterocolitica.*
330-1090	1.9e-16	HIA	227614	Autotransporter adhesin [Intracellular trafficking and secretion/ Extracellular structures] first identified in the oligomeric AT Hia of *Haemophilus influenzae.*
1014-1090	9.64e-14	YadA_anchor	252233	YadA-like C-terminal region. Represents the C-terminal 120 aa of several oligomeric AT including *Y. enterocolitica* YadA, *M. catarrhalis* UspA2, *Haemophilus ducreyi* DsrA and *E. coli* Eib. The C-terminal 9 aa, consisting of alternating hydrophobic aa ending in F or W, comprise a targeting motif for the OM of the Gram-negative cell envelope. This region is also important for oligomerization.

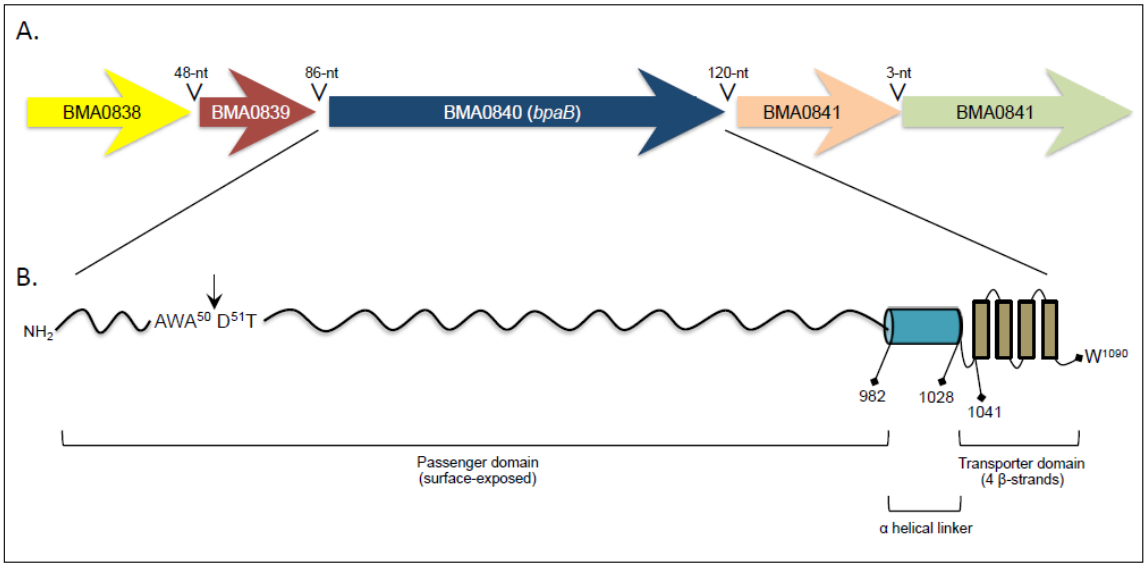

Figure 4.1. Schematic representation of the *B. mallei* ATCC 23344 *bpaB* genomic locus and gene product.

Panel A: Colored block arrows represent the *bpaB* ORF and surrounding genes in chromosome I of the organism. The length of intergenic regions is shown above block arrows. Panel B: Different regions of the predicted BpaB protein are depicted with positions of residues defining selected domains. The C-terminal transporter domain and helical linker were identified using the PSIPRED server. The arrow represents the predicted signal sequence cleavage site, which was identified using the SignalP 4.1 server.

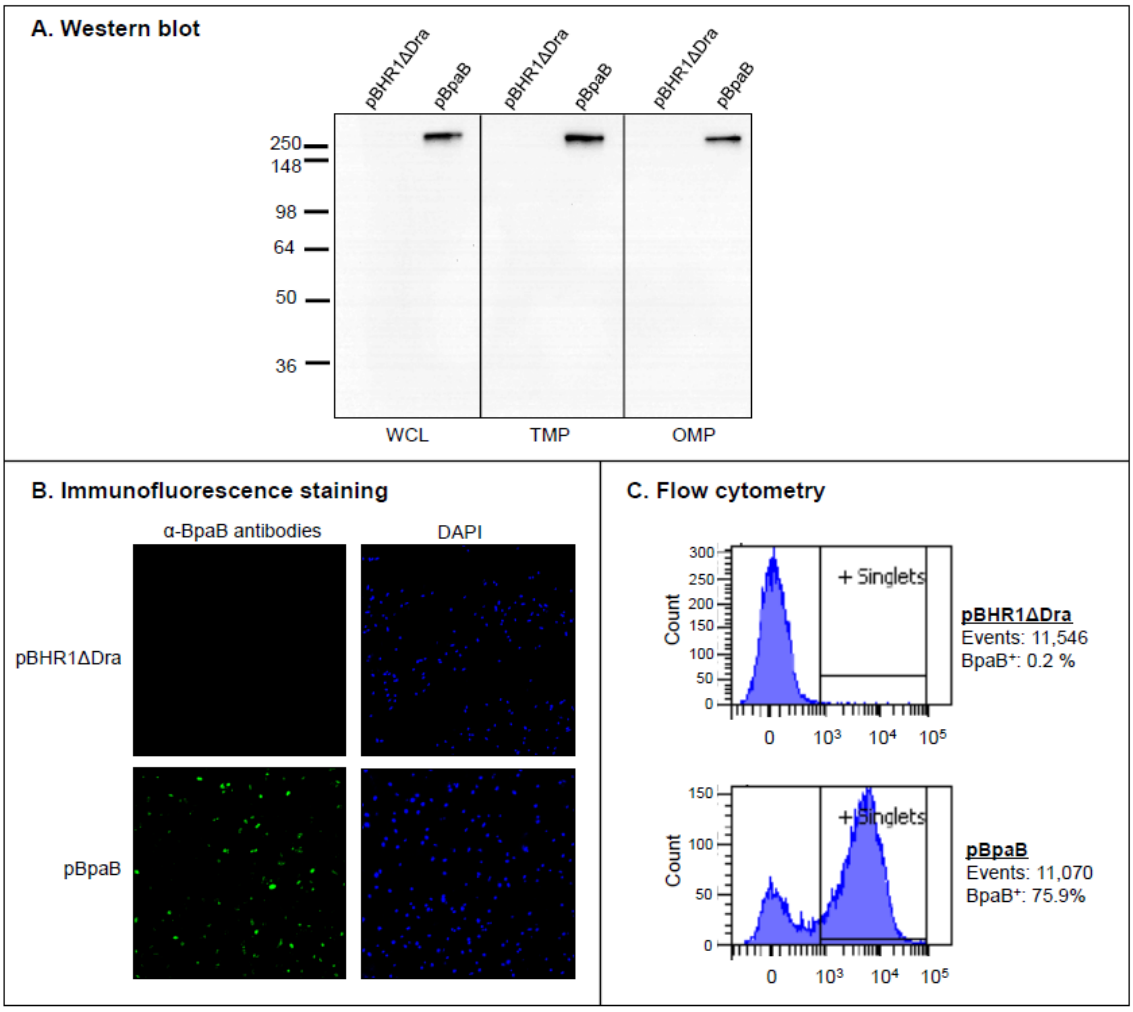

Figure 4.2. BpaB production by recombinant *E. coli* strains.

Panel A: Equivalent amounts of whole cell lysates (WCL), total membrane proteins (TMP) and sarkosyl-insoluble fractions containing OM proteins (OMP) were resolved by SDS-PAGE, transferred to PVDF membranes and analyzed by western blot with the monoclonal antibody BpaB-MAb#4. Molecular weight markers are shown to the left in kilodaltons. Panel B: Non-permeabilized *E. coli* strains were fixed onto glass slides and fluorescently-labeled with DAPI (blue) and with α-BpaB polyclonal antibodies (green) as described in Materials and Methods. Bacteria were visualized by microscopy using a

Nikon Eclipse Ti confocal system. Representative microscopic fields are shown. Panel C: Non-permeabilized *E. coli* strains were incubated with polyclonal antibodies against BpaB and fluorescently-labeled with a goat α-mouse antibody conjugated with the fluorochrome Alexa Fluor 488. Labeled bacteria were analyzed using a BD LSR II flow cytometer. The *x*-axis represents the level of fluorescence, and the *y*-axis corresponds to the particles counted in arbitrary units. The number of cells analyzed, and the percentage of those producing BpaB on their surface, is shown.

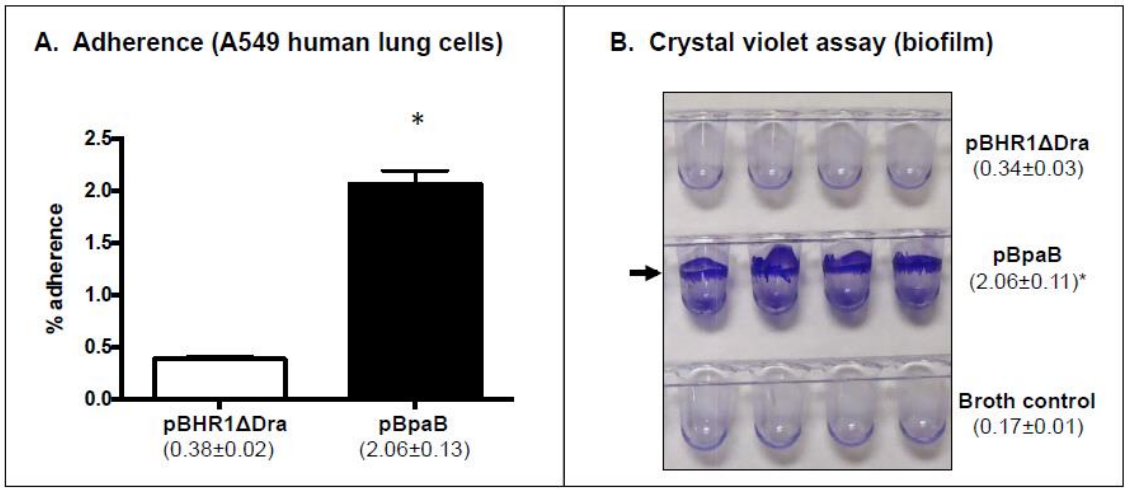

Figure 4.3. Adherence and biofilm assays with *E. coli* recombinant strains.

Panel A: *E. coli* strains were incubated with epithelial cells for 30 min at 37°C. Following this, cells were washed to remove unbound bacteria, lysed, diluted, and spread onto agar plates to calculate the number of bound bacteria. The results are expressed as the mean percentage (± standard error) of inoculated bacteria attached to A549 cells. The values in parentheses show the actual percentage. Panel B: *E. coli* strains were cultured in the wells of PVC microplates, stained with crystal violet, washed with deionized water, and the wells were photographed. The arrow shows biofilm formation, which was quantitated by extracting crystal violet with methanol and measuring absorbance at 570 nm. The results are shown in parentheses and are expressed as the mean (± standard error) absorbance. Both panels: The asterisks indicate that the increase in adherence and biofilm formation of *E. coli* carrying pBpaB, compared to *E. coli* harboring pBHR1ΔDra, is statistically significant (*P* values < 0.05, Mann-Whitney test).

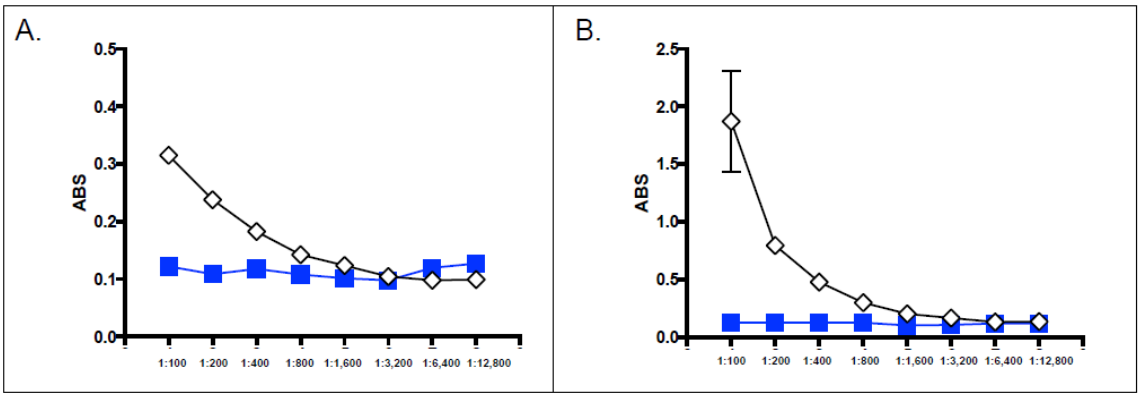

Figure 4.4. ELISA with sera from mice that survived aerosol challenge with *B. mallei*. Serum samples were serially diluted and placed in duplicate wells of plates coated with GST-tagged BpaB (panel A) and CPS (panel B). Goat α-mouse antibodies (light and heavy chains) conjugated to alkaline phosphatase were used as secondary antibodies. The y-axis shows absorbance at a wavelength of 405 nm, which is indicative of antibodies binding to antigens coating the plates. The x-axis represents serial two-fold dilutions of sera. The results are expressed the mean absorbance (± standard error). Open diamonds show sera from mice that survived challenge with *B. mallei* ATCC 23344. Blue squares represent sera from control mice that were inoculated with 50 µL of PBS using the MicroSprayer. These serum samples were generated in the context of a previously published study (169).

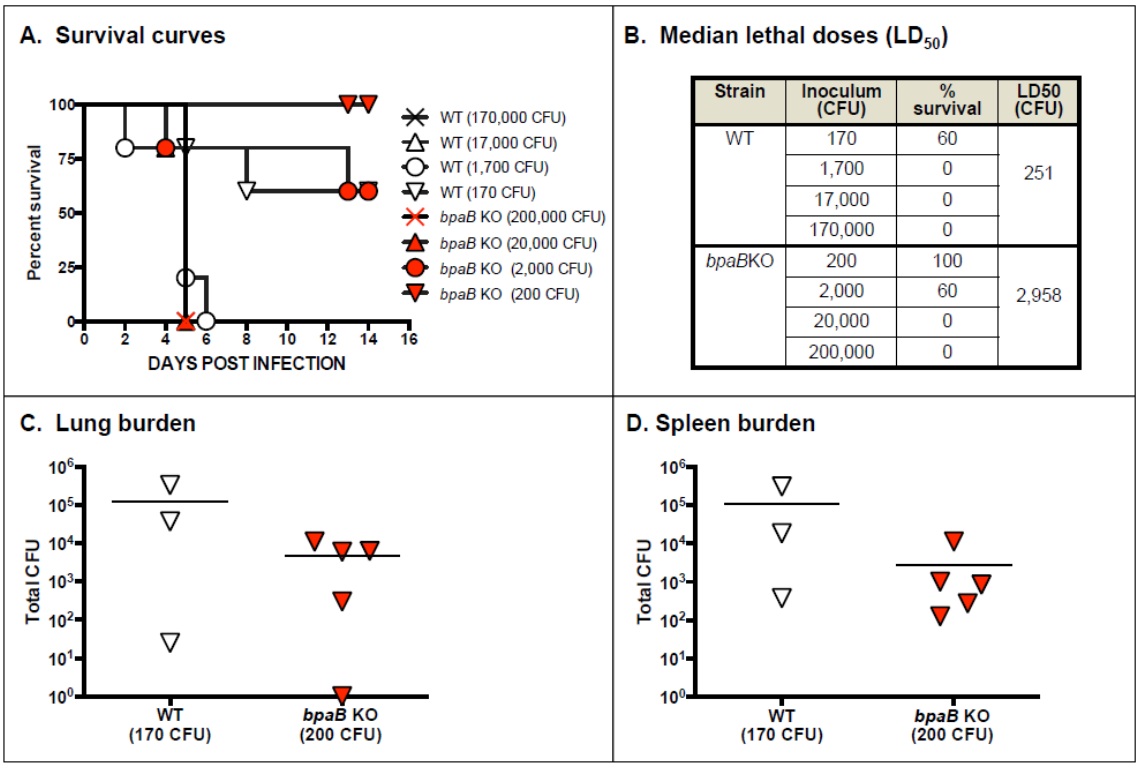

Strain	Inoculum (CFU)	% survival	LD50 (CFU)
WT	170	60	251
	1,700	0	
	17,000	0	
	170,000	0	
*bpaB*KO	200	100	2,958
	2,000	60	
	20,000	0	
	200,000	0	

Figure 4.5. Median lethal dose determination of wild-type *B. mallei* and *bpaB* KO mutant strains.

Mice were inoculated intratracheally using a Microsprayer device to aerosolize the indicated number of bacterial CFU directly into the lungs (n=5 mice/dose). Animals were then monitored daily for clinical signs of illness and morbidity. Panel A: Survival curves. Panel B: Calculated LD_{50} values. Panels C and D: Tissues were collected from mice that survived challenge with 10^2 CFU, homogenized, diluted, and spread on agar plates to determine bacterial loads. Symbols show data for individual animals.

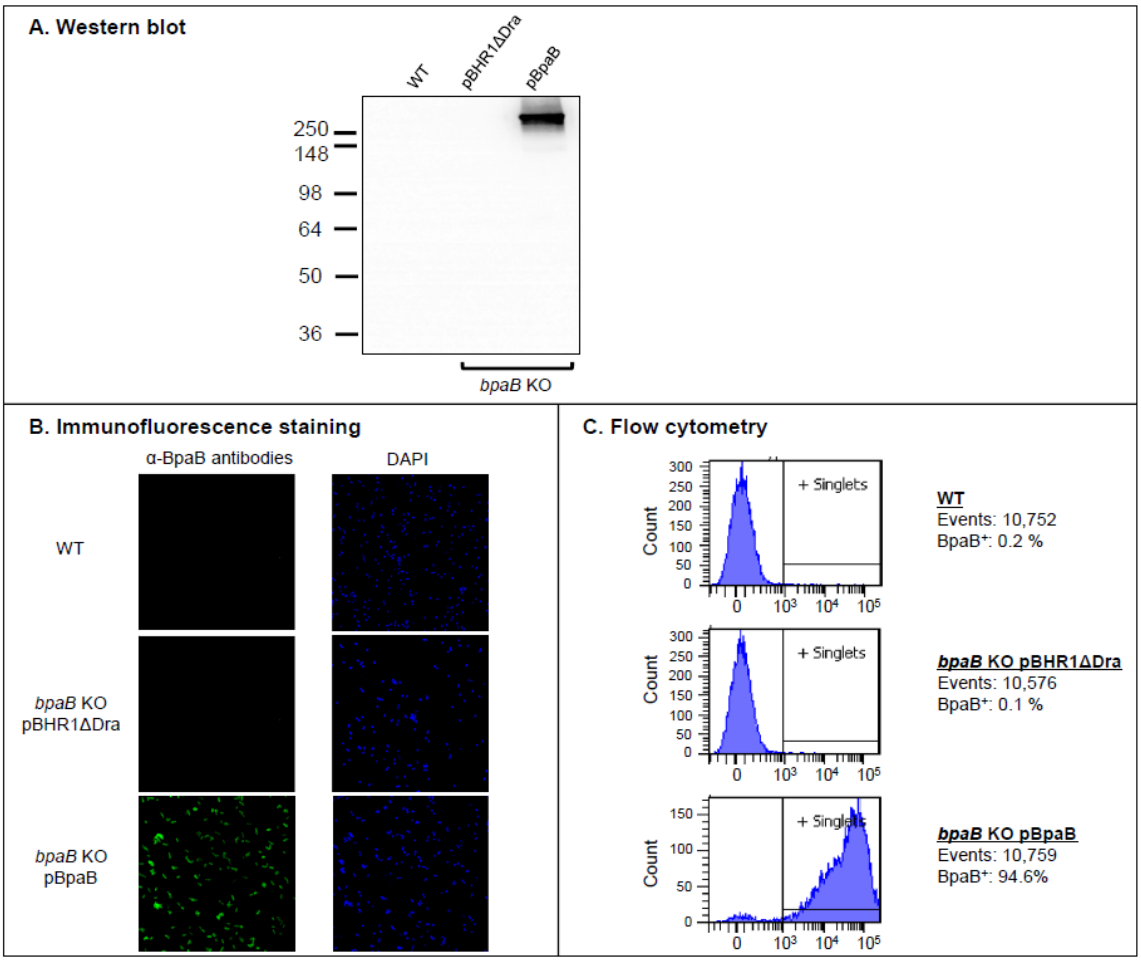

Figure 4.6. BpaB production by wild-type and recombinant *B. mallei* strains.

Panel A: Equivalent amounts of whole cell lysate preparations were resolved by SDS-PAGE, transferred to PVDF membranes and analyzed by western blot with BpaB-MAb#4. Molecular weight markers are shown to the left in kilodaltons. Panel B: Non-permeabilized *B. mallei* strains were fixed onto glass slides and fluorescently-labeled with DAPI (blue) and with α-BpaB polyclonal antibodies (green) as described in Materials and Methods. Bacteria were visualized by microscopy using a Nikon Eclipse Ti confocal system. Representative microscopic fields are shown. Panel C: Paraformaldehyde-fixed *B. mallei* strains were incubated with polyclonal antibodies

against BpaB and fluorescently-labeled with a goat α-mouse antibody conjugated with the fluorochrome Alexa Fluor 488. Labeled bacteria were analyzed using a BD LSR II flow cytometer. The *x*-axis represents the level of fluorescence, and the *y*-axis corresponds to the particles counted in arbitrary units. The number of cells analyzed, and the percentage of those producing BpaB on their surface, is shown.

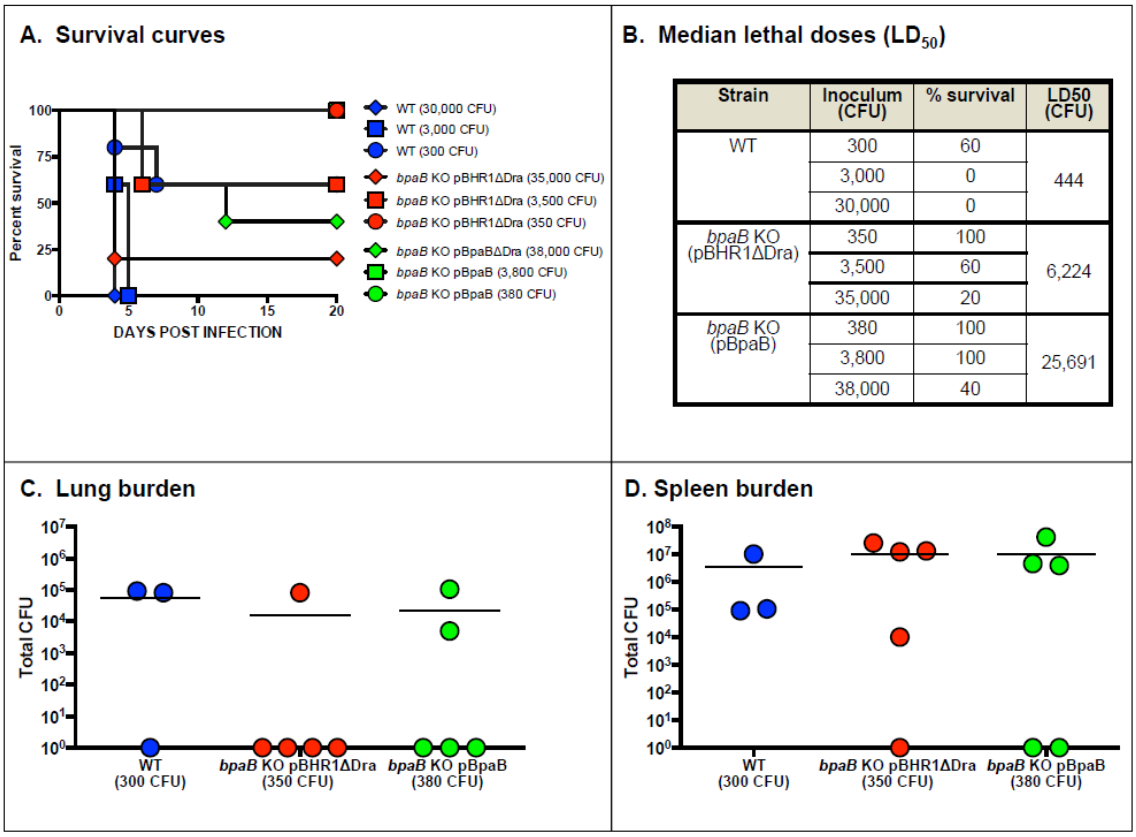

Strain	Inoculum (CFU)	% survival	LD50 (CFU)
WT	300	60	444
	3,000	0	
	30,000	0	
bpaB KO (pBHR1ΔDra)	350	100	6,224
	3,500	60	
	35,000	20	
bpaB KO (pBpaB)	380	100	25,691
	3,800	100	
	38,000	40	

Figure 4.7. Median lethal dose determination of wild-type *B. mallei* and recombinant *bpaB* KO strains.

Mice were inoculated intratracheally using a Microsprayer device to aerosolize the indicated number of bacterial CFU directly into the lungs (n=5 mice/dose). Animals were then monitored daily for clinical signs of illness and morbidity. Panel A: Survival curves. Panel B: Calculated LD_{50} values. Panels C and D: Tissues were collected from mice that survived challenge with 10^2 CFU, homogenized, diluted, and spread on agar plates to determine bacterial loads. Symbols show data for individual animals.

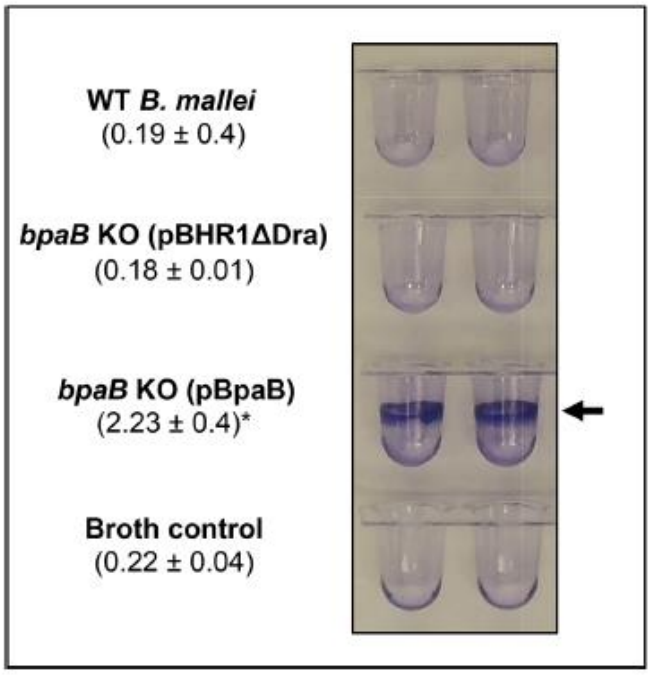

Figure 4.8. Biofilm assay with wild-type and recombinant *B. mallei* strains.

B. mallei strains were cultured in the wells of PVC microplates, stained with crystal violet, washed with deionized water, and the wells were photographed. The arrow shows biofilm formation, which was quantitated by extracting crystal violet with methanol and measuring absorbance at 570 nm. The results are shown in parentheses and are expressed as the mean (± standard error) absorbance. The asterisk indicates that the increase in biofilm formation by bacteria carrying pBpaB is statistically significant (*P* values < 0.05, Mann-Whitney test).

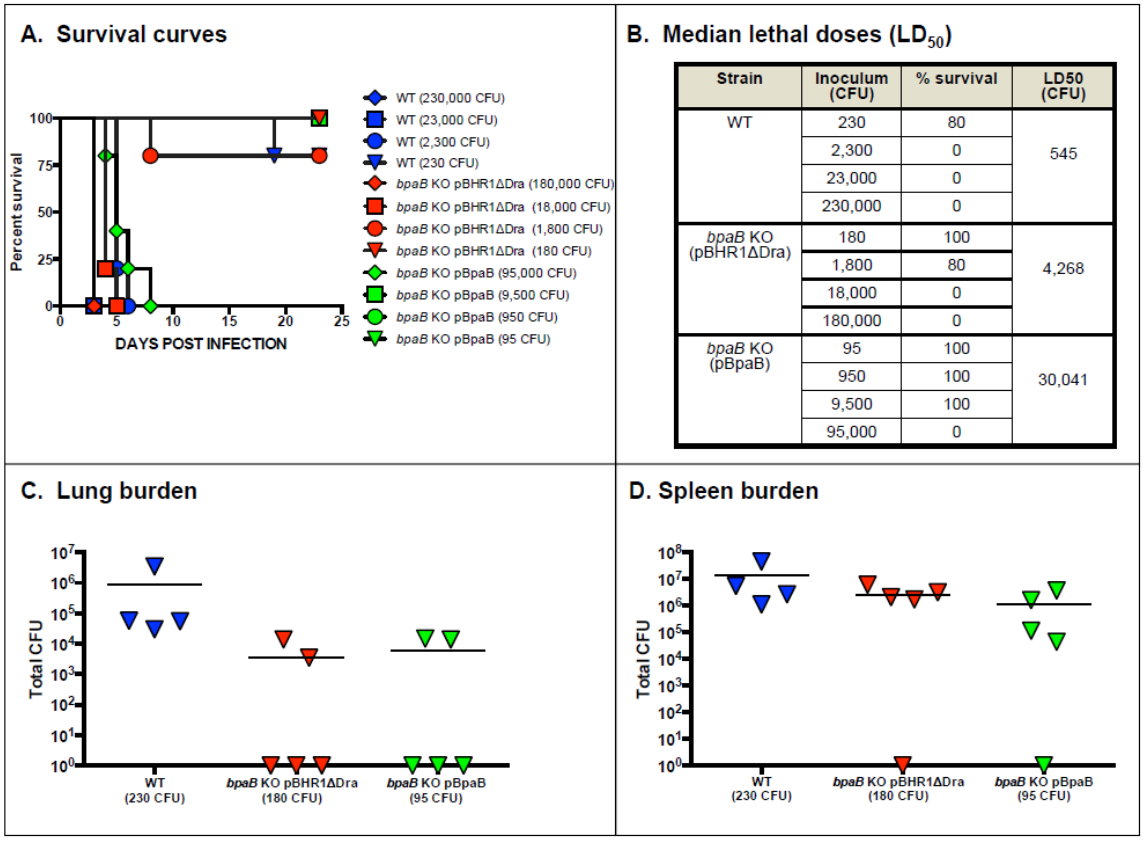

Strain	Inoculum (CFU)	% survival	LD50 (CFU)
WT	230	80	545
	2,300	0	
	23,000	0	
	230,000	0	
bpaB KO (pBHR1ΔDra)	180	100	4,268
	1,800	80	
	18,000	0	
	180,000	0	
bpaB KO (pBpaB)	95	100	30,041
	950	100	
	9,500	100	
	95,000	0	

Figure 4.9. (Supplementary Figure 1) Median lethal dose determination of wild-type *B. mallei* and recombinant *bpaB* KO strains.

Mice were inoculated intratracheally using a Microsprayer device to aerosolize the indicated number of bacterial CFU directly into the lungs (n=5 mice/dose). Animals were then monitored daily for clinical signs of illness and morbidity. Panel A: Survival curves. Panel B: Calculated LD_{50} values. Panels C and D: Tissues were collected from mice that survived challenge with 10^2 CFU, homogenized, diluted, and spread on agar plates to determine bacterial loads. Symbols show data for individual animals.

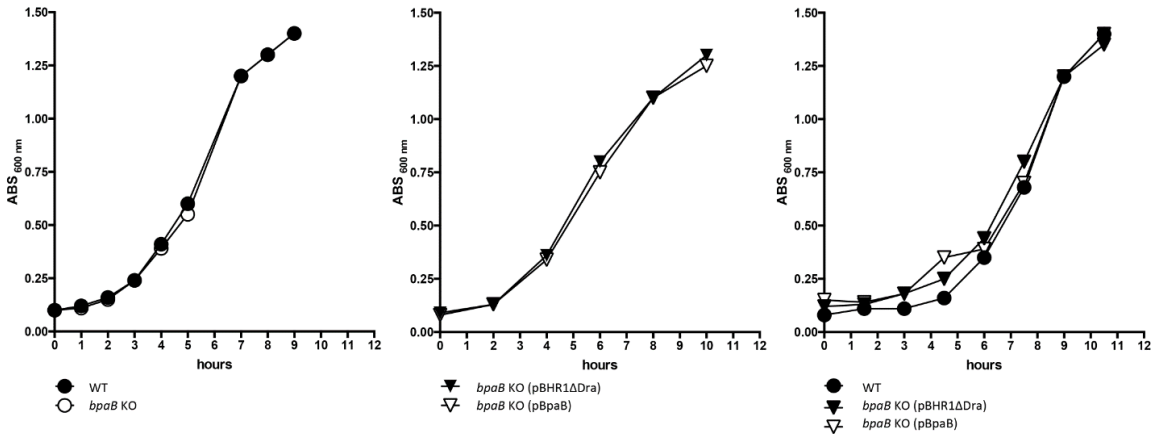

Figure 4.10 (Supplementary Figure 2) Growth rates of wild-type *B. mallei* and recombinant *bpaB* KO strains in liquid cultures.

Plate-grown bacteria (40-hr) were suspended in broth to an optical density at wavelength 600 nm (ABS_{600nm}) of ~ 0.1. Following this, suspended bacteria were incubated at 37°C and the optical density of cultures was measured at the indicated time intervals. Strains were tested on at least 3 separate occasions. Representative experiments are shown.

CHAPTER 5

CHARACTERIZATION OF A NOVEL LIVE ATTENUATED MUTANT STRAIN OF *BURKHOLDERIA MALLEI* ATCC 23344[1]

[1] Zimmerman SM, Dyke JS, Long ME, Jelesijevic T, Michel F, Lafontaine ER, Hogan RJ. To be submitted to *PLOS Pathogens.*

5.1 Abstract

Autotransporter proteins (AT) form one of the largest families of virulence factors in Gram-negative bacteria. Based on the structure of the C-terminus, AT are classified as either conventional or oligomeric. The genome of *Burkholderia mallei* strain ATCC 23344 contains eight AT gene products (6 oligomeric and 2 conventional). To date only three oligomeric AT (BoaA, BimA, and BpaC) have been functionally characterized, and of these, only BimA has been shown to contribute to virulence *in vivo*. In this study, we report the characterization of a conventional AT specified by *B. mallei* termed BatA. To gain insight into the contribution of this AT to virulence *in vivo*, a *batA* mutation was introduced into the genome of *B. mallei* ATCC 23344. Experiments using a mouse model of aerosol infection revealed that the *batA* mutation attenuates virulence at least 250-fold, and that tissues from survivors are transiently colonized. We also discovered that vaccination with the *batA* mutant strain provides 77% and 68% protection against acute infection with *B. mallei* ATCC 23344 and *B. pseudomallei* 1026b, respectively. Furthermore, 56% of the vaccinated mice that survived back-challenge with wild-type *B. pseudomallei* developed sterilizing immunity. To evaluate the contribution of antibodies to this protection, serum obtained from vaccinated mice that survived back-challenge with *B. mallei* (immune sera) was passively transferred intraperitoneally to naïve mice, and these mice were then challenged with wild-type *B. mallei* ATCC 23344. We determined that immune sera provided protective immunity in a dose-dependent manner, and we also discovered that immune sera contain increased antibody titers against multiple unique antigens. Furthermore, these antibodies opsonize *B. mallei*, resulting in increased phagocytosis and decreased intracellular survival in murine macrophages. Our

data demonstrate that BatA is an important virulence factor of *B. mallei* and that studying AT provides a platform to gain new knowledge about immunity against the organism, including protective antigen discovery.

5.2 Introduction

Glanders is a fatal, zoonotic, respiratory disease caused by the bacterial agent, *Burkholderia mallei*. *B. mallei* is a non-spore forming, encapsulated, non-motile, aerobic, host-adapted, Gram-negative bacterium that is endemic to Asia, Africa, the middle East, and South America. Infection occurs via percutaneous inoculation or inhalation of contaminated aerosol particles, causing severe pneumonia and eventually sepsis in humans and most veterinary species, particularly solipeds (horses, ponies, donkeys, and mules). Affected veterinary species are not treated and must be culled. The mortality rate of untreated glanders disease in humans is 100%, and the treated mortality rate remains over 50%. While the reason for high mortality remains unknown, it is likely complicated by limited diagnostic testing ability, intrinsic antimicrobial resistance, and the lack of an efficacious vaccine for *B. mallei* (2-4, 9, 10, 21, 23).

Melioidosis is a fatal respiratory disease caused by the bacterial agent, *Burkholderia pseudomallei*. *B. pseudomallei* is a ubiquitous, encapsulated, motile, aerobic, Gram-negative bacillus that is endemic to the soil and water in Asia and northern Australia. Infection occurs primarily via percutaneous inoculation, inhalation, and ingestion. *B. pseudomallei* has a broad host range, including but not limited to humans, domestic animals (livestock and companion animals), and even exotic species (camels, dolphins, and birds). The clinical presentation and gross and histologic lesions caused by

B. pseudomallei are similar to that of *B. mallei*, and mortality rates in humans and animals are just as high (1, 3, 6, 11, 18, 22).

Overall, *B. mallei* and *B. pseudomallei* are remarkably similar pathogens. Not only are their genomes 99% identical, but they also possess similar virulence factors and are resistant to most antimicrobials (3). Given that neither pathogen is present in North America yet both are highly fatal, difficult to diagnose, resistant to treatment, and lack preventative measures, there is concern that *B. mallei* and *B. pseudomallei* could be utilized in present-day biological warfare, especially since *B. mallei* has already been used in this manner (38). Therefore, the Federal Select Agent Program (SAP) has classified *B. mallei* and *B. pseudomallei* as Tier 1 Select Agents, and the United States has made the development of therapeutic and preventative measures against these pathogens a priority (41).

B. mallei and *B. pseudomallei* share many virulence traits, including several autotransporter (AT) proteins. AT are often used by Gram-negative bacteria for motility, adherence, invasion, serum resistance, phospholipolysis, cytotoxicity, intracellular survival, and biofilm formation. They are also highly immunogenic, and AT-based vaccines have been shown to be effective at protecting against infection with Gram-negative organisms (13). One of the best characterized is the *Bordetella pertussis* AT, Pertactin, which is a component of the licensed DTaP vaccine used to protect humans against whooping cough (DAPTACEL®, Infanrix®, Tripedia®, Pediarix®, KINRIX®, Adacel®, Pentacel®, and Boostrix®) (83).

AT consist of three functional domains: an N-terminal passenger domain, a C-terminal transporter domain, and an α-helical linker region. The N-terminus specifies the

biologic function of the AT, while the C-terminus is composed of hydrophobic β-strands that tether the protein to the outer membrane. Structurally, AT are also characterized by their C-terminus. Those consisting of 10-12 antiparallel β-strands are termed conventional, while those consisting of a trimer of 4 antiparallel β-strands are termed oligomeric.

AT secretion at the inner membrane (IM) is mediated by a signal peptide that chaperones the protein via the Sec-translocase pathway. The molecular pathway by which AT are secreted across the outer membrane (OM) is still under investigation; however, two models are proposed. The first is the hairpin model that states the AT secretes itself by inserting its C-terminal translocator domain into the OM, after which it forms a β-barrel pore to secrete its own internal passenger domain. The second is the Bam model, which argues that the β-barrel pore is too narrow to accommodate a large, completely folded protein, so the AT must either hijack or work cooperatively with existing secretion machinery (e.g. Bam or Lol complexes) to secrete themselves across the OM (62, 67, 68, 75, 248).

Once on the extracellular side of the OM, AT may remain embedded in the outer membrane with their passenger domain exposed. Alternatively, AT can also release a portion of their passenger domain into the extracellular milieu. Many AT utilize internal protease domains to autoproteolytically cleave themselves (e.g. Hap of *H. influenzae*), while others rely on neighboring OM proteins or AT to cleave their passenger domains (e.g. IcsA of *Shigella sp.* or NalP of *N. meningitidis*) (62, 67).

The genome of *B. mallei* encodes two conventional AT, *Burkholderia* conventional autotransporter 1 (Bca1, BMAA1263) and *Burkholderia* autotransporter A

(BatA, BMA1647). Interestingly, the amino acid sequence of BatA resembles another conventional AT, McaP, which has been characterized in *Moraxella catarrhalis* by Timpe *et al*. They determined that McaP was a surface exposed AT with lipolytic enzyme activity and a passenger domain that mediated adherence to A549 human lung epithelial cells, which implicates it as an important factor in bacterial pathogenesis and a potential vaccine antigen (85, 249). In this study, we characterize the function of BatA, report on its contribution to the virulence of *B. mallei*, and describe the protective immune response elicited by *BmbatA*KO, a novel live attenuated mutant strain of *B. mallei* ATCC 23344.

5.3 Materials and Methods

5.3.1 Strains, plasmids, tissue culture cell lines, and growth conditions.

Strains and plasmids used in this study are described in Table 5.1. *Burkholderia mallei* strains were grown at 37°C for 48 hours on Brucella medium (BD) supplemented with 5% (v/v) glycerol. Antibiotics were supplemented in the medium when necessary at the following concentrations: 7.5 µg/mL Polymyxin B (MP Biomedicals), 5 µg/mL kanamycin (MP Biomedicals), and/or 7.5 µg/mL zeocin (Life Technologies™). *Burkholderia thailandensis* and *Escherichia coli* strains were grown at 37°C on either Luria Bertani (LB) media (Fisher Scientific) or Low Salt Luria Bertani (LSLB) media (Teknova). *Burkholderia thailandensis* were cultured for 48 hours, while *Escherichia coli* were cultured for 24 hours. Antibiotics were supplemented when indicated at the following concentrations: 100 µg/mL ampicillin (Sigma-Aldrich®), 15 µg/mL chloramphenicol (Fisher Scientific), 50 µg/mL kanamycin (MP Biomedicals), and/or 50 µg/mL zeocin

(Life Technologies™). Murine macrophages (J774A.1; ATCC TIB-67) were grown as per Balder *et al.* (79) in DMEM media (Corning® Cellgro®) supplemented with 10% fetal bovine serum (Hyclone®, Thermo Scientific) at 37°C and in the presence of 7.5% CO_2. 5.3.2 Recombinant DNA methods.

Standard molecular biology techniques were performed as described previously (250). All genomic DNA was isolated using the Easy-DNA™ Kit (Life Technologies™), and all plasmid DNA was isolated using the QIAprep Spin Miniprep kit (QIAGEN). All PCR experiments were performed as per the manufacturer's instructions using Platinum® Pfx DNA Polymerase (Life Technologies™). All restriction enzyme digests and ligations were performed as per the manufacturer's instructions using reagents (various restriction endonucleases and T4 DNA ligase) purchased from New England BioLabs® Inc. All PCR products and plasmids were purified from 0.7% agarose gels with the High Pure PCR Product Purification Kit (Roche Applied Science) and blunted by treating with the End-It™ DNA End Repair Kit (epicentre® Illumina®). Sanger sequencing was performed on all plasmids by the University of Michigan DNA Sequencing Core (http://seqcore.brcf.med.umich.edu) to verify PCR did not introduce mutations that would result in amino acid (aa) substitutions to the *batA* gene product.

The chloramphenicol resistance marker in a broad host range plasmid pBHR1 (MoBiTec Molecular Biotechnology) was disrupted by deleting a 339-nucleotide (nt) fragment internal to the marker. This disruption was achieved by digesting pBHR1 with *Dra*I, excising and purifying from an agarose gel, and re-

ligating. The resulting plasmid, pBHR1.ΔDra, was sequenced to verify the deletion and also tested to confirm that it no longer confers resistance to chloramphenicol.

A 2,975-nt DNA fragment containing the *batA* gene was amplified from the genome of *B. pseudomallei* 1026b with the following primers; P1 (5'-CAACCGTGATTCCCGACCCG-3'), P2 (5'-GTCCTGTCGGCCGCGAATCT-3'). Next, the pCC.batA plasmid was generated by cloning the *batA* amplicon into the pCC1^{TM} vector using the CopyControl^{TM} PCR cloning kit (epicentre® Illumina®). Plasmid pBatA was created by amplifying a 2,998-nt DNA fragment containing *batA* from the genome of *B. pseudomallei* K96243 with the following primers; P3 (5'-CGGAATTCAACGGTTCGCCGCGCATTT-3') and P4 (5'-GGCATGTCGCTCGTGTACTA-3'). This *batA* amplicon was then digested with *Eco*RI and subcloned into the *Eco*RI-*Sca*I site of pBHR1.ΔDra. Plasmid pCC.batA.zeo was constructed by digesting pCC.batA with *Aat*II to remove a 1,300-nt fragment internal to the *batA* ORF, end-repairing, and then ligating with a blunt 400-nt zeocin resistance marker. Plasmid pKAS.batA.zeo was generated by amplifying the 2,075-nt knock-out (KO) *batA* insert from pCC.batA.zeo with the following primers; P5 (5'-TAATACGACTCACTATAGGG-3') and P6 (5'-TACGCCAAGCTATTTAGGTGAGA-3'). The *batA* KO insert was then digested with *Eco*RV and subcloned into the *Eco*RV site of pKAS45 (251).

PCR product specifying aa 30 to 307 of the *batA* ORF was amplified from *B. pseudomallei* 1026b genomic DNA with the following primers; P7 (5'-CCCAAGCTTGGCGACAGCCTGACCGACAAT-3'; *Hind*III site underlined)

and P8 (5'-GGTTAATTAAAGCCCAAGCACCGGCGCGGTCGA-3'; *Pac*I site underlined). The plasmid pHis.BatA was generated by gel-purifying this 831-nt amplicon, digesting with *Hind*III and *Pac*I, and ligating in-frame with the N-terminal His-tag of vector pETcoco-1 (EMD Millipore). Likewise, a PCR product specifying aa 30 to 307 of the *batA* ORF was amplified from *B. pseudomallei* 1026b genomic DNA with the following primers; P9 (5'-CGGGATCCGGCGACAGCCTGACCGACAAT-3'); *Bam*HI site underlined) and P10 (5'-CCGCTCGAGTCCCAAGCACCGGCGCGGTCGA-3'; *Xho*I site underlined). The plasmid pGST.BatA was generated by gel-purifying this 831-nt amplicon, digesting with *Bam*HI and *Xho*I, and ligating in-frame with the N-terminal GST-tag of vector pGEX4T-2 (GE Healthcare Life Sciences).

5.3.3 Construction of the *batA* isogenic mutant in *B. mallei* ATCC23344.

Horizontal gene transfer from *E. coli* strain *s17* to *B. mallei* ATCC23344 via conjugation was used to generate the *batA* knock-out (KO) mutation, as reported previously (79, 252). After conjugation, the desired *B. mallei* ATCC23344 colonies were selected for resistance to polymyxin B (to prevent growth of *E. coli* S17) and zeocin (to select *B. mallei* ATCC23344 strains containing the disrupted copy of *batA* in their genome). Potential mutants were first screened for sensitivity to kanamycin to identify strains that do not contain the suicide vector pKAS46 integrated in their genome and then tested by PCR to identify strains with the mutated *batA* gene (data not shown). When compared by agarose gel electrophoresis, the *batA* KO mutant amplicon is smaller in size (4,700-nt) compared to the wild-type strain (6,000-nt). This 1,300-nt size

difference is compatible with the deletion of the internal 1,300-nt fragment from *batA* and subsequent insertion of the 400-nt zeocin resistance marker. The following primers were used: P11 (5'-AAGAGGGCATCAACATCCAG-3') and P12 (5'-GACGCCCGTCATCTATCTGT-3'). Lastly, the amplicon generated from the isogenic *batA* KO mutant strain was sequenced to verify proper allelic exchange and disruption of the *batA* gene.

Complementation of the *batA* KO mutant was also achieved by horizontal gene transfer via conjugation. Specifically, recombinant *E. coli* S17 strains containing the plasmids pBHR1.ΔDra and pBatA were conjugated with the *B. mallei batA* KO mutant (*BmbatA*KO). Transconjugates were selected for resistance to zeocin (indicating the presence of the *batA* KO mutation), kanamycin (indicating the presence of the plasmid of interest, either pBHR1.ΔDra or pBatA), and polymyxin B (to prevent the growth of *E. coli* S17).

5.3.4 Nucleotide sequence and bioinformatic analyses.

Chromatograms were assembled using Sequencher® 5 software (Gene Codes Corporation), and sequence analyses were performed using Vector NTI (Life Technologies™). Bioinformatic analyses were performed using various online tools available through the ExPASy Bioinformatics Resource Portal (http://www.expasy.org). Specifically, signal sequence cleavage sites were determined using the SignalP 4.1 server (http://www.cbs.dtu.dk/services/SignalP), and the structural features of the BatA protein were identified using the PSIPIRED Protein Structure Prediction server (http://bioinf.cs.ucl.ac.uk/psipred). Conserved domains were identified within the BatA gene (locus tag BMA1647)

using both the NCBI gene database (http://www.ncbi.nlm.nih.gov/gene) and the Pfam Database (http://pfam.xfam.org).

5.3.5 Lipolytic enzyme assays.

Lipolytic enzyme activity was quantified as reported by others (85, 253). Specifically, 10 mM stock solutions of p-nitrophenyl esters of acetate, butyrate, caproate, caprate, laurate, myristate, palmitate, and stearate were prepared in 2-propanol. These stock solutions were serially diluted to 1 mM in PBS (pH = 8.0) supplemented with 2.3 mg deoxycholic acid and 1.1 mg of gum arabic. Plate-grown bacteria were suspended in this PBS reagent (pH = 8.0) to a density of 75 Klett. 950-uL of each bacterial suspension was combined with 50-uL of each p-nitrophenyl ester. The absorbance of each sample was measured at 410 and 580 nm in order to determine esterase activity and bacterial cell density, respectively. Optical density was measured at time (T) 0 and 10 minutes at room temperature while shaking at 80 RPM. Enzyme activity was determined using the following formula: Rate = [((OD410 T_{10})-(OD410 T_0))/(OD580)]/10 minutes. These assays were performed on duplicate samples on at least three different occasions. Statistical analyses were performed using the Mann-Whitney test (GraphPad Prism 6 software), and *P* values < 0.05 are reported as statistically significant.

5.3.6 Murine macrophage assays.

Murine macrophage assays were performed as per Balder *et al*. (79). For macrophage killing assays with both *B. mallei* ATCC23344 and *B. thailandensis* DW503, bacteria were resuspended in 5-mL of sterile PBS to a density of 10^7 CFU/mL, and this suspension was then diluted to 10^6 CFU/mL (MOI 10:1). This

bacterial suspension was used to infect 24-well tissue culture (TC) plates containing duplicate monolayers of J774A.1 cells (immortalized BALB/c mouse macrophages) seeded at 5.0 x 10^5 cells/well. TC plates were centrifuged (165 x g for 5 minutes) and incubated for 1 hour at 37°C to allow for infection. The TC medium was then replaced with fresh TC medium supplemented with 50 µg/mL streptomycin to kill any remaining extracellular bacteria. After another incubation (1.5 hours at 37°C) the TC medium was replaced with fresh TC medium lacking antibiotics. One plate was incubated an additional 7.5 hours at 37°C to allow for intracellular replication of the bacteria in macrophages. The other TC plate was washed with TC medium one time prior to lysing the cells with saponin. Serial dilutions of each TC well were plated to determine the number of bacteria phagocytosed by the macrophages. This experiment was performed with duplicate samples on three separate occasions. Statistical analyses were performed using the Mann-Whitney test (GraphPad Prism 6 software), and *P* values < 0.05 are reported as statistically significant.

5.3.7 Antigen and antibody preparation and analysis.

Total membrane proteins and the sarkosyl-soluble fractions containing outer membrane (OM) proteins were obtained as described by Carlone *et al.* (220). The method used to prepare whole cell lysates (WCL) and perform western blot experiments are described previously (217). To express and purify His- and GST-tagged BatA proteins, the plasmids pHis.BatA and pGST.BatA were electroporated in the *E. coli* strain TUNER^{TM} (EMD Millipore). Both proteins were extracted from inclusion bodies and purified under denaturing conditions as

previously described by the Lafontaine laboratory (85, 221). Purified capsular polysaccharides (CPS) from the *Burkholderia pseudomallei* LPS^- mutant strain MB100 (58) were kindly provided by Donald E. Woods at the University of Calgary.

Polyclonal α-BatA antibodies were obtained by immunizing female BALB/c mice (Frederick National Laboratory for Cancer Research) with a 1:1 mixture composed of purified His-tagged BatA emulsified in Freund's adjuvant (SIGMA-ALDRICH®) as reported previously by Lafontaine and colleagues (223). Serum antibodies were demonstrated to recognize BatA by western blot using purified GST-tagged BatA (data not shown). The BatA-specific monoclonal antibody was generated by fusing splenocytes from a vaccinated mouse with Sp2/mIL6 cells (ATCC CRL 2016). The fused cells were plated in methylcellulose medium containing hypoxanthine, aminopterin, and thymidine using a ClonaCell HY kit per the manufacturer's specifications (Stemcell Technologies). Hybridomas secreting antibodies specific for BatA were identified by ELISA using purified GST-tagged BatA.

Naïve and immune polyclonal mouse sera obtained from lethal challenge experiments were treated in two ways. First, untreated polyclonal sera was filter sterilized with a 0.22 μm syringe filter (Millex®). Next, polyclonal sera were incubated with 2.0 mL *B. mallei* ATCC 23344 at room temperature and continuously mixed using a rotisserie mixer for 30-min in a biosafety cabinet in order to bind and remove host antibodies with affinity for constitutively expressed antigens on the surface of *B. mallei*, like capsular polysaccharide [CPS] and

lipopolysaccharide [LPS]. The supernate (adsorbed sera) was then separated from the bacteria via centrifugation at 4000-RPM for 10 minutes and filter sterilized as mentioned previously. Immunoglobins from filter-sterilized naïve and immune sera were also affinity purified using filter columns coated with recombinant fusion proteins A and G (NAb^{TM} Protein A/G Spin Columns, Pierce® Thermo Scientific), after which both constitutive and *in vivo* expressed antibodies (purified antibodies) were eluted with 100 mM glycine (pH = 2.5), neutralized, and dialyzed.

For ELISA, duplicate wells of Immulon^{TM} 2HB plates (Thermo Scientific Nunc) were coated with purified antigens and incubated overnight at 4°C. Unbound antigens were washed off with 1x wash solution (KPL) and the wells were filled with 10% BSA Diluent/Blocking solution (KPL) diluted to 0.5% with PBS and supplemented with 3% (wt/vol) dry milk (blocking buffer). After incubating 1 hour at room temperature, the wells were washed with the wash solution and probed for 1 hour with primary antibody diluted in blocking buffer. Primary antibodies used include sera from mice that survived aerosol infection with *B. mallei* ATCC23344, serum from mice immunized with His-tagged BatA, and culture supernates from fused splenocytes producing monoclonal anti-BatA antibodies). After incubation, the wells were washed with the wash solution and incubated at room temperature with goat anti-mouse secondary antibodies conjugated to alkaline phosphatase (KPL) diluted in blocking buffer. Excess secondary antibodies were removed by washing with wash buffer, and 100 µL of pNPP substrate solution (KPL) was added. The absorbance of this colormetric

assay was measured at an optical density (OD) of 405 nm using a μQuant™ Microplate Reader Spectrophotometer (BioTek®).

5.3.8. Immunofluorescence assays.

The binding of treated and untreated immune sera to antigens on the surface of *B. mallei* was measured by flow cytometry as described by Lipski and colleagues (199). Plate-grown bacteria (incubated 40-hr) were fixed with 4% (wt/vol) paraformaldehyde, probed with the appropriate polyclonal antibodies, and incubated with a goat α-mouse antibody labeled with Alexa Fluor 488. Labeled bacteria were analyzed using a BD LSR II flow cytometer.

5.3.9. Aerosol infection, vaccination, and passive transfer experiments.

Female BALB/c mice, aged 14-28 weeks, were purchased from Frederic National Laboratory for Cancer Research. The animals were anesthetized via intraperitoneal injections with 250 mg/kg of 2, 2, 2 tribromoethanol (TBE, SIGMA-ALDRICH®). Once completely anesthetized, 50 μL of bacterial suspensions were administered intratracheally using a Microsprayer® model I-1C (PennCentury™), as reported previously by the Lafontaine Laboratory (169, 254). Infected mice were monitored twice daily, and food and water were provided *ad libitum*. Humane end-points as referenced previously (169) were strictly observed. Mice exhibiting moderate to severe signs of discomfort were euthanized via intraperitoneal injection with TBE followed by cervical dislocation, in accordance with the 2013 AVMA Guidelines on Euthanasia. Pulmonary and splenic tissues were aseptically collected, homogenized with 15-mL Fisherbrand™ disposable tissue grinders (Thermo Scientific), serially-diluted, and plated on agar to

determine bacterial burdens. Survival data were analyzed using the Kaplan-Meir method, and the LD_{50} values were calculated according to Reed and Muench (174).

Mice were vaccinated with the *Bmbat*AKO strain via the aerosol route using the Microsprayer device as described above. Thirty days post-vaccination, these mice were challenged with 10 LD_{50} of *B. mallei* ATCC 23344 (8,000 CFU) or 5 LD_{50} of *B. pseudomallei* strain 1026b (25,000 CFU). For passive transfer experiments, mice were administered serum samples via intraperitoneal injection ($\leq$ 1-mL). Forty eight hours later, mice were challenged with 10 LD_{50} of *B. mallei* ATCC 23344. The lungs, spleen, and liver from surviving animals were homogenized in 2-mL of sterile PBS, serially diluted, and spread onto agar medium to determine bacterial burden. The results are expressed as total CFU in tissues. Symbols represent individual animals.

5.3.10 Compliance and animal research ethics statements.

The University of Georgia's Institutional Biosafety Committee (IBC) approved the experiments in this study. All experiments with live *B. mallei* were performed inside a Class II Biosafety Cabinet in a BSL3 laboratory in compliance with the rules and regulations of the U.S. Federal Select Agent Program (SAP).

The University of Georgia's Institutional Animal Care and Use Committee (IACUC) approved the animal experiments in this study. All animal experiments were carried out in strict accordance with the recommendations in the Guide for the Care and Use of Laboratory Animals of the National Institutes of Health (NIH). Every effort was made to minimize animal suffering.

5.4 Results

5.4.1 Features of *batA* genomic locus and gene product.

Sequence analysis identified the *B. mallei* ATCC23344 *batA* ortholog on chromosome 1 of the published genome (locus tag BMA1647), with an open reading frame (ORF) that is 1,833-nt in length and predicted to specify a 610-aa protein with a molecular mass of 64 kDa. The BatA protein has the features of a conventional AT, including a large barrel-shaped, membrane-anchoring transporter domain at the C-terminus composed of 12 anti-parallel β-strands, an alpha-helical linker region, and a surface-exposed passenger domain at the N-terminus. A putative signal sequence cleavage site is predicted to occur between amino acid residues 24 and 25. Comparison of BatA to other protein sequences also identified the presence of GDSL-hydrolase in the passenger domain (Figure 5.1, Table 5.2). While GDSL hydrolases are members of a diverse family of lipases and esterases, they possess a unique tertiary fold and an active site that closely resembles the Ser-His-Asp (Glu) triad of serine hydrolases. Experimentally, they have been demonstrated to be promiscuous enzymes, acting on a variety of substrates, and they are thought to catalyze the fatty acid transfer between phosphatidylcholine and sterols (255, 256).

5.4.2 Expression and functional analysis of the BatA protein in *B. thailandensis.*

Since the sequence and predicted structure of BatA resembles that of other known bacterial virulence factors, like McaP, a bacterial adhesin with lipolytic enzyme activity in *Moraxella catarrhalis,* we hypothesized that BatA would have lipolytic enzyme activity. To determine if BatA directly mediates lipolytic

enzyme activity, the *batA* gene of *B. mallei* ATCC23344 was cloned and expressed in the recombinant background of *B. thailandensis* DW503. BatA expression was verified by western blot analysis using whole cell lysates (WCL), concentrated culture supernates (SUP), heated bacterial pellets (HEAT), total membrane proteins (TMP), and sarkosyl-insoluble fractions containing outer membrane proteins (OMP) prepared from *B. thailandensis* DW503 harboring either the plasmid pBHR1.ΔDra (control) or the pBatA plasmid (specifies *batA* from *B. mallei* ATCC23344), respectively. Figure 5.2 demonstrates that polyclonal murine sera reacts with all protein fractions in *B. thailandensis* expressing BatA. An additional band is noted in both the SUP and HEAT samples. The smaller band at 64 kDa is compatible with recombinant bacteria expressing the AT in its monomer form, while the larger band just below 148 kDa likely indicates the presence of AT dimers (predicted molecular mass ~138 kDa). This result is not surprising as many AT are capable of polymerizing when secreted or released from bacteria via heat (257-262).

Next, we tested the recombinant *B. thailandensis* strains for lipolytic enzyme activity using a colormetric assay with p-nitrophenyl esters and lipids. As shown in Figure 5.3 A and B, *B. thailandensis* constitutively expressing BatA preferentially cleaves the carboxylic ester bond in p-nitrophenyl acetate, suggesting it may function as an acetylesterase. No significant difference was observed between the recombinant *B. thailandensis* strains regarding their ability to cleave the other esters and lipids tested (Figure 5.3 A).

5.4.3 Expression and functional analysis of the BatA protein in *B. mallei.*

To examine the function of the BatA gene product in its native background of *B. mallei*, we constructed an isogenic *batA* knock-out (KO) mutant of *B. mallei* ATCC23344. Western blots of WCLs prepared from WT and recombinant mutant strains were examined and verified lack of BatA expression in the isogenic KO mutant complemented with pBHR1.ΔDra and constitutive BatA expression in the mutant complemented with pBatA. Interestingly, BatA expression was not detected in WT *B. mallei* when grown *in vitro* (Figure 5.4).

To determine if BatA plays a role in the virulence of *B. mallei*, we determined the median lethal dose (LD_{50}) of the mutant using a mouse model of aerosol infection. To determine *in vivo* fitness, we also collected pulmonary and splenic tissues from survivors and quantified the bacterial loads in these organs. All mice infected with WT *B. mallei* succumbed to infection within 7 days. In contrast, > 60% of mice infected with the *batA* KO mutant (*BmbatA*KO) survived infection (Figure 5.5 A). We discovered that the *batA* mutation attenuates *B. mallei* virulence >1000-fold (Figure 5.5 B), and that at equivalent inoculating doses, bacterial loads in the lungs (Figure 5.5 C) and spleen (Figure 5.5 D) of the survivors were markedly reduced to even absent in mice infected with the *batA* mutant. This attenuation could not be attributed to *in vitro* defects in the mutant growth rate (data not shown).

To determine if *BmbatA*KO persistently colonized the mouse after infection, the lethal challenge experiment was repeated but extended from 15 to 30 days post-infection. Once again, mice infected with the ≥ 3,549 CFU (LD_{50})

WT *B. mallei* succumbed to infection, while mice had to be infected with ≥ 885,437 CFU (LD_{50}) to succumb to infection with *BmbatA*KO, indicating substantial (250-fold) attenuation in the virulence of *B. mallei* (Figures 5.6 A and B). Furthermore, the tissues collected from survivor mice at 30-days post-infection with *BmbatA*KO were agent-free, compared to the tissues collected from survivor mice at 30-days post-infection with WT *B. mallei* (Figures 5.6 C and D). This finding indicates that mice are transiently colonized with *BmbatA*KO, compared to their persistently infected WT *B. mallei* counterparts.

The functional properties of BatA and its contribution to virulence were further evaluated by complementing the *batA* KO mutant with either a plasmid that constitutively-expresses BatA (pBatA) or a plasmid that lacks BatA expression (pBHRI.ΔDra). Figure 5.4 demonstrates that the recombinant *B. mallei* strain expresses a 64 kDa antigen compatible with BatA, as expected. Interestingly, lethal challenge experiments with the plasmid-complemented *batA* KO mutant (*BmbatA*KO pBatA) revealed > 60% of infected mice survived infection compared to just 20% survival with the isogenic *batA* KO mutant-infected mice (*BmbatA*KO pBHRI.ΔDra) and no survival with WT *B. mallei* (Figure 5.7 A). The *batA* KO mutant carrying the control plasmid, pBHR1.ΔDra demonstrated >1000-fold reductions in LD_{50} when compared to WT (Figure 5.7 B), which is consistent with the >1000-fold attenuation in virulence measured for the mutant without the plasmid (Figure 5.5 B). However, the LD_{50} of the *batA* KO mutant possessing the pBatA plasmid was 3-fold lower than the mutant possessing the control plasmid and >3500- fold lower that the WT strain (Figure

5.7 B). Likewise, bacterial loads in the lungs (Figures 5.7 C) and spleen (Figure 5.7 D) of surviving mice were either markedly reduced to absent in the *batA* KO mutant and complemented *batA* KO mutant strains when compared to WT *B. mallei*.

Since BatA plays a substantial role in the virulence of *B. mallei,* we next sought to determine if the isogenic *batA* KO mutant was impaired in its ability to survive and replicate in host cells. Specifically, we compared the intracellular replication of *BmbatA*KO in J774.A1 murine macrophages to WT *B. mallei* and an isogenic *ilv1* KO mutant in *B. mallei*, which is has a well-characterized intracellular replication defect (263). Like the isogenic *ilv1* KO mutant, the isogenic *batA* KO mutant exhibited significantly decreased intracellular survival in murine macrophages when compared to WT *B. mallei* (Figure 5.8).

Given the mutation in *batA* greatly attenuates *B. mallei* virulence and results in transient tissue colonization with a reduced the ability of *B. mallei* to replicate within murine macrophages, we hypothesized that vaccination with the *batA* mutant strain would elicit protective immunity against back-challenge with wild-type *B. mallei* and *B. pseudomallei*. To test this, mice vaccinated with 10^5 CFU of the isogenic *batA* KO mutant strain (*BmbatA*KO) were challenged 30 days later with lethal doses of WT *B. mallei* ATCC 23344 or *B. pseudomallei* 1026b. We discovered in replicate experiments that vaccination with *BmbatA*KO provides 77% and 68% protection against acute infection with *B. mallei* and *B. pseudomallei*, respectively. These experiments also revealed that 56% of mice

that survived *B. pseudomallei* infection developed sterilizing immunity (Table 5.4).

5.4.4 Characterization of the protective immune response elicited by the live attenuated isogenic *batA* mutant strain.

The contribution of humoral-derived antibodies to the protection elicited by vaccinating mice with *BmbatA*KO was determined by performing passive transfer experiments. Specifically, serum was collected from mice vaccinated with the *BmbatA*KO 30 days prior, and different volumes of this sera and was transferred to naïve mice via intraperitoneal injection (0.2 mL or 1.0 mL per mouse). Two days after serum transfer, animals were challenged with a lethal dose of *B. mallei* ATCC 23344. We discovered that mice immunized with 0.2 mL of immune sera succumbed to infection. However, mice immunized with 1.0 mL immune sera were protected against lethal challenge. Specifically, 100% survival was observed during acute infection, and 71% survival was observed up to 45 days post challenge (Table 5.4). These findings indicate that protective antibodies are generated upon vaccination with *BmbatA*KO, but that this protection is dose-dependent.

To determine if the protective antibodies in this immune sera were against antigens expressed either constitutively or *in vivo*, the immune sera was treated as referenced in the Materials and Methods and outlined in Figure 5.9 to generate both adsorbed sera and affinity-purified antibodies. ELISAs were performed to detect these antibodies using plates coated with either paraformaldehyde-fixed *B. mallei,* purified *B. pseudomallei* capsular polysaccharides (CPS), or purified

oligosaccharide chains of *B. pseudomallei* LPS (OPS). These experiments revealed that the immune sera contain increased antibody titers against unique antigens expressed *in vivo*, rather than to constitutively expressed antigens like CPS and OPS (Figure 5.10). Passive transfer experiments were also repeated as before using the aforementioned immune sera, adsorbed sera, and purified antibodies. These experiments allowed us to determine that the unique antibodies in immune sera provide robust protection against infection with WT *B. mallei* and *B. pseudomallei* strains when compared to their naïve sera counterparts (Table 5.5).

Lastly, we sought to determine if constitutive and *in vivo* expressed antibodies would opsonize *B. mallei* ATCC 23344 for phagocytosis by J774.A1 murine macrophages. First, we determined that the *in vivo* antibodies in this immune mouse sera were capable of binding to the surface of *B. mallei* ATCC 23344 (Top Panel, Figure 5.11). Next, we incubated *B. mallei* with the following antibody treatments for 30 minutes at 37°C and 80 RPM: no serum, naïve sera, immune sera, naïve adsorbed sera, immune adsorbed sera, purified naïve antibodies, and purified immune antibodies. After this incubation, J774.A1 murine macrophages were infected as described previously, and the amount of *B. mallei* that were phagocytosed (Middle Panel, Figure 5.11) and then replicated intracellularly (Bottom Panel, Figure 5.11) were determined. We demonstrate that immune sera, immune adsorbed sera, and purified immune antibodies not only increase the phagocytosis of *B. mallei* by murine macrophages but also decrease their intracellular replication when compared to their naïve counterparts and no

serum. These results indicate that antibodies against both constitutively and *in vivo* expressed antigens on the surface of the bacteria contribute to the opsonization, phagocytosis, and intracellular destruction of *B. mallei* ATCC 23344 by murine macrophages.

5.5 Discussion

This study demonstrates that BatA is a conventional AT that may function as an acetylesterase, contributes to the intracellular survival of *B. mallei* in murine macrophages, and is also critical for the virulence of *B. mallei* in a murine model of aerosol infection. We demonstrate that BatA is expressed *in vivo* and elicits the production of unique antibodies that protect against infection with *B. mallei*, suggesting BatA possesses properties of an excellent vaccine candidate. Furthermore, we show that vaccination with the live-attenuated isogenic *batA* KO mutant (*BmbatA*KO) protects against acute and chronic infection with both *B. mallei* and *B. pseudomallei*.

We report that the constitutive expression of BatA by recombinant *B. thailandensis* DW503 indicates this AT may function as an acetylesterase that preferentially cleaves the carboxylic ester bond in p-nitrophenyl acetate, yielding acetate and alcohol. Experiments are currently underway to determine if the isogenic *batA* KO mutant has impaired acetylesterase activity, and if this activity can be restored by plasmid complementation of this mutant. Precedents in the literature exist to support the role bacterial esterases can play in virulence. One of the most compelling is Streptococcal secreted esterase (Sse), a CovRS-regulated virulence factor that has been demonstrated to be important for the virulence of Group A *Streptococcus* in subcutaneous infection in

mice (264) by hydrolyzing platelet-activating factor (PAF) to impede neutrophil recruitment and evade the host immune system (265).

We also demonstrate that BatA contributes to the intracellular survival of *B. mallei* in J774.A1 murine macrophages. While the exact mechanism by which BatA promotes the intracellular survival of *B. mallei* remains to be determined, there is precedence in the literature for enzymes with GDSL motifs contributing to the intracellular survival and dissemination of other lung pathogens. For example, it has been demonstrated that *Legionella pneumophila* uses PlaC to hydrolyze phosphatidylcholine and acylate host cell cholesterol, enabling it to attack host cell membranes (266, 267). Similarly, phospholipase B1 (Plb1) produced by *Cryptococcus neoformans* has been shown to be critical for its intracellular growth in host macrophages, as deletion of *plb1* causes a decrease in intracellular proliferation and increased killing within the phagosome (268).

To our knowledge, this is the first report of a conventional AT contributing to the pathogenesis and virulence of either *B. mallei* or *B. pseudomallei.* Recently, Galyov *et al*. reported that mutating the *B. pseudomallei* ortholog of *batA* (BPSL2237) had no effect on the survival of *B. pseudomallei* in J774.2 murine macrophages, and that this mutation also failed to attenuate the virulence of *B. pseudomallei* in a murine model of intraperitoneal infection (269). Likewise, we demonstrated that an isogenic *batA* mutation introduced into the genome of *B. pseudomallei* did not attenuate virulence in our murine model of aerosol infection (Table 5.3). These contradictory findings may simply reflect a fundamental difference in the lifestyle and pathogenesis of these two bacterial species. However, it is known that the temporal expression of surface-exposed antigens by

bacterial organisms can play a significant role in their pathogenesis (270, 271). It would be interesting to examine the effects of constitutive BatA expression by *B. pseudomallei,* particularly as neither us nor Galyov and colleagues performed such experiments.

The discovery that constitutive expression of BatA by the isogenic *batA* KO mutant (*BmbatA*KO) further attenuated rather than restored the virulence of *B. mallei* was very surprising. Median lethal dose experiments determined that the *BmbatA*KO mutant possessing pBHRI.ΔDra reduced virulence >1000-fold compared to WT *B. mallei* (Figure 5.7), whereas the *BmbatA*KO mutant possessing pBatA and constitutively expressing BatA reduced virulence >3500-fold compared to WT. We also demonstrate that WT *B. mallei* do not express BatA when cultured *in vitro* (Figure 5.4). These data suggest that the expression of BatA by *B. mallei* during host infection must be closely and temporally regulated, as both the lack of expression and the constitutive expression of BatA are detrimental to the virulence of *B. mallei in vivo.* We previously reported on a similar phenomenon with the oligomeric AT, BpaB, which functions as a novel biofilm factor and contributes to the virulence of *B. mallei* in a murine model of aerosol infection (14). Other precedents also exist in the literature to support this finding. For example, the constitutive expression of *Salmonella enterica* flagellum (243), *Yersinia pestis* F1 capsule (244), and *Cryptococcus neoformans* adhesin Cf11 (242) have been demonstrated to substantially attenuate virulence. This unique phenomenon has led to the emergence of a novel live-attenuated vaccine strategy referred to as Attenuating Gene Expression (AGE) (245). The exact mechanism by which constitutive BatA expression attenuates virulence is currently being investigated.

This study also demonstrated that the isogenic *batA* KO mutant (*BmbatA*KO) was a novel live-attenuated mutant strain of *B. mallei* with excellent vaccinogenic potential. To date, the Federal Select Agent Program has not approved the exclusion of an attenuated *B. mallei* strain from the Tier 1 Select Agent list for experimental use. Ulrich *et al*. reported the characterization of two live-attenuated *B. mallei* strains, a capsule mutant (DD3008) and a branched-chain amino acid auxotroph (Ilv1), and evaluated their potential as vaccines against aerosol-initiated glanders in mice. Their study showed that vaccination with *B. mallei* ILV1 protected 50% of mice against acute infection with WT *B. mallei*, and yielded high IgG1 titers (263). Similar to our study, they also report the transient colonization of mice with *B. mallei* ILV1 and the persistence of WT *B. mallei* in the tissues of chronically-infected mice. Unlike our study, they did not evaluate whether *B. mallei* ILV1 protected against infection with *B. pseudomallei*, and they did not perform passive transfer experiments with the IgG1 antibodies to determine if they were truly protective *in vivo*.

Other live-attenuated *B. mallei* strains have been characterized to date, such as the *tonB* mutant (272, 273) and *ctpA* mutant (274). While these mutants offer protection against challenge, both persist in murine tissues after infection, and neither has equaled the robust protection elicited by vaccination with *B. mallei* ILV1 and *BmbatA*KO. Unlike these other studies, we also report that the unique *in vivo* expressed antibodies generated by vaccination with *BmbatA*KO likely function as opsonins, given *B. mallei* incubated with immune serum, adsorbed serum, and purified antibodies are phagocytosed in larger numbers by murine macrophages when compared to their naïve serum and no serum counterparts. Even more exciting, opsonized *B. mallei* once internalized by murine

macrophages, fail to replicate within the host cells, suggesting the ability of murine macrophages to kill engulfed *B. mallei* may be restored.

Overall, our data demonstrate that BatA is an important virulence factor of *B. mallei* and that studying AT provides a platform to gain new knowledge about immunity against the organism, including protective antigen discovery. There is currently no vaccine available for *B. mallei,* and there is concern that the organism may be used as a biological warfare agent. Hence, our findings are relevant to the development of medical countermeasures and improved diagnostic tests for glanders.

5.6 Acknowledgements

This study was supported by DTRA contract HDTRA1-12-C0081 and a Zoetis-Morris Animal Foundation Veterinary Fellowship for Advanced Study to Shawn M. Zimmerman (D12ZO-902).

Table 5.1. Strains and plasmids.

Strain or plasmid	Description	Source or reference
Strains		
B. mallei		
ATCC 23344	Wild-type strain (equine clinical isolate); resistant to Polymyxin B and sensitive to kanamycin and zeocin	(5)
batA KO	Isogenic *batA* mutant strain of ATCC23344; resistant to Polymyxin B and sensitive to kanamycin and zeocin	This study
B. thailandensis		
DW503	Parental strain (B. thailandensis E264 derivative); resistant to Polymyxin B and sensitive to kanamycin and zeocin	(216)
E. coli		
EPI300™	Electrocompetent cloning strain	epicentre® Illumina®
S17	Strain used for conjugational transfer of plasmids pBHR1.ΔDra, pBatA, and pKASbatA.zeo to *B. mallei*; sensitive to Polymyxin B	(246)
TUNER™	Expression strain used for purification of His- and GST-tagged BatA proteins	EMD Millipore
Plasmids		
pBHR1	Broad host range cloning vector; resistant to chloramphenicol and kanamycin resistance markers	MoBiTec Molecular Biotechnology
pBHR1.ΔDra	pBHR1 containing a 339-nt deletion in the chloramphenicol resistance marker; resistant only to kanamycin	This study
pBatA	pBHR1ΔDra containing the *B. mallei* ATCC 23344 *batA* gene; resistant to kanamycin	This study
pCC1™	Cloning vector; contains chloramphenicol resistance marker	epicentre® Illumina®
pCC.batA	pCC1 containing the *B. mallei* ATCC 23344 *batA* gene; resistant to chloramphenicol	This study
pCC.batA.zeo	pCC.batA in which a 1.3-kb fragment internal to the *batA* ORF is replace with a 0.4-kb zeocin resistance cassette; resistant to chloramphenicol and zeocin	This study
pKAS46	Mobilizable suicide plasmid; resistant to kanamycin	(246)
pKAS.batA.zeo	pKAS46 containing the insert from pCC.batA.zeo; resistant to kanamycin and zeocin	This study
pEM7/ZEO	Source of the zeocin resistance marker	Life Technologies™
pETcoco™-1	Protein expression vector; chloramphenicol resistant	EMD Millipore
pHis.BatA	pETcoco-1 expressing BatA residues 30-307 joined to an N-terminal His-tag; resistant to chloramphenicol	This study
pGEX4T-2	Protein expression vector; resistant to ampicillin	GE Healthcare Life Sciences
pGST.BatA	pGEX4T-2 expressing BatA residues 30-307 joined to an N-terminal GST-tag; resistant to ampicillin	This study

Table 5.2. Regions of BatA gene product with high level of sequence similarity to conserved domains in the NCBI Entrez Conserved Domain Database (CDD).

BatA residues	E-value	CDD domain	CDD number	Description
25-293	9.21e-63	Fatty-acyltransfase-like subfamily of SGNH Hydrolase Superfamily	238882	Fatty acyltransferase-like subfamily of the SGNH hydrolases or GDSL hydrolases, a diverse family of lipases and esterases. The tertiary fold of the enzyme is substantially different from that of the α/β hydrolase family and is unique among all known hydrolases. Its active site closely resembles the Ser-His-Asp (Glu) triad of other serine hydrolases. They may catalyze fatty acid transfer between phosphatidylcholine and sterols.
345-593	2.42e-22	Outer Membrane Channel Superfamily	214872	Autotransporter β-domain. A member of the porin superfamily; these intermembrane outer membrane channels have a beta-barrel domain that transports the protein. This domain is found at the C-terminus of the protein, while the N-terminus contains the variable passenger domain that translocates across the membrane. Once the passenger domain is exported it is cleaved auto-catalytically in some proteins, in others a different peptidase is used and in some cases no cleavage occurs.

Table 5.3. Mutation of *batA* does not attenuate the virulence of *B. pseudomallei.*

Strain	**Inoculum (CFU)**	**% survival**	**LD50(CFU)**
WT	650	100	2,741
	6,500	20	
	65,000	0	
	650,000	0	
*bca2*KO	690	20	≤ 690
	6,900	0	
	69,000	0	
	690,000	0	

Table 5.4. The live attenuated BmbatAKO strain protects against lethal challenge with *B. mallei* and *B. pseudomallei.*

# of independent experiments	Vaccine	Agent used in challenge	Total # of mice challenged	Survival, acute (1-10 dpi)	Survival, chronic (11-45 dpi)	Sterilizing immunity
8	*Bmbat*AKO	*Bm* ATCC 23344	66	77%	65%	0%
	Saline (control)		64	6%	3%	0%
6	*Bmbat*AKO	*Bp* 1026b	58	68%	67%	56%
	Saline (control)		50	0%	0%	0%

Table 5.5. Passive transfer of immune sera and antibodies protects against challenge with *B. mallei.*

Treatment	Total # of mice challenged	Survival, acute (1-10 dpi)	Survival, chronic (11-45 dpi)
Vaccinated with *Bmbat*AKO	10	100%	70%
Immune serum	7	100%	71%
Naïve serum (control)	7	0%	0%
Adsorbed immune serum	7	86%	57%
Adsorbed naïve serum (control)	6	17%	0%
Purified immune antibodies	5	80%	60%
Purified naive antibodies	5	0%	0%

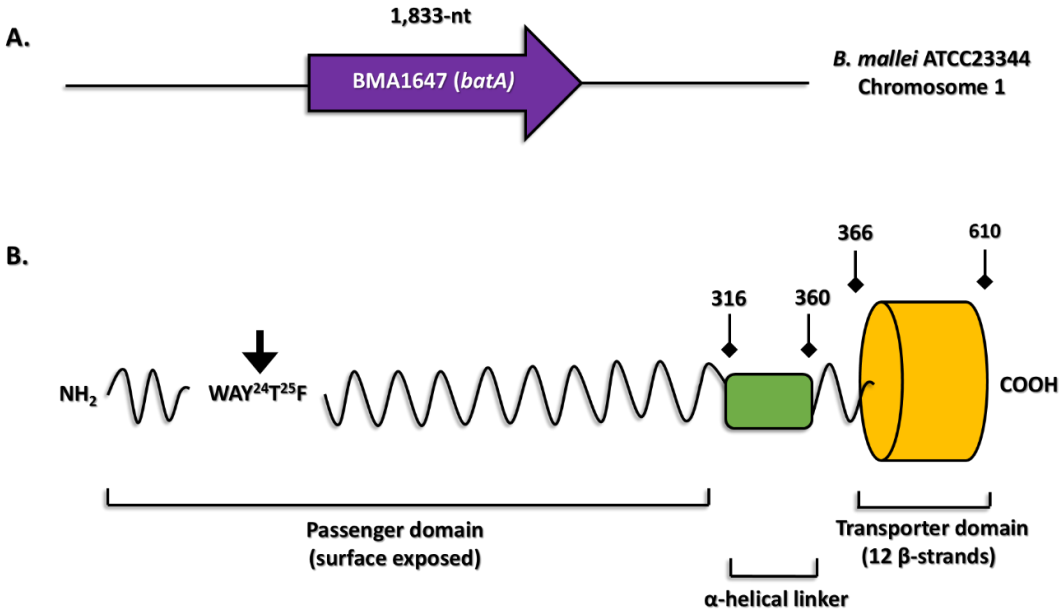

Figure 5.1. Schematic representation of the *B. mallei* ATCC23344 *batA* gene and gene product.

Panel A: Colored block arrow represents the *batA* ORF in chromosome I of *B. mallei* ATCC 23344. Panel B: Different regions of the predicted BatA protein are depicted with positions of residues defining selected domains. The C-terminal transporter domain and helical linker were identified using the PSIPRED server. The arrow represents the predicted signal sequence cleavage site, which was identified using the SignalP 4.1 server.

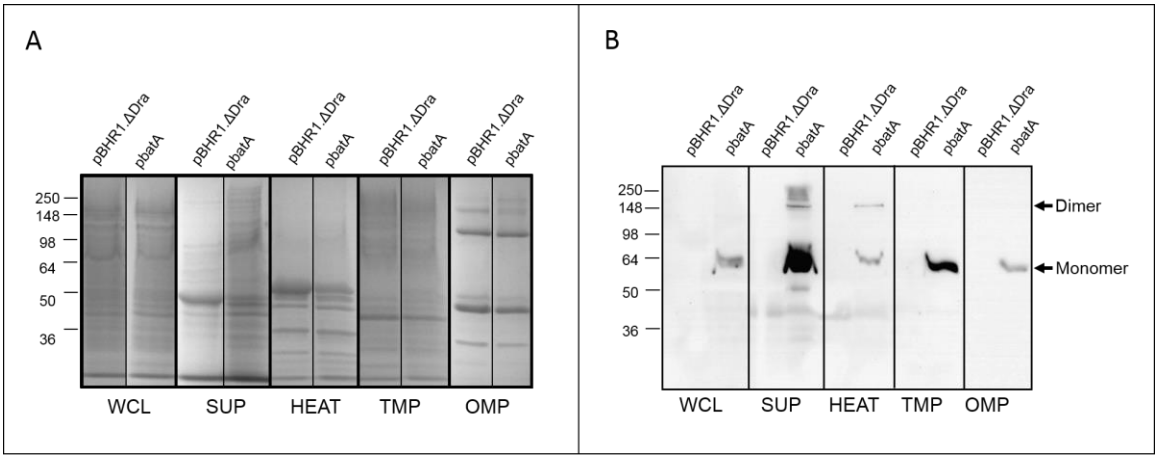

Figure 5.2. BatA expression by recombinant *B. thailandensis* strains.

Panel A: Equivalent amounts of whole cell lysates (WCL), precipitated culture supernate (SUP), precipitated heated cell pellet (HEAT), total membrane proteins (TMP), and sarkosyl-insoluble fractions containing OM proteins (OMP) were resolved by SDS-PAGE. Panel B: The bacterial fractions shown in Panel A were transferred to PVDF membranes and analyzed by western blot with α-batA polyclonal antibodies as described in the Materials and Methods. Molecular weight markers are shown to the left in kilodaltons (kDa).

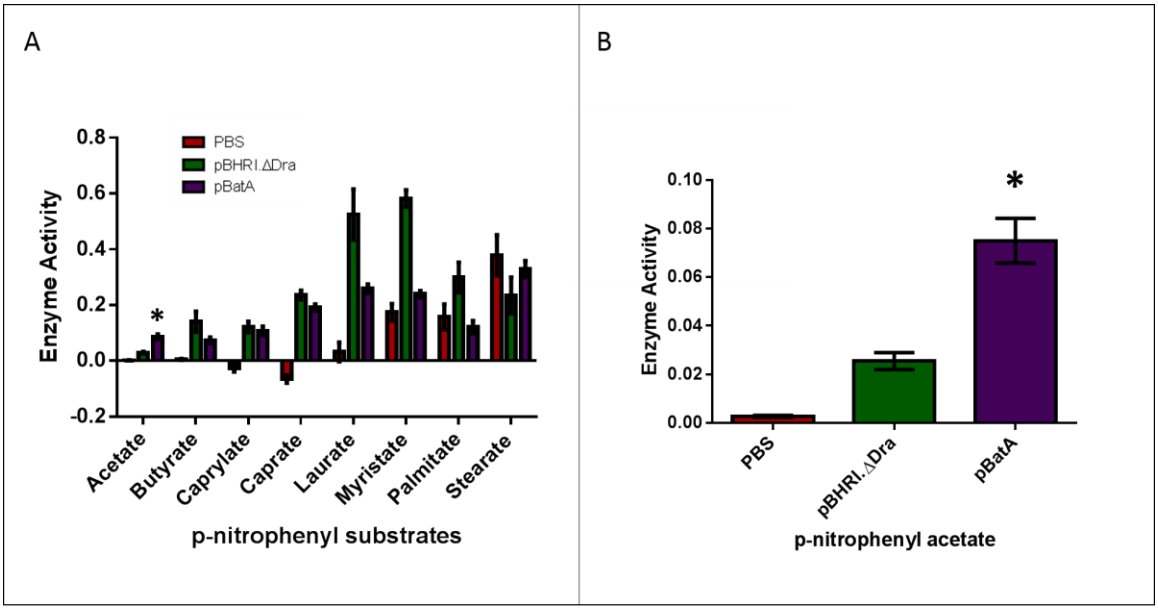

Figure 5.3. Acetylesterase activity exhibited by recombinant *B. thailandensis* strains.

Duplicate wells containing 950 uL of either phosphate-buffered saline at pH = 8.0 (PBS), *B. thailandensis* DW503 with the control plasmid (pBHRI.ΔDra), or *B. thailandensis* DW503 were prepared and the optical density at 580 nm was measured. Each well was then spiked with 50 uL of 1 mM pNP-acetate, incubated at 80 RPM at room temperature, and the optical density (410 nm) measured at 0 and 10 minutes. Enzyme activity was determined using the following formula: Rate = [((OD410 T_{10})-(OD410 T_0))/(OD580)]/10 minutes. These assays were performed on duplicate samples on at least three different occasions. (*) indicates the $P \leq 0.05$. Panel A: Summary of enzymatic activity exhibited by recombinant *B. thailandensis* strains for all the p-nitrophenyl substrates tested. Panel B: Acetylesterase activity exhibited by recombinant *B. thailandensis* strains.

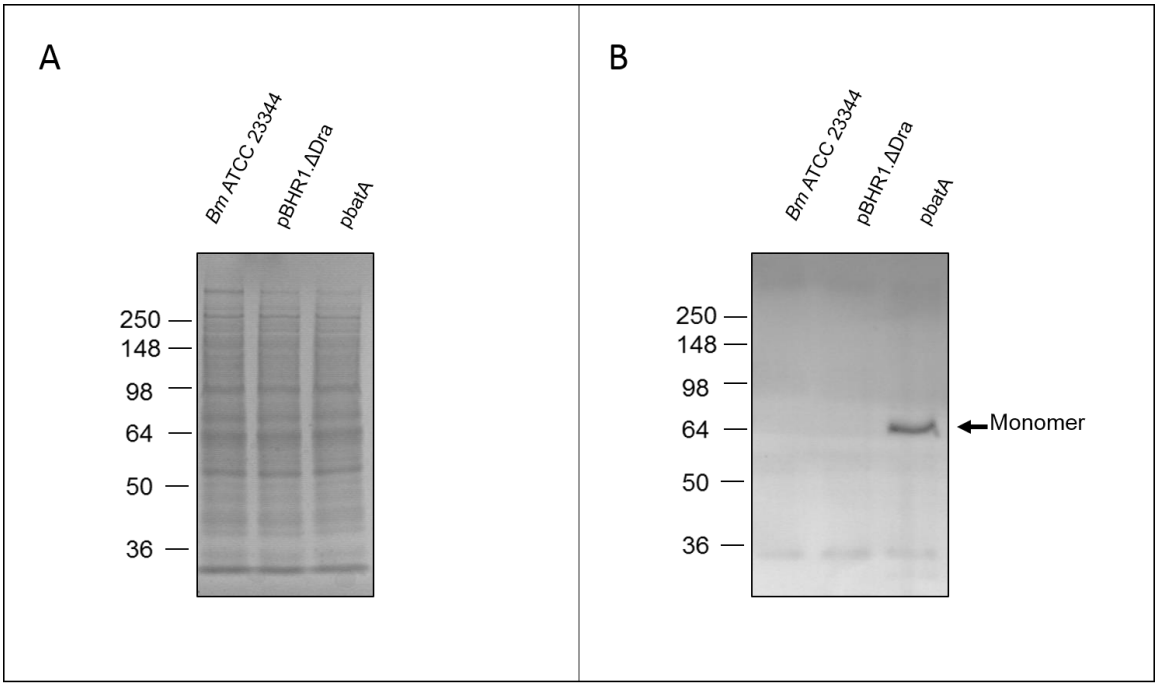

Figure 5.4. BatA expression by wild-type and recombinant *B. mallei* strains.

Panel A: Equivalent amounts of whole cell lysate (WCL) preparations were resolved by SDS-PAGE. Panel B: Whole cell lysate preparations were transferred to PVDF membranes and analyzed by western blot with α-batA polyclonal antibodies. Molecular weight markers are shown to the left in kilodaltons (kDa).

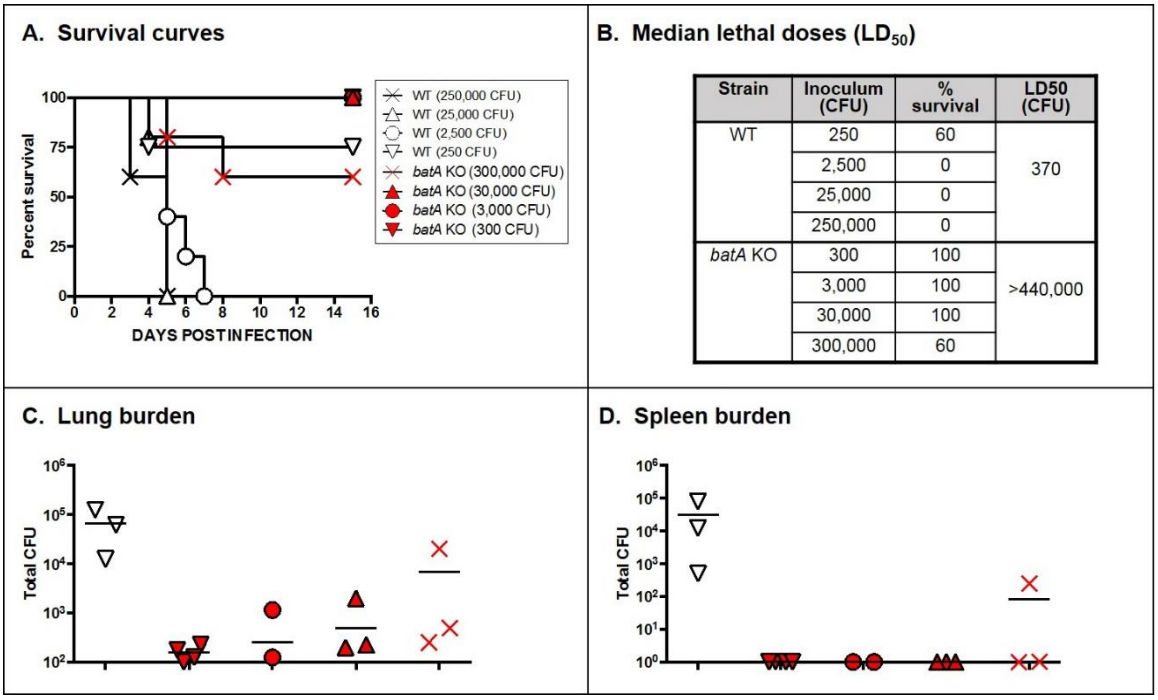

Strain	Inoculum (CFU)	% survival	LD50 (CFU)
WT	250	60	370
	2,500	0	
	25,000	0	
	250,000	0	
batA KO	300	100	>440,000
	3,000	100	
	30,000	100	
	300,000	60	

Figure 5.5. Mutation of *batA* attenuates the virulence of *B. mallei* and reduces bacterial burdens in mouse tissues.

Mice were inoculated intratracheally using a Microsprayer device to aerosolize the indicated number of bacterial CFU directly into the lungs (n=5 mice/dose). Animals were then monitored daily for clinical signs of illness and morbidity. The experimental duration was 15 days. Panel A: Survival curves. Panel B: Calculated LD_{50} values. Panels C and D: Tissues were collected from mice that survived challenge with 10^2 CFU, homogenized, diluted, and spread on agar plates to determine bacterial loads. Symbols show data for individual animals.

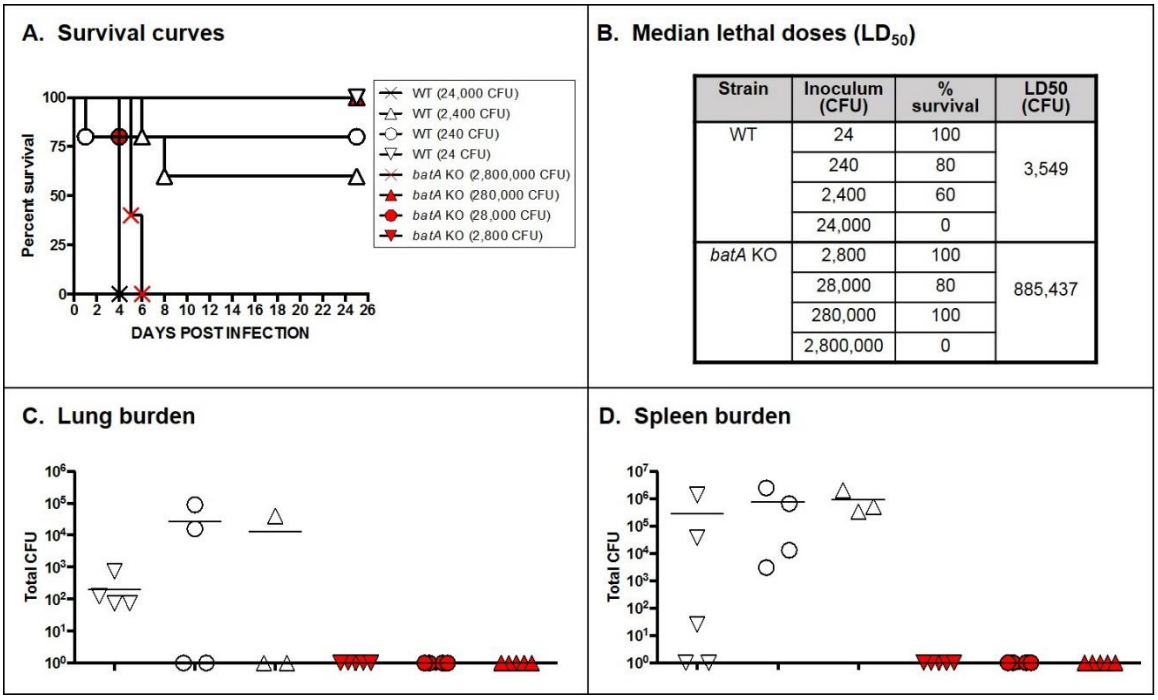

Strain	Inoculum (CFU)	% survival	LD50 (CFU)
WT	24	100	3,549
	240	80	
	2,400	60	
	24,000	0	
batA KO	2,800	100	885,437
	28,000	80	
	280,000	100	
	2,800,000	0	

Figure 5.6. Mutation of *batA* attenuates the virulence of *B. mallei* and transiently colonizes mouse tissues.

Mice were inoculated intratracheally using a Microsprayer device to aerosolize the indicated number of bacterial CFU directly into the lungs (n=5 mice/dose). Animals were then monitored daily for clinical signs of illness and morbidity. The experimental duration was 30 days. Panel A: Survival curves. Panel B: Calculated LD_{50} values. Panels C and D: Tissues were collected from mice that survived challenge with 10^2 CFU, homogenized, diluted, and spread on agar plates to determine bacterial loads. Symbols show data for individual animals.

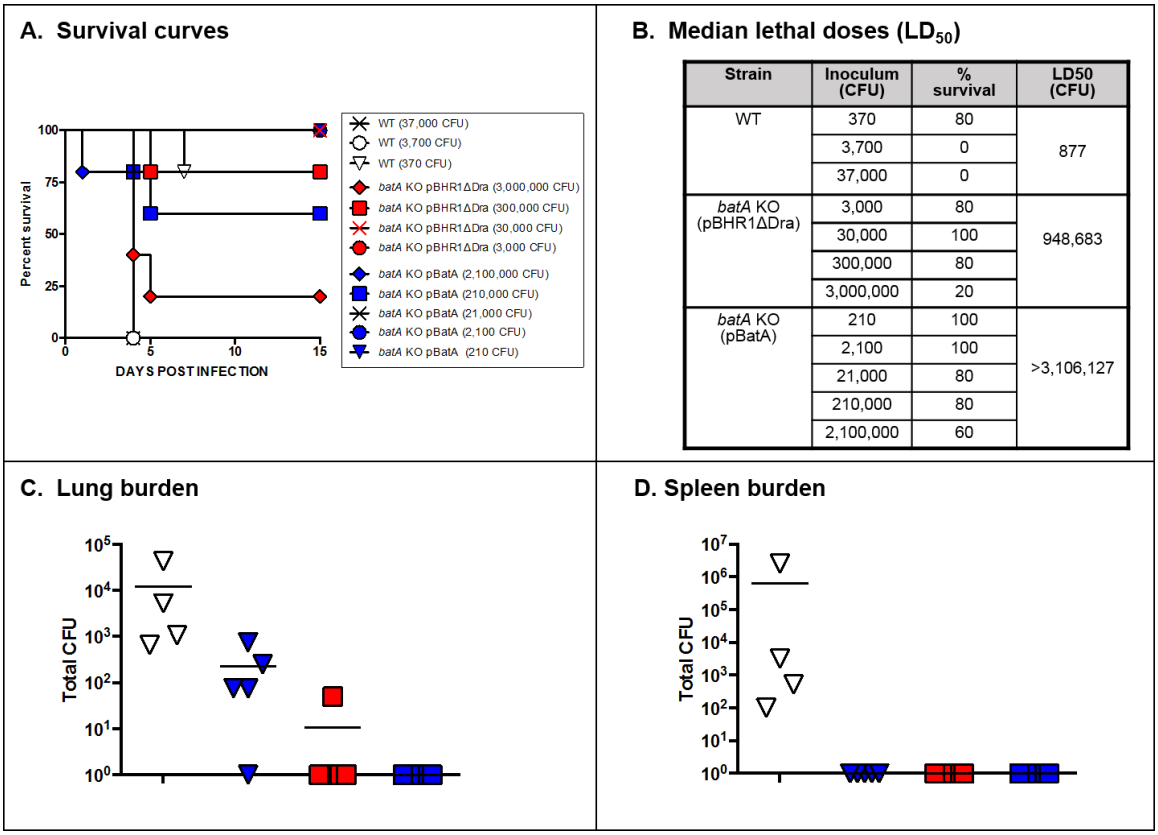

Strain	Inoculum (CFU)	% survival	LD50 (CFU)
WT	370	80	877
	3,700	0	
	37,000	0	
batA KO (pBHR1ΔDra)	3,000	80	948,683
	30,000	100	
	300,000	80	
	3,000,000	20	
batA KO (pBatA)	210	100	>3,106,127
	2,100	100	
	21,000	80	
	210,000	80	
	2,100,000	60	

Figure 5.7. Constitutive expression of *batA* by the plasmid-complemented isogenic *batA* KO mutant further attenuates the virulence of *B. mallei* and reduces bacterial burdens in mouse tissues.

Mice were inoculated intratracheally using a Microsprayer device to aerosolize the indicated number of bacterial CFU directly into the lungs (n=5 mice/dose). Animals were then monitored daily for clinical signs of illness and morbidity. Panel A: Survival curves. Panel B: Calculated median lethal dose (LD_{50}) values. Panels C and D: Tissues were collected from mice that survived challenge, homogenized, diluted, and spread on agar plates to determine bacterial loads. Symbols show data for individual animals.

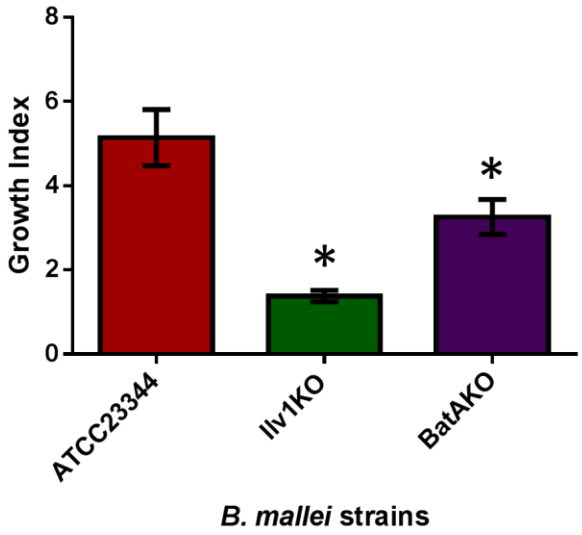

Figure 5.8. Intracellular growth of the isogenic *batA* KO mutant is reduced in murine macrophages.

Duplicate plates of J774.A1 murine macrophages were infected with *B. mallei* ATCC 23344 at MOI = 10:1 for 1 hour at 37°C. Extracellular bacteria were killed by incubating with kanamycin for 1.5 hours at 37°C, at which point, the macrophages were washed. One plate was immediately processed by lysing the macrophage membranes and plating their contents on culture media to enumerate the number of phagocytosed bacteria. After incubating an additional 7.5 hours at 37°C, the second plate was processed in a similar manner to enumerate the number of bacteria that replicated within these macrophages. The growth index (ratio) is reported here and was calculated as follows: Growth Index = Mean Intracellular Replication CFU/Mean Phagocytosis CFU**.** (*) indicates the $P \leq 0.05$.

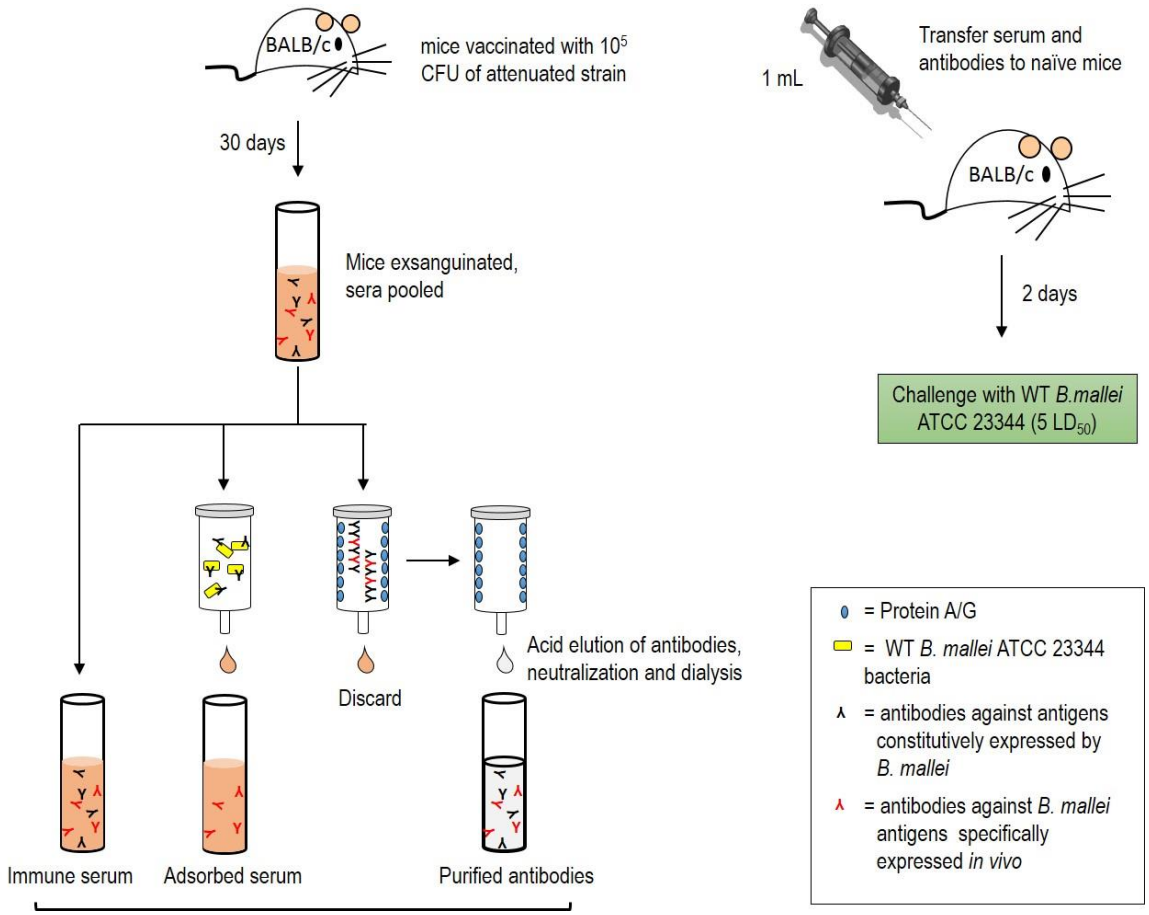

Figure 5.9. Schematic overview of passive transfer methodology in murine model of aerosol infection with *B. mallei*.

Passive transfer experiments were performed. Specifically, serum was collected from mice vaccinated with the isogenic *batA* knock out mutant in *B. mallei* ATCC 23344 (BmbatAKO) 30 days prior. This sera and was then administered to naïve mice via intraperitoneal injection (0.2 or 1.0 mL per mouse). Two days after serum transfer, animals were challenged with a lethal dose of *B. mallei* ATCC 23344. ELISAs and additional passive transfer experiments were also performed with naïve and immune sera that underwent various antibody treatments. Specifically, naïve and immune sera were incubated with *B. mallei* ATCC 23344 to bind host antibodies against constitutively

expressed surface antigens. This adsorbed sera was then separated from the bacteria via centrifugation and filter sterilized. Naïve and immune sera were also filtered through an antibody-coated column that would bind recombinant A and G fusion proteins, after which both constitutive and *in vivo* expressed antibodies (purified antibodies) were eluted with glycine, neutralized, and dialyzed.

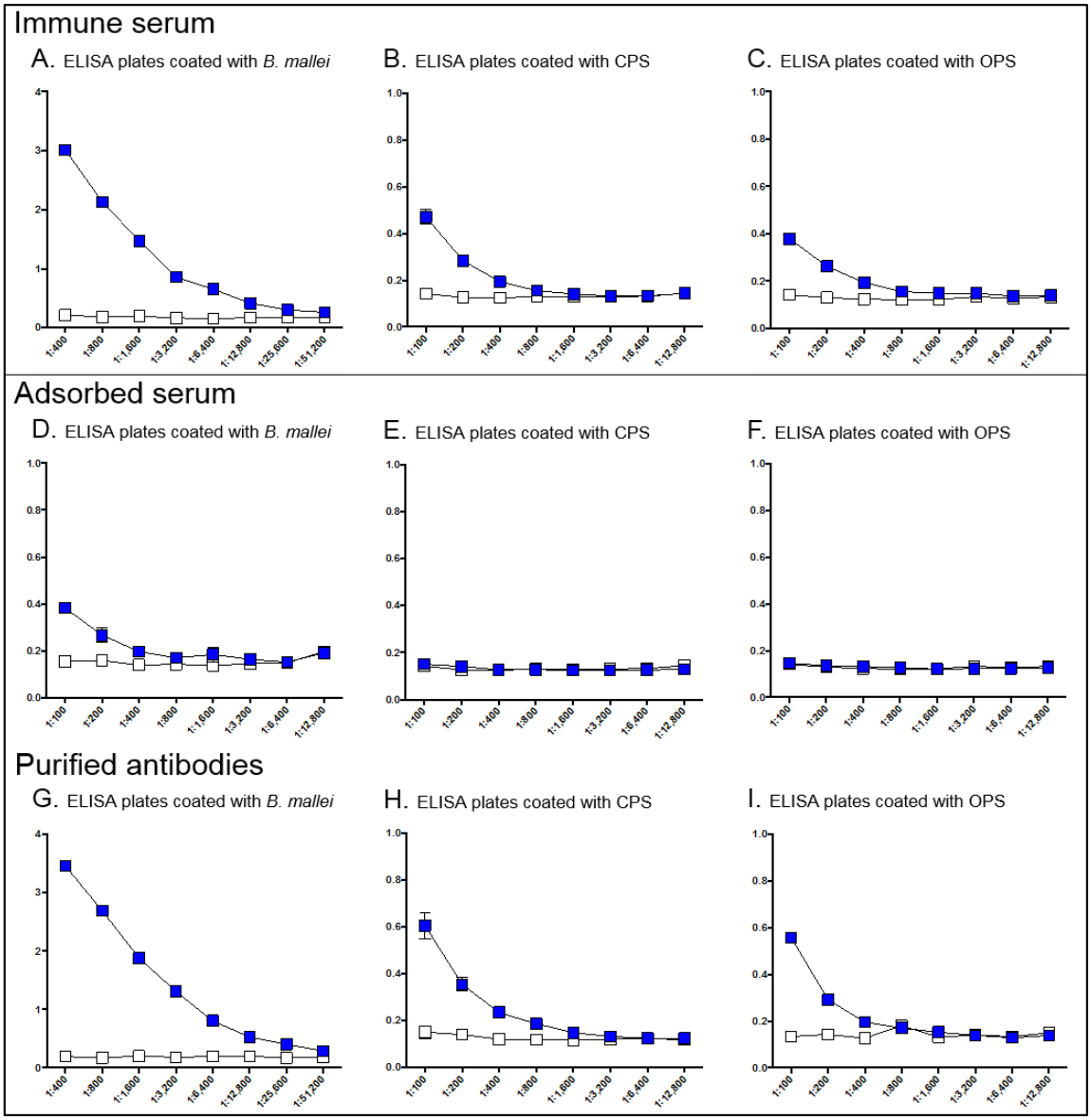

Figure 5.10. Immune serum and purified antibodies recognize unique antigens expressed by *B. mallei.*

Antibody titers were measured in serum by ELISA. Enzyme immunoassay plates were coated with paraformaldehyde-fixed *B. mallei* ATCC 23344 bacteria, purified *B. pseudomallei* capsular polysaccharides (CPS), or purified oligosaccharide chains of *B. pseudomallei* LPS (OPS). Serum samples were serially diluted and placed in duplicate

wells of coated ELISA plates. Goat α-mouse antibodies (light and heavy chains) conjugated to alkaline phosphatase were used as secondary antibodies. The y-axis shows absorbance at a wavelength of 405 nm, which is indicative of antibodies binding to antigens coating the plates. The x-axis represents serial two-fold dilutions of sera. The results are expressed as the mean absorbance (± standard error).

Flow cytometry

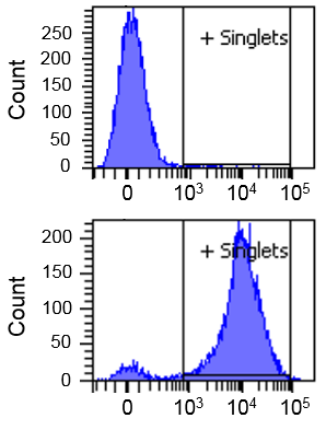

Naïve serum
Events: 10,805
Antibody$^+$: 0.5 %

Immune serum
Events: 10,492
Antibody$^+$: 87.5%

Phagocytosis by macrophages

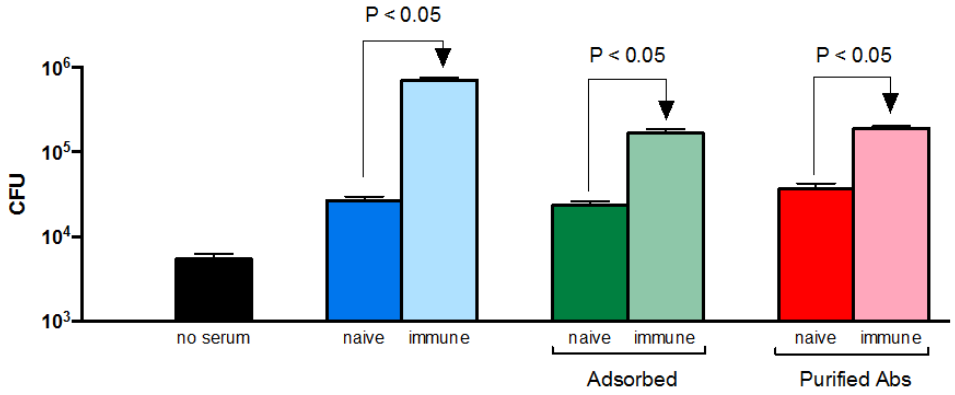

Replication inside macrophages

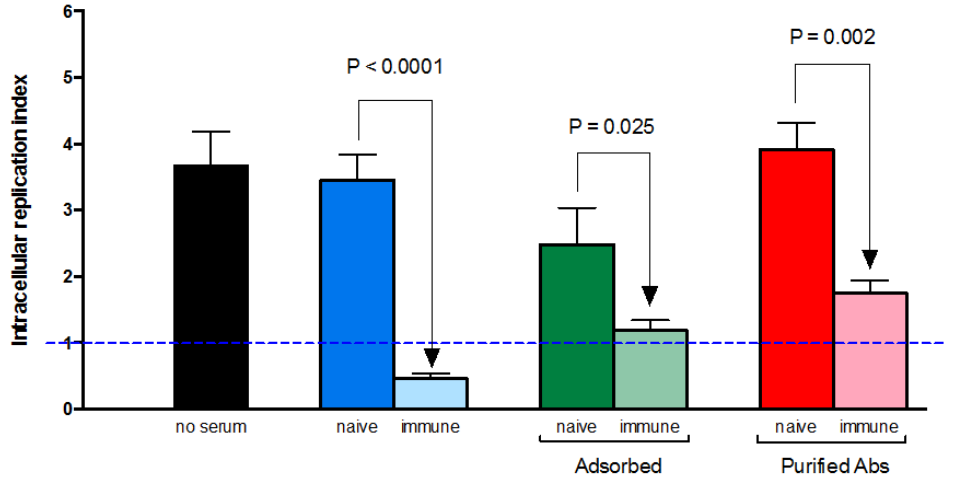

Figure 5.11. Immune sera binds to antigens at the surface of *B. mallei*, resulting in increased phagocytosis and decreased intracellular survival in murine macrophages.

Top Panel: Non-permeabilized *B. mallei* strains were incubated with the indicated polyclonal antibodies and fluorescently-labeled with a goat α-mouse antibody conjugated with the fluorochrome Alexa Fluor 488. Labeled bacteria were analyzed using a BD LSR II flow cytometer. The *x*-axis represents the level of fluorescence, and the *y*-axis corresponds to the particles counted in arbitrary units. The number of cells analyzed, and the percentage of those producing BpaB on their surface, are shown. Middle and Bottom Panels: Duplicate plates of J774.A1 murine macrophages were infected with *B. mallei* ATCC 23344 at MOI = 10:1 for 1 hour at 37°C. Extracellular bacteria were killed by incubating with kanamycin for 1.5 hours at 37°C, at which point, the macrophages were washed. Middle Panel: One plate was immediately processed by lysing the macrophage membranes and plating their contents on culture media to enumerate the number of phagocytosed bacteria. Bottom Panel: After incubating an additional 7.5 hours at 37°C, the second plate was processed in a similar manner to enumerate the number of bacteria that replicated within these macrophages.

CHAPTER 6

CONCLUSION

Several small animal models have been developed to study the pathogenesis of and test medical countermeasures (MCM) against glanders (164-169); however, there have been few reports describing the use of large animal models, particularly non-human primates, as surrogates to study glanders and validate lead MCM candidates (170-172). This dissertation reports on the establishment of a marmoset model of intranasal infection for *B. mallei* and supplies data that indicate the common marmoset (*Callithrix jacchus*) is a suitable surrogate for studying glanders. Marmosets provide an advantage over other large animal models for a number of reasons. First, marmosets develop clinical signs and pathologic lesions that are characteristic of glanders in experimental models (123, 125, 130). The onset and clinical progression observed in marmosets also resembles those noted in natural cases of disease in both humans and animals (8, 9, 23, 145, 146, 153-156). In terms of ease of use and safety in biocontainment, the small size of the common marmoset is preferable for manipulation when compared other large animal models like the horse and macaque. Not only is the anatomy and physiology of the common marmoset similar to humans, but recently the whole genome of the common marmoset was sequenced and work is already underway to generate transgenic marmosets for biomedical research (275-280), which further underscores the usefulness of this large animal model. The potential availability of a nonhuman primate species (NHP) with both

outbred and transgenic animals makes the common marmoset a very powerful tool for studying the pathogenesis of *B. mallei,* particularly with respect to characterizing the host immune response to *B. mallei* and the development of MCM. The United States Department of Human Health and Services Food and Drug Administration Center for Biologics Evaluation and Research (CBER) regulates the testing of new MCM, and it requires that all promising vaccine candidates be validated in both a small animal (rodent) model and a large animal (non-rodent) model during pre-clinical studies, as novel target compounds may affect one species differently from another. For all these reasons, the common marmoset is an ideal animal model for future studies to investigate lead MCM against *B. mallei.*

Currently, there is no vaccine to protect against infection with *B. mallei* and *B. pseudomallei.* These organisms share many virulence traits that are important in pathogenesis, including several autotransporter (AT) proteins. Subunit vaccines containing AT have been very successful at protecting against infection with other bacterial organisms. Most notable would be pertactin, an AT in *Bordetella pertussis,* which is a component of the licensed DTaP vaccine used to protect humans against whooping cough (DAPTACEL®, Infanrix®, Tripedia®, Pediarix®, KINRIX®, Adacel®, Pentacel®, and Boostrix®) (83). Another vaccine recently approved by the FDA is Bexsero® (Pfizer), which contains Neisseria adhesin A (NadA), an immunogenic AT that is used to protect humans against bacterial meningitis (281).

With this in mind, the genome of *Burkholderia mallei* strain ATCC 23344 was examined and determined to contain eight AT gene products that are 99-100% identical to AT gene products in *B. pseudomallei* (six oligomeric and two conventional). Prior to

this study, only three oligomeric AT (BoaA, BimA, and BpaC) had been functionally characterized, and of these, only BimA has been shown to contribute to virulence *in vivo*. We report the characterization and immunogenic potential of two AT in *B. mallei* ATCC 23344 that contribute to virulence, namely, an oligomeric AT termed BpaB and a conventional AT termed BatA.

Comparative sequence analyses indicate that BpaB is a trimeric autotransporter of 1,090 amino acids with a predicted molecular weight of 105-kDa. Consistent with this finding, we determined recombinant bacteria expressing *bpaB* produce a protein of ≥300-kDa on their surface that reacts with a BpaB-specific monoclonal antibody. Analysis of sera from mice infected with *B. mallei* indicated that animals produce antibodies against BpaB during the course of disease, thus establishing production of the autotransporter *in vivo*. Median lethal dose experiments in mice revealed that the *bpaB* mutation attenuates the virulence of *B. mallei* 8-14 fold, and that constitutive BpaB expression further attenuates virulence. Furthermore, we also discovered constitutive production of BpaB on the surface of both *B. thailandensis* and *B. mallei* promotes biofilm formation. To our knowledge, this is the first report of a biofilm factor for this organism.

While it has been determined that BpaB is expressed *in vivo* and that *in vitro* it contributes to biofilm formation, its exact role *in vivo* has yet to be determined. Recently, the Lafontaine lab developed an immunohistochemistry (IHC) protocol for identifying *B. mallei* in tissues. A study using this IHC protocol on infected marmoset tissues is currently underway to determine if and where BpaB is expressed *in vivo*. Should BpaB expression be identified in these marmoset tissues, attempts to identify biofilm polysaccharide components in marmoset tissues could be pursued, especially given that

an antibody to the capsular polysaccharide of *B. pseudomallei* is commercially available (Life Technologies®).

Additionally, the exact immunogenic potential of BpaB remains unclear. Previous experiments indicate that vaccination with purified BpaB protein is not sufficient to protect against infection with *B. mallei* and *B. pseudomallei* (data not shown). While the isogenic *bpaB* KO mutant attenuates virulence, it also still results in mortality, which suggests it would be unsuccessful and inappropriate to use as a live-attenuated strain for vaccination studies. Passive transfer experiments have not yet been performed, but they could be pursued to determine if the α-BpaB antibodies produced by mice during infection are protective against lethal challenge with *B. mallei* and *B. pseudomallei*. Additionally, the ability of BpaB to prime the innate immune system or contribute to cell-mediated immunity has also not yet been explored. Future experiments to explore if vaccination with purified BpaB can elicit the production of protective immune cytokines (TNF-α, IL-1, IL-6, and IFN-γ) or an expansion of T-cells would be of value. Should this priming of the innate immune system or a cell-mediated immune response be observed, it would then be pertinent to determine which innate cells (natural killer (NK) cells, neutrophils, macrophages, dendritic cells) and T-cell subsets (cytotoxic, helper, and regulatory T-cells) are contributing to this protective immune response. Furthermore, immunohistochemistry or fluorescent microscopy could be performed on affected marmoset tissues to examine the immune response elicited in tissues (e.g. B-cell, T-cell, NK-cell, neutrophils, macrophages, or dendritic cells), which may shed more light on the exact interaction between host cells and *B. mallei* during pathogenesis.

This dissertation also reports on the characterization of a conventional AT in *B. mallei* ATCC 23344 identified as BatA. Comparative sequence analyses indicated that BatA is composed of 610 amino acids with a predicted molecular weight of 64-kDa and a putative GDSL-hydrolase in its passenger domain. Consistent with this finding, we determined recombinant *B. thailandensis* and *B. mallei* that constitutively express BatA produce a protein of 64-kDa that reacts with α-BatA polyclonal antibodies, and in *B. thailandensis*, we demonstrate this protein acts as an esterase in the presence an acetate substrate. To investigate the impact of BatA expression on virulence *in vivo*, a *batA* mutation was introduced into the genome of *B. mallei* ATCC 23344. Median lethal dose experiments in our mouse model of aerosol infection revealed that *batA* mutation attenuates virulence at least 250-fold, that constitutive BatA expression further attenuates virulence, and that tissues from survivors are transiently colonized by this isogenic mutant. We also determined that vaccination with the *batA* mutant strain provides robust protection against acute infection with *B. mallei* ATCC 23344 and *B. pseudomallei* 1026b, respectively. Furthermore, 56% of the vaccinated mice that survived *B. pseudomallei* infection developed sterilizing immunity. Using passive transfer experiments with our murine model, we also determined that antibodies contribute to this protective immune response in a dose-dependent manner, and that the immune sera contains increased antibody titers against multiple unique antigens that opsonize *B. mallei* for phagocytosis and destruction by murine macrophages. These results indicate BatA is an important virulence factor of *B. mallei*, and that future studies should be aimed at further characterizing the immunogenic potential of BatA.

First and foremost, it would be of great benefit to perform a proteomic microarray on immune sera to identify which unique antigenic targets of *B. mallei* result in the generation of these novel protective antibodies found immune mouse serum. Once identified, such antigenic targets could then be evaluated for their role in the virulence of *B. mallei* and *B. pseudomallei*, and they could also be used as components in novel vaccine strategies. Specifically, the mouse model of aerosol infection could be used to screen whether these purified antigens offer protection when used in either subunit vaccines or when expressed by viral vectored vaccines.

Additionally, the ability of BatA to prime the innate immune system or contribute to cell-mediated immunity and long-term memory has also not yet been explored. Future experiments to explore if vaccination with either purified BatA or the isogenic *batA* KO mutant can elicit the production of protective immune cytokines (TNF-α, IL-1, IL-6, and IFN-γ) would be of tremendous value. Likewise, it would be very useful to determine if the adoptive transfer of T-cells from vaccinated to naïve mice can protect against lethal challenge with *B. mallei* and *B. pseudomallei.* Should priming of the innate immune system or a cell-mediated immune response be observed, it would then be pertinent to use flow cytometry to determine which innate immune cells (natural killer cells, neutrophils, macrophages, dendritic cells) and T-cell subsets are contributing to the protective immune response both systemically and within relevant tissues (spleen, liver, and lung). Furthermore, immunohistochemistry or fluorescent microscopy could be employed to examine which immune cells (B-cells, T-cells, neutrophils, macrophages, and dendritic cells) are associated with *B. mallei*-induced lesions in marmosets to better determine the role these cells may be playing in the pathogenesis of glanders.

In this dissertation, it was also determined *in vitro* that BatA is important for the survival and replication of *B. mallei* in murine macrophages, and that it may also function as an esterase. This work has yet to be explored *in vivo.* Experiments are currently underway using the aforementioned IHC and fluorescent microscopy techniques to determine if and in what tissues and cell types *B. mallei* expressing BatA are expressed *in vivo* using tissues from marmosets with glanders.

This dissertation makes several scientific contributions to the study of *B. mallei* and *B. pseudomallei.* Specifically, we identify the common marmoset as excellent, biologically-relevant, non-human primate model for examining the pathogenesis of *B. mallei* and for evaluating lead medical countermeasure candidates. We characterized BpaB and BatA as being two novel virulence factors that are important for the virulence of *B. mallei.* We also report on the characterization of a novel live-attenuated strain of *B. mallei* ATCC 23344 that protects against lethal challenge with WT *B. mallei* and *B. pseudomallei.* Given *B. mallei* and *B. pseudomallei* are zoonotic pathogens and potential biological warfare agents that result in significant morbidity and mortality world-wide, the findings of this dissertation are of tremendous value as they further our knowledge on the pathogenesis of *B. mallei* and *B. pseudomallei* and offer improved tools for studying, diagnosing, and combating the infections caused by these bacterial organisms.

REFERENCES

1. Cheng AC, Currie BJ. Melioidosis: epidemiology, pathophysiology, and management. Clinical microbiology reviews. 2005;18(2):383-416.

2. Dvorak GD, Spickler AR. Glanders. Journal of the American Veterinary Medical Association. 2008;233(4):570-7.

3. Galyov EE, Brett PJ, Deshazer D. Molecular Insights into Burkholderia pseudomallei and Burkholderia mallei Pathogenesis. Annu Rev Microbiol. 2010;64:495-517.

4. Whitlock GC, Estes DM, Torres AG. Glanders: off to the races with Burkholderia mallei. FEMS Microbiol Lett. 2007;277(2):115-22.

5. Nierman WC, DeShazer D, Kim HS, Tettelin H, Nelson KE, Feldblyum T, et al. Structural flexibility in the Burkholderia mallei genome. Proceedings of the National Academy of Sciences of the United States of America. 2004;101(39):14246-51.

6. Hampton V, Kaestli M, Mayo M, Choy JL, Harrington G, Richardson L, et al. Melioidosis in birds and Burkholderia pseudomallei dispersal, Australia. Emerging infectious diseases. 2011;17(7):1310.

7. Limmathurotsakul D, Thammasart S, Warrasuth N, Thapanagulsak P, Jatapai A, Pengreungrojanachai V, et al. Melioidosis in animals, Thailand, 2006–2010. Emerging Infectious Diseases. 2012;18(2):325.

8. Wernery U, Wernery R, Joseph M, Al-Salloom F, Johnson B, Kinne J, et al. Natural Burkholderia mallei infection in dromedary, Bahrain. Emerging infectious diseases. 2011;17(7):1277.

9. Kahn C, Line S. Merck Veterinary Manual. Whitehouse Station (NJ): Merck & Co. Inc; 2010.

10. Alibasoglu M, Yesildere T, Calislar T, Inal T, Calsikan U. Glanders outbreak in lions in the Istanbul zoological garden]. Berliner und Münchener tierärztliche Wochenschrift. 1986;99(2):57.

11. Currie BJ, Dance DA, Cheng AC. The global distribution of Burkholderia pseudomallei and melioidosis: an update. Transactions of the Royal Society of Tropical Medicine and Hygiene. 2008;102(Supplement 1):S1-S4.

12. Jelesijevic T, Zimmerman SM, Harvey SB, Mead DG, Shaffer TL, Estes DM, et al. Use of the Common Marmoset to Study Burkholderia mallei Infection. 2015.

13. Lazar Adler NR, Stevens JM, Stevens MP, Galyov EE. Autotransporters and Their Role in the Virulence of Burkholderia pseudomallei and Burkholderia mallei. Frontiers in microbiology. 2011;2:151.

14. Zimmerman SM, Michel F, Hogan RJ, Lafontaine ER. The Autotransporter BpaB Contributes to the Virulence of Burkholderia mallei in an Aerosol Model of Infection. 2015.

15. Stoyanova M, Pavlina I, Moncheva P, Bogatzevska N. Biodiversity and incidence of Burkholderia species. BIOTECHNOLOGY AND BIOTECHNOLOGICAL EQUIPMENT. 2007;21(3):306.

16. Yabuuchi E, Kosako Y, Oyaizu H, Yano I, Hotta H, Hashimoto Y, et al. Proposal of Burkholderia gen. nov. and transfer of seven species of the genus Pseudomonas homology group II to the new genus, with the type species Burkholderia cepacia (Palleroni and Holmes 1981) comb. nov. Microbiology and immunology. 1992;36(12):1251.

17. Wiersinga WJ, Currie BJ, Peacock SJ. Melioidosis. New England Journal of Medicine. 2012;367(11):1035-44.

18. Lazar Adler NR, Govan B, Cullinane M, Harper M, Adler B, Boyce JD. The molecular and cellular basis of pathogenesis in melioidosis: how does Burkholderia pseudomallei cause disease? FEMS microbiology reviews. 2009;33(6):1079-99.

19. Holden MT, Titball RW, Peacock SJ, Cerdeño-Tárraga AM, Atkins T, Crossman LC, et al. Genomic plasticity of the causative agent of melioidosis, Burkholderia pseudomallei. Proceedings of the National Academy of Sciences of the United States of America. 2004;101(39):14240-5.

20. Whitlock GC, Mark Estes D, Torres AG. Glanders: off to the races with Burkholderia mallei. FEMS microbiology letters. 2007;277(2):115-22.

21. Larsen JC, Johnson NH. Pathogenesis of Burkholderia pseudomallei and Burkholderia mallei. Military medicine. 2009;174(6):647-51.

22. Currie BJ. Advances and remaining uncertainties in the epidemiology of Burkholderia pseudomallei and melioidosis. Transactions of the Royal Society of Tropical Medicine and Hygiene. 2008;102(3):225-7.

23. Srinivasan A, Kraus CN, DeShazer D, Becker PM, Dick JD, Spacek L, et al. Glanders in a military research microbiologist. New England Journal of Medicine. 2001;345(4):256-8.

24. Sharrer GT. The great glanders epizootic, 1861-1866: a civil war legacy. Agricultural history. 1995;69(1):79-97.

25. Derbyshire JB. The eradication of glanders in Canada. The Canadian Veterinary Journal. 2002;43(9):722.

26. Wilkinson L. Glanders: medicine and veterinary medicine in common pursuit of a contagious disease. Medical history. 1981;25(4):363.

27. Brett PJ, Burtnick MN, Snyder DS, Shannon JG, Azadi P, Gherardini FC. Burkholderia mallei expresses a unique lipopolysaccharide mixture that is a potent activator of human Toll-like receptor 4 complexes. Molecular microbiology. 2007;63(2):379-90.

28. Parthasarathy N, DeShazer D, England M, Waag DM. Polysaccharide microarray technology for the detection of Burkholderia pseudomallei and Burkholderia mallei antibodies. Diagnostic microbiology and infectious disease. 2006;56(3):329-32.

29. Neubauer H, Sprague L, Zacharia R, Tomaso H, Al Dahouk S, Wernery R, et al. Serodiagnosis of Burkholderia mallei Infections in Horses: State-of-the-art and Perspectives. Journal of Veterinary Medicine, Series B. 2005;52(5):201-5.

30. Naureen A, Saqib M, Muhammad G, Hussain MH, Asi MN. Comparative evaluation of Rose Bengal plate agglutination test, mallein test, and some conventional serological tests for diagnosis of equine glanders. Journal of veterinary diagnostic investigation. 2007;19(4):362-7.

31. Verma R, Sharma J, Venkateswaran K, Batra H. Development of an avidin-biotin dot enzyme-linked immunosorbent assay and its comparison with other serological tests for diagnosis of glanders in equines. Veterinary microbiology. 1990;25(1):77-85.

32. Scholz HC, Joseph M, Tomaso H, Al Dahouk S, Witte A, Kinne J, et al. Detection of the reemerging agent Burkholderia mallei in a recent outbreak of glanders in the United Arab Emirates by a newly developed fliP-based polymerase chain reaction assay. Diagnostic microbiology and infectious disease. 2006;54(4):241-7.

33. Ulrich MP, Norwood DA, Christensen DR, Ulrich RL. Using real-time PCR to specifically detect Burkholderia mallei. Journal of medical microbiology. 2006;55(5):551-9.

34. Alexander D. Manual of diagnostic tests and vaccines for terrestrial animals. Office of International Des Epizooties, Paris, France. 2012.

35. Brown CaT, A. Foreign Animal Diseases—The Gray Book. Cited 1/3/2013, 2008.

36. Public Health Agency of Canada. Office of Laboratory Security. Material safety data sheet—Burkholderia (Pseudomonas) mallei 2011 [26/2/2013]. Available from: http://www.phac-aspc.gc.ca/lab-bio/res/psds-ftss/msds25e-eng.php.

37. Thibault F, Hernandez E, Vidal D, Girardet M, Cavallo J-D. Antibiotic susceptibility of 65 isolates of Burkholderia pseudomallei and Burkholderia mallei to 35 antimicrobial agents. Journal of Antimicrobial Chemotherapy. 2004;54(6):1134-8.

38. Wheelis M. First shots fired in biological warfare. Nature. 1998;395(6699):213-.

39. Wheelis M. Biological sabotage in World War I. Geissler EMoon JEvC, ed Biological and toxin weapons: research, development, and use from the Middle Ages to 1945 Oxford: Oxford University Press. 1999:35-72.

40. Frischknecht F. The history of biological warfare. EMBO reports. 2003;4:S47-S52.

41. Robinson JP. Public health response to biological and chemical weapons: WHO guidance: WHO; 2004.

42. McGavin MD, Zachary JF. Pathologic basis of veterinary disease: Mosby; 2010.

43. The Joint Center of Pathology. Veterinary Systemic Pathology Program. Case P-B08: Glanders - lung - horse [8/11/2011]. Available from: http://www.askjpc.org/vspo/index.php.

44. Ahmed K, Enciso HD, Masaki H, Tao M, Omori A, Tharavichikul P, et al. Attachment of Burkholderia pseudomallei to pharyngeal epithelial cells: a highly pathogenic bacteria with low attachment ability. American Journal of Tropical Medicine and Hygiene. 1999;60(1):90-3.

45. Comolli JC, Waite LL, Mostov KE, Engel JN. Pili binding to asialo-GM1 on epithelial cells can mediate cytotoxicity or bacterial internalization byPseudomonas aeruginosa. Infection and immunity. 1999;67(7):3207-14.

46. Essex-Lopresti AE, Boddey JA, Thomas R, Smith MP, Hartley MG, Atkins T, et al. A type IV pilin, PilA, contributes to adherence of Burkholderia pseudomallei and virulence in vivo. Infection and immunity. 2005;73(2):1260-4.

47. Stevens MP, Friebel A, Taylor LA, Wood MW, Brown PJ, Hardt W-D, et al. A Burkholderia pseudomallei type III secreted protein, BopE, facilitates bacterial invasion of epithelial cells and exhibits guanine nucleotide exchange factor activity. Journal of bacteriology. 2003;185(16):4992-6.

48. Stevens MP, Stevens JM, Jeng RL, Taylor LA, Wood MW, Hawes P, et al. Identification of a bacterial factor required for actin-based motility of Burkholderia pseudomallei. Molecular microbiology. 2005;56(1):40-53.

49. Stevens MP, Wood MW, Taylor LA, Monaghan P, Hawes P, Jones PW, et al. An Inv/Mxi-Spa-like type III protein secretion system in Burkholderia pseudomallei modulates intracellular behaviour of the pathogen. Molecular microbiology. 2002;46(3):649-59.

50. Jones A, DeShazer D, Woods D. Identification and characterization of a two-component regulatory system involved in invasion of eukaryotic cells and heavy-metal resistance in Burkholderia pseudomallei. Infection and immunity. 1997;65(12):4972-7.

51. Gong L, Cullinane M, Treerat P, Ramm G, Prescott M, Adler B, et al. The Burkholderia pseudomallei type III secretion system and BopA are required for evasion of LC3-associated phagocytosis. PLoS One. 2011;6(3):e17852.

52. Ekchariyawat P, Pudla S, Limposuwan K, Arjcharoen S, Sirisinha S, Utaisincharoen P. Burkholderia pseudomallei-induced expression of suppressor of cytokine signaling 3 and cytokine-inducible src homology 2-containing protein in mouse macrophages: a possible mechanism for suppression of the response to gamma interferon stimulation. Infection and immunity. 2005;73(11):7332-9.

53. Ekchariyawat P, Pudla S, Limposuwan K, Arjcharoen S, Sirisinha S, Utaisincharoen P. Expression of suppressor of cytokine signaling 3 (SOCS3) and cytokine-inducible Src homology 2-containing protein (CIS) induced in Burkholderia pseudomallei—infected mouse macrophages requires bacterial internalization. Microbial pathogenesis. 2007;42(2):104-10.

54. Utaisincharoen P, Arjcharoen S, Limposuwan K, Tungpradabkul S, Sirisinha S. Burkholderia pseudomallei RpoS regulates multinucleated giant cell formation and inducible nitric oxide synthase expression in mouse macrophage cell line (RAW 264.7). Microbial pathogenesis. 2006;40(4):184-9.

55. Lengwehasatit I, Nuchtas A, Tungpradabkul S, Sirisinha S, Utaisincharoen P. Involvement of B. pseudomallei RpoS in apoptotic cell death in mouse macrophages. Microbial pathogenesis. 2008;44(3):238-45.

56. Reckseidler-Zenteno SL, DeVinney R, Woods DE. The capsular polysaccharide of Burkholderia pseudomallei contributes to survival in serum by reducing complement factor C3b deposition. Infection and immunity. 2005;73(2):1106-15.

57. Deshazer D, Brett PJ, Woods DE. The type II O-antigenic polysaccharide moiety of Burkholderia pseudomallei lipopolysaccharide is required for serum resistance and virulence. Molecular microbiology. 1998;30(5):1081-100.

58. Burtnick MN, Woods DE. Isolation of Polymyxin B-Susceptible Mutants ofBurkholderia pseudomallei and Molecular Characterization of Genetic Loci Involved in Polymyxin B Resistance. Antimicrobial agents and chemotherapy. 1999;43(11):2648-56.

59. Taweechaisupapong S, Kaewpa C, Arunyanart C, Kanla P, Homchampa P, Sirisinha S, et al. Virulence of Burkholderia pseudomallei does not correlate with biofilm formation. Microbial pathogenesis. 2005;39(3):77-85.

60. Desvaux M, Parham NJ, Henderson IR. The autotransporter secretion system. Research in microbiology. 2004;155(2):53-60.

61. Henderson IR, Navarro-Garcia F, Nataro JP. The great escape: structure and function of the autotransporter proteins. Trends in microbiology. 1998;6(9):370-8.

62. Grijpstra J, Arenas J, Rutten L, Tommassen J. Autotransporter secretion: varying on a theme. Research in microbiology. 2013;164(6):562-82.

63. Chagnot C, Zorgani MA, Astruc T. Proteinaceous determinants of surface colonization in bacteria: bacterial adhesion and biofilm formation from a protein secretion perspective. Frontiers in microbiology. 2013;4.

64. Cotter SE, Surana NK, Grass S, Geme JWS. Trimeric autotransporters require trimerization of the passenger domain for stability and adhesive activity. Journal of bacteriology. 2006;188(15):5400-7.

65. Cotter SE, Surana NK, St Geme III JW. Trimeric autotransporters: a distinct subfamily of autotransporter proteins. Trends in microbiology. 2005;13(5):199-205.

66. Oomen CJ, van Ulsen P, Van Gelder P, Feijen M, Tommassen J, Gros P. Structure of the translocator domain of a bacterial autotransporter. The EMBO journal. 2004;23(6):1257-66.

67. Leyton DL, Rossiter AE, Henderson IR. From self sufficiency to dependence: mechanisms and factors important for autotransporter biogenesis. Nature Reviews Microbiology. 2012;10(3):213-25.

68. White D. The physiology and biochemistry of prokaryotes. 4th Ed. New York: Oxford University Press, 2012.

69. Junker M, Schuster CC, McDonnell AV, Sorg KA, Finn MC, Berger B, et al. Pertactin β-helix folding mechanism suggests common themes for the secretion and folding of autotransporter proteins. Proceedings of the National Academy of Sciences of the United States of America. 2006;103(13):4918-23.

70. Oliver DC, Huang G, Fernandez RC. Identification of secretion determinants of the Bordetella pertussis BrkA autotransporter. Journal of bacteriology. 2003;185(2):489-95.

71. Leyton DL, Sevastsyanovich YR, Browning DF, Rossiter AE, Wells TJ, Fitzpatrick RE, et al. Size and conformation limits to secretion of disulfide-bonded loops in autotransporter proteins. Journal of Biological Chemistry. 2011;286(49):42283-91.

72. Rossiter AE, Leyton DL, Tveen-Jensen K, Browning DF, Sevastsyanovich Y, Knowles TJ, et al. The essential β-barrel assembly machinery complex components BamD and BamA are required for autotransporter biogenesis. Journal of bacteriology. 2011;193(16):4250-3.

73. Ruiz-Perez F, Henderson IR, Leyton DL, Rossiter AE, Zhang Y, Nataro JP. Roles of periplasmic chaperone proteins in the biogenesis of serine protease autotransporters of Enterobacteriaceae. Journal of bacteriology. 2009;191(21):6571-83.

74. Knowles TJ, Scott-Tucker A, Overduin M, Henderson IR. Membrane protein architects: the role of the BAM complex in outer membrane protein assembly. Nature Reviews Microbiology. 2009;7(3):206-14.

75. Veiga E, De Lorenzo V, Fernández LA. Probing secretion and translocation of a β-autotransporter using a reporter single-chain Fv as a cognate passenger domain. Molecular microbiology. 1999;33(6):1232-43.

76. Roussel-Jazédé V, Grijpstra J, van Dam V, Tommassen J, van Ulsen P. Lipidation of the autotransporter NalP of Neisseria meningitidis is required for its function in the release of cell-surface-exposed proteins. Microbiology. 2013;159(Pt 2):286-95.

77. Henderson IR, Navarro-Garcia F, Desvaux M, Fernandez RC, Ala'Aldeen D. Type V protein secretion pathway: the autotransporter story. Microbiol Mol Biol Rev. 2004;68(4):692-744.

78. Oliver DC, Huang G, Nodel E, Pleasance S, Fernandez RC. A conserved region within the Bordetella pertussis autotransporter BrkA is necessary for folding of its passenger domain. Molecular microbiology. 2003;47(5):1367-83.

79. Balder R, Lipski S, Lazarus J, Grose W, Wooten R, Hogan R, et al. Identification of Burkholderia mallei and Burkholderia pseudomallei adhesins for human respiratory epithelial cells. BMC microbiology. 2010;10(1):250.

80. Stevens JM, Ulrich RL, Taylor LA, Wood MW, DeShazer D, Stevens MP, et al. Actin-binding proteins from Burkholderia mallei and Burkholderia thailandensis can functionally compensate for the actin-based motility defect of a Burkholderia pseudomallei bimA mutant. Journal of bacteriology. 2005;187(22):7857-62.

81. Campos CG, Borst L, Cotter PA. Characterization of BcaA, a putative classical autotransporter protein in Burkholderia pseudomallei. Infection and immunity. 2013.

82. Adler NRL, Dean RE, Saint RJ, Stevens MP, Prior JL, Atkins TP, et al. Identification of a Predicted Trimeric Autotransporter Adhesin Required for Biofilm Formation of Burkholderia pseudomallei. PloS one. 2013;8(11):e79461.

83. Scheifele D, Halperin SA, Rubin E, Tapiero B, Guasparini R, Meekison W, et al. Safety and Immunogenicity of a Pentavalent Combination Vaccine (Diphtheria, Tetanus, Acellular Pertussis, Polio and Haemophilus Influenzae Type b Conjugate) When Administered as a Fourth Dose at 15 to 18 Months of Age. Human vaccines. 2005;1(5):180-6.

84. Attia AS, Lafontaine ER, Latimer JL, Aebi C, Syrogiannopoulos GA, Hansen EJ. The UspA2 protein of Moraxella catarrhalis is directly involved in the expression of serum resistance. Infection and immunity. 2005;73(4):2400.

85. Lipski SL, Akimana C, Timpe JM, Wooten RM, Lafontaine ER. The Moraxella catarrhalis autotransporter McaP is a conserved surface protein that mediates adherence to human epithelial cells through its N-terminal passenger domain. Infection and immunity. 2007;75(1):314-24.

86. Balder R, Hassel J, Lipski S, Lafontaine ER. Moraxella catarrhalis strain O35E expresses two filamentous hemagglutinin-like proteins that mediate adherence to human epithelial cells. Infection and immunity. 2007;75(6):2765.

87. Wiersinga WJ, van der Poll T. Immunity to Burkholderia pseudomallei. Current opinion in infectious diseases. 2009;22(2):102-8.

88. Wiersinga WJ, Wieland CW, Dessing MC, Chantratita N, Cheng AC, Limmathurotsakul D, et al. Toll-like receptor 2 impairs host defense in gram-negative sepsis caused by Burkholderia pseudomallei (Melioidosis). PLoS medicine. 2007;4(7):e248.

89. West TE, Ernst RK, Jansson-Hutson MJ, Skerrett SJ. Activation of Toll-like receptors by Burkholderia pseudomallei. BMC immunology. 2008;9(1):46.

90. Utaisincharoen P, Tangthawornchaikul N, Kespichayawattana W, Anuntagool N, Chaisuriya P, Sirisinha S. Kinetic studies of the production of nitric oxide (NO) and tumour necrosis factor-alpha (TNF-α) in macrophages stimulated with Burkholderia pseudomallei endotoxin. Clinical & Experimental Immunology. 2000;122(3):324-9.

91. Wiersinga WJ, van't Veer C, Wieland CW, Gibot S, Hooibrink B, Day NP, et al. Expression profile and function of triggering receptor expressed on myeloid cells-1 during melioidosis. Journal of Infectious Diseases. 2007;196(11):1707-16.

92. Wiersinga WJ, Wieland CW, Roelofs JJ, van der Poll T. MyD88 dependent signaling contributes to protective host defense against Burkholderia pseudomallei. PLoS One. 2008;3(10):e3494.

93. Yu HB, Finlay BB. The caspase-1 inflammasome: a pilot of innate immune responses. Cell host & microbe. 2008;4(3):198-208.

94. Hii C-S, Sun GW, Goh JWK, Lu J, Stevens MP, Gan Y-H. Interleukin-8 induction by Burkholderia pseudomallei can occur without Toll-like receptor signaling but requires a functional type III secretion system. Journal of Infectious Diseases. 2008;197(11):1537-47.

95. Wiersinga WJ, Van der Poll T, White NJ, Day NP, Peacock SJ. Melioidosis: insights into the pathogenicity of Burkholderia pseudomallei. Nature Reviews Microbiology. 2006;4(4):272-82.

96. Wiersinga WJ, Dessing MC, Kager PA, Cheng AC, Limmathurotsakul D, Day NP, et al. High-throughput mRNA profiling characterizes the expression of inflammatory molecules in sepsis caused by Burkholderia pseudomallei. Infection and immunity. 2007;75(6):3074-9.

97. LaRosa SP, Opal SM, Utterback B, Yan SCB, Helterbrand J, Simpson AJ, et al. Decreased protein C, protein S, and antithrombin levels are predictive of poor outcome in Gram-negative sepsis caused by Burkholderia pseudomallei. International journal of infectious diseases. 2006;10(1):25-31.

98. Levi M, van der Poll T. Two-way interactions between inflammation and coagulation. Trends in cardiovascular medicine. 2005;15(7):254-9.

99. Esmon CT. The interactions between inflammation and coagulation. British journal of haematology. 2005;131(4):417-30.

100. Wiersinga W, Meijers J, Levi M, Van't Veer C, Day N, Peacock S, et al. Activation of coagulation with concurrent impairment of anticoagulant mechanisms correlates with a poor outcome in severe melioidosis. Journal of Thrombosis and Haemostasis. 2008;6(1):32-9.

101. Cullinane M, Gong L, Li X, Lazar-Adler N, Tra T, Wolvetang E, et al. Stimulation of autophagy suppresses the intracellular survival of Burkholderia pseudomallei in mammalian cell lines. Autophagy. 2008;4(6):744-53.

102. Easton A, Haque A, Chu K, Lukaszewski R, Bancroft GJ. A critical role for neutrophils in resistance to experimental infection with Burkholderia pseudomallei. Journal of Infectious Diseases. 2007;195(1):99-107.

103. Breitbach K, Klocke S, Tschernig T, van Rooijen N, Baumann U, Steinmetz I. Role of inducible nitric oxide synthase and NADPH oxidase in early control of Burkholderia pseudomallei infection in mice. Infection and immunity. 2006;74(11):6300-9.

104. Cheng AC, Limmathurotsakul D, Chierakul W, Getchalarat N, Wuthiekanun V, Stephens DP, et al. A randomized controlled trial of granulocyte colony-stimulating factor for the treatment of severe sepsis due to melioidosis in Thailand. Clinical Infectious Diseases. 2007;45(3):308-14.

105. Haque A, Chu K, Easton A, Stevens MP, Galyov EE, Atkins T, et al. A Live Experimental Vaccine against Burkholderia pseudomallei Elicits CD4+ T Cell–Mediated Immunity, Priming T Cells Specific for 2 Type III Secretion System Proteins. Journal of Infectious Diseases. 2006;194(9):1241-8.

106. Sarkar-Tyson M, Titball RW. Progress toward development of vaccines against melioidosis: a review. Clinical therapeutics. 2010;32(8):1437-45.

107. Lertmemongkolchai G, Cai G, Hunter CA, Bancroft GJ. Bystander activation of CD8+ T cells contributes to the rapid production of IFN-γ in response to bacterial pathogens. The Journal of Immunology. 2001;166(2):1097-105.

108. Barnes J, Warner J, Melrose W, Durrheim D, Speare R, Reeder J, et al. Adaptive immunity in melioidosis: a possible role for T cells in determining outcome of infection with Burkholderia pseudomallei. Clinical Immunology. 2004;113(1):22-8.

109. Nelson M, Prior JL, Lever MS, Jones HE, Atkins TP, Titball RW. Evaluation of lipopolysaccharide and capsular polysaccharide as subunit vaccines against experimental melioidosis. Journal of medical microbiology. 2004;53(12):1177-82.

110. Brett PJ, Woods DE. Structural and immunological characterization of Burkholderia pseudomallei O-polysaccharide-flagellin protein conjugates. Infection and immunity. 1996;64(7):2824-8.

111. Atkins T, Prior R, Mack K, Russell P, Nelson M, Prior J, et al. Characterisation of an acapsular mutant of Burkholderia pseudomallei identified by signature tagged mutagenesis. Journal of medical microbiology. 2002;51(7):539-53.

112. Breitbach K, Köhler J, Steinmetz I. Induction of protective immunity against Burkholderia pseudomallei using attenuated mutants with defects in the intracellular life

cycle. Transactions of the Royal Society of Tropical Medicine and Hygiene. 2008;102(Supplement 1):S89-S94.

113. Stevens MP, Haque A, Atkins T, Hill J, Wood MW, Easton A, et al. Attenuated virulence and protective efficacy of a Burkholderia pseudomallei bsa type III secretion mutant in murine models of melioidosis. Microbiology. 2004;150(8):2669-76.

114. Barnes JL, Ketheesan N. Development of protective immunity in a murine model of melioidosis is influenced by the source of Burkholderia pseudomallei antigens. Immunology and cell biology. 2007;85(7):551-7.

115. Razak CN, Ismail G, Embi N, Omar O. Protection studies using whole cells and partially purified toxic material (PPTM) of Pseudomonas pseudomallei. Malaysian applied biology: Biologi gunaan Malaysia. 1986.

116. Whitlock GC, Deeraksa A, Qazi O, Judy BM, Taylor K, Propst KL, et al. Protective response to subunit vaccination against intranasal Burkholderia mallei and B. pseudomallei challenge. Procedia in vaccinology. 2010;2(1):73-7.

117. Chen Y-S, Hsiao Y-S, Lin H-H, Yen C-M, Chen S-C, Chen Y-L. Immunogenicity and anti-Burkholderia pseudomallei activity in Balb/c mice immunized with plasmid DNA encoding flagellin. Vaccine. 2006;24(6):750-8.

118. Warawa JM. Evaluation of surrogate animal models of melioidosis. Frontiers in microbiology. 2010;1.

119. Stundick M, Albrecht M, Houchens C, Smith AP, Dreier T, Larsen J. Animal Models for Francisella tularensis and Burkholderia Species Scientific and Regulatory Gaps Toward Approval of Antibiotics Under the FDA Animal Rule. Veterinary Pathology Online. 2013;50(5):877-92.

120. Fukushima A, Yamaguchi T, Ishida W, Fukata K, Taniguchi T, Liu F-T, et al. Genetic background determines susceptibility to experimental immune-mediated blepharoconjunctivitis: comparison of Balb/c and C57BL/6 mice. Experimental eye research. 2006;82(2):210-8.

121. OLVER SD, PRICE P. Contrasting phenotypes of liver-infiltrating leucocytes isolated from MCMV-infected BALB/c and C57 BL/6 mice. International journal of experimental pathology. 1998;79(1):33.

122. Leakey AK, Ulett GC, Hirst RG. BALB/c and C57Bl/6 mice infected with virulent Burkholderia pseudomallei provide contrasting animal models for the acute and chronic forms of human melioidosis. Microbial pathogenesis. 1998;24(5):269-75.

123. Fritz D, Vogel P, Brown D, Deshazer D, Waag D. Mouse model of sublethal and lethal intraperitoneal glanders (Burkholderia mallei). Veterinary Pathology Online. 2000;37(6):626-36.

124. Jeddeloh J, Fritz D, Waag D, Hartings J, Andrews G. Biodefense-driven murine model of pneumonic melioidosis. Infection and immunity. 2003;71(1):584-7.

125. Fritz D, Vogel P, Brown D, Waag D. The hamster model of intraperitoneal Burkholderia mallei (glanders). Veterinary Pathology Online. 1999;36(4):276-91.

126. Lever MS, Nelson M, Stagg AJ, Beedham RJ, Simpson AJ. Experimental acute respiratory Burkholderia pseudomallei infection in BALB/c mice. International journal of experimental pathology. 2009;90(1):16-25.

127. Revelli DA, Boylan JA, Gherardini FC. A non-invasive intratracheal inoculation method for the study of pulmonary melioidosis. Frontiers in cellular and infection microbiology. 2012;2.

128. Trevino SR, Permenter AR, England MJ, Parthasarathy N, Gibbs PH, Waag DM, et al. Monoclonal antibodies passively protect BALB/c mice against Burkholderia mallei aerosol challenge. Infection and immunity. 2006;74(3):1958-61.

129. Liu B, Koo GC, Yap EH, Chua KL, Gan Y-H. Model of differential susceptibility to mucosal Burkholderia pseudomallei infection. Infection and immunity. 2002;70(2):504-11.

130. Lopez J, Copps J, Wilhelmsen C, Moore R, Kubay J, St-Jacques M, et al. Characterization of experimental equine glanders. Microbes and infection. 2003;5(12):1125-31.

131. Soffler C. The development and characterization of caprine infection models of melioidosis: COLORADO STATE UNIVERSITY; 2013.

132. Yeager JJ, Facemire P, Dabisch PA, Robinson CG, Nyakiti D, Beck K, et al. Natural History of Inhalation Melioidosis in Rhesus Macaques (Macaca mulatta) and African Green Monkeys (Chlorocebus aethiops). Infection and immunity. 2012;80(9):3332-40.

133. Nelson M, Dean RE, Salguero FJ, Taylor C, Pearce PC, Simpson AJ, et al. Development of an acute model of inhalational melioidosis in the common marmoset (Callithrix jacchus). International journal of experimental pathology. 2011;92(6):428-35.

134. Nelson M, Salguero FJ, Dean RE, Ngugi SA, Smither SJ, Atkins TP, et al. Comparative experimental subcutaneous glanders and melioidosis in the common marmoset (Callithrix jacchus). International journal of experimental pathology. 2014;95(6):378-91.

135. Gan YH, Chua KL, Chua HH, Liu B, Hii CS, Chong HL, et al. Characterization of Burkholderia pseudomallei infection and identification of novel virulence factors using a Caenorhabditis elegans host system. Molecular microbiology. 2002;44(5):1185-97.

136. Inglis TJ, Robertson T, Woods DE, Dutton N, Chang BJ. Flagellum-mediated adhesion by Burkholderia pseudomallei precedes invasion of Acanthamoeba astronyxis. Infection and immunity. 2003;71(4):2280-2.

137. Inglis TJ, Rigby P, Robertson TA, Dutton NS, Henderson M, Chang BJ. Interaction between Burkholderia pseudomallei and Acanthamoeba species results in coiling phagocytosis, endamebic bacterial survival, and escape. Infection and immunity. 2000;68(3):1681-6.

138. O'quinn A, Wiegand E, Jeddeloh J. Burkholderia pseudomallei kills the nematode Caenorhabditis elegans using an endotoxin-mediated paralysis. Cellular microbiology. 2001;3(6):381-93.

139. Schell MA, Lipscomb L, DeShazer D. Comparative genomics and an insect model rapidly identify novel virulence genes of Burkholderia mallei. Journal of bacteriology. 2008;190(7):2306-13.

140. Fisher NA, Ribot WJ, Applefeld W, DeShazer D. The Madagascar hissing cockroach as a novel surrogate host for Burkholderia pseudomallei, B. mallei and B. thailandensis. BMC microbiology. 2012;12(1):117.

141. Carr-Gregory B, Waag DM. Glanders. In: Dembek ZF, editor. Medical Aspects of Biological Warfare: Borden Institute, Office of the Surgeon General, AMEDD Center and School; 2007. p. 121-46.

142. Dvorak GD, Spickler AR. Glanders. Journal of the American Veterinary Medical Association. 2008;233(4):570-7.

143. Slater J. From glanders to Hendra virus: 125 years of equine infectious diseases. The Veterinary record. 2013;173(8):186-9.

144. Waag DM, Deshazer D. Glanders: New insights into an old disease. In: Lindler LE LF, Korch GW, editor. Biological Weapons Defense: Infectious Diseases and Counterbioterrorism. Totowa, New Jersey: Humana Press Inc; 2004.

145. Van Zandt KE, Greer MT, Gelhaus HC. Glanders: an overview of infection in humans. Orphanet journal of rare diseases. 2013;8:131.

146. Howe C. Glanders. In: Christian HA, editor. The Oxford Medicine: Oxford University Press, New York, NY; 1950. p. 185-202.

147. Derbyshire JB. The eradication of glanders in Canada. The Canadian veterinary journal La revue veterinaire canadienne. 2002;43(9):722-6.

148. Sharrer GT. The great glanders epizootic, 1861-1866: a Civil War legacy. Agricultural history. 1995;69(1):79-97.

149. Kovalev GK. [Glanders (review)]. Zhurnal mikrobiologii, epidemiologii, i immunobiologii. 1971;48(1):63-70.

150. Scholz HC, Pearson T, Hornstra H, Projahn M, Terzioglu R, Wernery R, et al. Genotyping of Burkholderia mallei from an outbreak of glanders in Bahrain suggests multiple introduction events. PLoS neglected tropical diseases. 2014;8(9):e3195.

151. Khan I, Wieler LH, Melzer F, Elschner MC, Muhammad G, Ali S, et al. Glanders in animals: a review on epidemiology, clinical presentation, diagnosis and countermeasures. Transboundary and emerging diseases. 2013;60(3):204-21.

152. Wernery U, Wernery R, Joseph M, Al-Salloom F, Johnson B, Kinne J, et al. Natural Burkholderia mallei infection in Dromedary, Bahrain. Emerging infectious diseases. 2011;17(7):1277-9.

153. Howe C, Miller WR. Human glanders: report of six cases. Ann Intern Med. 1947;26:93-115.

154. Robins G. A study of chronic glanders in man with report of a case: analysis of 156 cases collected from nature. Studies from the Royal Victoria Hospital Montreal. 1906;1:1-98.

155. Arun S, Neubauer H, Gurel A, Ayyildiz G, Kuscu B, Yesildere T, et al. Equine glanders in Turkey. The Veterinary record. 1999;144(10):255-8.

156. Neubauer H, Meyer H, Finke EJ. Human glanders. Revue Internationale des Services de Sante des Forces Armees. 1997;70:258-65.

157. Srinivasan A, Kraus CN, DeShazer D, Becker PM, Dick JD, Spacek L, et al. Glanders in a military research microbiologist. N Engl J Med. 2001;345(4):256-8.

158. Lipsitz R, Garges S, Aurigemma R, Baccam P, Blaney DD, Cheng AC, et al. Workshop on Treatment of and Postexposure Prophylaxis for Burkholderia pseudomallei and B. mallei infection, 2010. Emerging infectious diseases. 2012;18(12):online report.

159. Wheelis M. First shots fired in biological warfare. Nature. 1998;395(6699):213.

160. Smart JK. History of chemical and biological warfare: an American perspective. R Zajtchuk and R F Bellarmy (ed), Textbook of Military Medicine Borden Institute and Office of the Army Surgeon General. 1997:16-64.

161. Regis E. The biology of doom. Henry Holt and Company, New York. 1999.

162. Alibek K, Handelman S. Biohazard: the chilling true story of the largest covert biological weapons programin the world: New York: Random House; 1999.

163. Lehavi O, Aizenstien O, Katz LH, Hourvitz A. [Glanders--a potential disease for biological warfare in humans and animals]. Harefuah. 2002;141 Spec No:88-91, 119.

164. Lopez J, Copps J, Wilhelmsen C, Moore R, Kubay J, St-Jacques M, et al. Characterization of experimental equine glanders. Microbes Infect. 2003;5(12):1125-31.

165. Fritz DL, Vogel P, Brown DR, Deshazer D, Waag DM. Mouse model of sublethal and lethal intraperitoneal glanders (Burkholderia mallei). Vet Pathol. 2000;37(6):626-36.

166. Fritz DL, Vogel P, Brown DR, Waag DM. The hamster model of intraperitoneal Burkholderia mallei (glanders). Vet Pathol. 1999;36(4):276-91.

167. Lever MS, Nelson M, Ireland PI, Stagg AJ, Beedham RJ, Hall GA, et al. Experimental aerogenic Burkholderia mallei (glanders) infection in the BALB/c mouse. J Med Microbiol. 2003;52(Pt 12):1109-15.

168. Woods DE. The use of animal infection models to study the pathogenesis of melioidosis and glanders. Trends Microbiol. 2002;10(11):483-4; discussion 4-5.

169. Lafontaine ER, Zimmerman SM, Shaffer TL, Michel F, Gao X, Hogan RJ. Use of a safe, reproducible, and rapid aerosol delivery method to study infection by Burkholderia pseudomallei and Burkholderia mallei in mice. PloS one. 2013;8(10):e76804.

170. Miller WR, Pannell L, Cravitz L, Tanner WA, Rosebury T. Studies on Certain Biological Characteristics of Malleomyces mallei and Malleomyces pseudomallei: II. Virulence and Infectivity for Animals. Journal of bacteriology. 1948;55(1):127-35.

171. Khomiakov Iu N, Manzeniuk IN, Naumov DV, Svetoch EA. [The principles of the therapy of glanders in monkeys]. Zhurnal mikrobiologii, epidemiologii, i immunobiologii. 1998(1):70-4.

172. Manzeniuk IN, Svetoch EA, Diadishev NR, Stepanshin Iu G, Buziun AV. [Various indices of the infectious process in treatment of glanders in monkeys]. Antibiotiki i khimioterapiia = Antibiotics and chemoterapy [sic] / Ministerstvo meditsinskoi i mikrobiologicheskoi promyshlennosti SSSR. 1996;41(1):13-8.

173. Nierman WC, DeShazer D, Kim HS, Tettelin H, Nelson KE, Feldblyum T, et al. Structural flexibility in the Burkholderia mallei genome. Proceedings of the National Academy of Sciences of the United States of America. 2004;101(39):14246-51.

174. Reed LJ, Muench H. A simple method for estimating fifty percent end points. . Am J Hyg. 1938;27:793-497.

175. Goodyear A, Kellihan L, Bielefeldt-Ohmann H, Troyer R, Propst K, Dow S. Protection from pneumonic infection with burkholderia species by inhalational immunotherapy. Infection and immunity. 2009;77(4):1579-88.

176. Jeddeloh JA, Fritz DL, Waag DM, Hartings JM, Andrews GP. Biodefense-driven murine model of pneumonic melioidosis. Infection and immunity. 2003;71(1):584-7.

177. Song H, Hwang J, Yi H, Ulrich RL, Yu Y, Nierman WC, et al. The early stage of bacterial genome-reductive evolution in the host. PLoS pathogens. 2010;6(5):e1000922.

178. Duval CW, White PG. The Histological Lesions of Experimental Glanders. The Journal of experimental medicine. 1907;9(4):352-80.

179. Ferster LN, Kurilov V. [Characteristics of the infectious process in animals susceptible and resistant to glanders]. Arkhiv patologii. 1982;44(11):24-30.

180. Burtnick MN, DeShazer D, Nair V, Gherardini FC, Brett PJ. Burkholderia mallei cluster 1 type VI secretion mutants exhibit growth and actin polymerization defects in RAW 264.7 murine macrophages. Infection and immunity. 2010;78(1):88-99.

181. DeShazer D, Waag DM, Fritz DL, Woods DE. Identification of a Burkholderia mallei polysaccharide gene cluster by subtractive hybridization and demonstration that the encoded capsule is an essential virulence determinant. Microbial pathogenesis. 2001;30(5):253-69.

182. Nelson M, Dean RE, Salguero FJ, Taylor C, Pearce PC, Simpson AJ, et al. Development of an acute model of inhalational melioidosis in the common marmoset (Callithrix jacchus). International journal of experimental pathology. 2011;92(6):428-35.

183. Saqib M, Muhammad G, Naureen A, Hussain MH, Asi MN, Mansoor MK, et al. Effectiveness of an antimicrobial treatment scheme in a confined glanders outbreak. BMC veterinary research. 2012;8:214.

184. da Silva KP, de Campos Takaki GM, da Silva LB, Saukas TN, Santos AS, Mota RA. Assessment of the effectiveness of the PPD-mallein produced in Brazil for diagnosing glanders in mules. Brazilian journal of microbiology : [publication of the Brazilian Society for Microbiology]. 2013;44(1):179-81.

185. Nelson M, Salguero FJ, Dean RE, Ngugi SA, Smither SJ, Atkins TP, et al. Comparative experimental subcutaneous glanders and melioidosis in the common marmoset (Callithrix jacchus). International journal of experimental pathology. 2014.

186. Klemm P, Hjerrild L, Gjermansen M, Schembri MA. Structure-function analysis of the self-recognizing Antigen 43 autotransporter protein from Escherichia coli. Mol Microbiol. 2004;51(1):283-96.

187. Heras B, Totsika M, Peters KM, Paxman JJ, Gee CL, Jarrott RJ, et al. The antigen 43 structure reveals a molecular Velcro-like mechanism of autotransporter-mediated bacterial clumping. Proceedings of the National Academy of Sciences of the United States of America. 2013.

188. Valle J, Mabbett AN, Ulett GC, Toledo-Arana A, Wecker K, Totsika M, et al. UpaG, a new member of the trimeric autotransporter family of adhesins in uropathogenic Escherichia coli. Journal of bacteriology. 2008;190(12):4147-67.

189. Sherlock O, Schembri MA, Reisner A, Klemm P. Novel roles for the AIDA adhesin from diarrheagenic Escherichia coli: cell aggregation and biofilm formation. Journal of bacteriology. 2004;186(23):8058-65.

190. Roggenkamp A, Ackermann N, Jacobi CA, Truelzsch K, Hoffmann H, Heesemann J. Molecular analysis of transport and oligomerization of the Yersinia enterocolitica adhesin YadA. Journal of bacteriology. 2003;185(13):3735-44.

191. Attia AS, Lafontaine ER, Latimer JL, Aebi C, Syrogiannopoulos GA, Hansen EJ. The UspA2 protein of Moraxella catarrhalis is directly involved in the expression of serum resistance. Infection and immunity. 2005;73(4):2400-10.

192. Capecchi B, Adu-Bobie J, Di Marcello F, Ciucchi L, Masignani V, Taddei A, et al. Neisseria meningitidis NadA is a new invasin which promotes bacterial adhesion to and penetration into human epithelial cells. Mol Microbiol. 2005;55(3):687-98.

193. Bullard B, Lipski S, Lafontaine ER. Regions important for the adhesin activity of Moraxella catarrhalis Hag. BMC microbiology. 2007;7:65.

194. Lipski SL, Holm MM, Lafontaine ER. Identification of a Moraxella catarrhalis gene that confers adherence to various human epithelial cell lines in vitro. FEMS Microbiol Lett. 2007;267(2):207-13.

195. Fexby S, Bjarnsholt T, Jensen PO, Roos V, Hoiby N, Givskov M, et al. Biological Trojan horse: Antigen 43 provides specific bacterial uptake and survival in human neutrophils. Infection and immunity. 2007;75(1):30-4.

196. Stevens JM, Ulrich RL, Taylor LA, Wood MW, Deshazer D, Stevens MP, et al. Actin-binding proteins from Burkholderia mallei and Burkholderia thailandensis can functionally compensate for the actin-based motility defect of a Burkholderia pseudomallei bimA mutant. Journal of bacteriology. 2005;187(22):7857-62.

197. Maroncle NM, Sivick KE, Brady R, Stokes FE, Mobley HL. Protease activity, secretion, cell entry, cytotoxicity, and cellular targets of secreted autotransporter toxin of uropathogenic Escherichia coli. Infection and immunity. 2006;74(11):6124-34.

198. Farn JL, Strugnell RA, Hoyne PA, Michalski WP, Tennent JM. Molecular characterization of a secreted enzyme with phospholipase B activity from Moraxella bovis. Journal of bacteriology. 2001;183(22):6717-20.

199. Lipski SL, Akimana C, Timpe JM, Wooten RM, Lafontaine ER. The Moraxella catarrhalis Autotransporter McaP Is a Conserved Surface Protein That Mediates Adherence to Human Epithelial Cells through Its N-Terminal Passenger Domain. Infection and immunity. 2007;75(1):314-24.

200. Timpe JM, Holm MM, Vanlerberg SL, Basrur V, Lafontaine ER. Identification of a Moraxella catarrhalis outer membrane protein exhibiting both adhesin and lipolytic activities. Infection and immunity. 2003;71(8):4341-50.

201. Cotter SE, Surana NK, St Geme JW, 3rd. Trimeric autotransporters: a distinct subfamily of autotransporter proteins. Trends Microbiol. 2005;13(5):199-205.

202. Henderson IR, Navarro-Garcia F, Nataro JP. The great escape: structure and function of the autotransporter proteins. Trends Microbiol. 1998;6(9):370-8.

203. Stathopoulos C, Hendrixson DR, Thanassi DG, Hultgren SJ, St Geme JW, 3rd, Curtiss R, 3rd. Secretion of virulence determinants by the general secretory pathway in gram-negative pathogens: an evolving story. Microbes Infect. 2000;2(9):1061-72.

204. Linke D, Riess T, Autenrieth IB, Lupas A, Kempf VA. Trimeric autotransporter adhesins: variable structure, common function. Trends Microbiol. 2006;14(6):264-70.

205. Hoiczyk E, Roggenkamp A, Reichenbecher M, Lupas A, Heesemann J. Structure and sequence analysis of *Yersinia* YadA and *Moraxella* UspAs reveal a novel class of adhesins. The EMBO journal. 2000;19(22):5989-99.

206. van Ulsen P, Rahman S, Jong WS, Daleke-Schermerhorn MH, Luirink J. Type V secretion: from biogenesis to biotechnology. Biochimica et biophysica acta. 2014;1843(8):1592-611.

207. Oomen CJ, Van Ulsen P, Van Gelder P, Feijen M, Tommassen J, Gros P. Structure of the translocator domain of a bacterial autotransporter. The EMBO journal. 2004;23(6):1257-66.

208. Alamuri P, Eaton KA, Himpsl SD, Smith SN, Mobley HL. Vaccination with proteus toxic agglutinin, a hemolysin-independent cytotoxin in vivo, protects against Proteus mirabilis urinary tract infection. Infection and immunity. 2009;77(2):632-41.

209. Liu DF, Mason KW, Mastri M, Pazirandeh M, Cutter D, Fink DL, et al. The C-terminal fragment of the internal 110-kilodalton passenger domain of the Hap protein of

nontypeable Haemophilus influenzae is a potential vaccine candidate. Infection and immunity. 2004;72(12):6961-8.

210. Cutter D, Mason KW, Howell AP, Fink DL, Green BA, St Geme JW, 3rd. Immunization with Haemophilus influenzae Hap adhesin protects against nasopharyngeal colonization in experimental mice. J Infect Dis. 2002;186(8):1115-21.

211. Bondi SK, Goldberg JB. Strategies toward vaccines against Burkholderia mallei and Burkholderia pseudomallei. Expert Rev Vaccines. 2008;7(9):1357-65.

212. Balder R, Lipski S, Lazarus JJ, Grose W, Wooten RM, Hogan RJ, et al. Identification of Burkholderia mallei and Burkholderia pseudomallei adhesins for human respiratory epithelial cells. BMC microbiology. 2010;10:250.

213. Lafontaine ER, Balder R, Michel F, Hogan RJ. Characterization of an autotransporter adhesin protein shared by Burkholderia mallei and Burkholderia pseudomallei. BMC microbiology. 2014;14:92.

214. Campos CG, Byrd MS, Cotter PA. Functional characterization of Burkholderia pseudomallei trimeric autotransporters. Infection and immunity. 2013;81(8):2788-99.

215. Sambrook J, Russell, D.W. Molecular Cloning: A Laboratory Manual (Third Edition). Third Edition ed: Cold Spring Harbor Laboratory Press; 2001.

216. Burtnick M, Bolton A, Brett P, Watanabe D, Woods D. Identification of the acid phosphatase (acpA) gene homologues in pathogenic and non-pathogenic Burkholderia spp. facilitates TnphoA mutagenesis. Microbiology. 2001;147(Pt 1):111-20.

217. Bullard B, Lipski SL, Lafontaine ER. Hag directly mediates the adherence of Moraxella catarrhalis to human middle ear cells. Infection and immunity. 2005;73(8):5127-36.

218. Balder R, Krunkosky TM, Nguyen CQ, Feezel L, Lafontaine ER. Hag mediates adherence of Moraxella catarrhalis to ciliated human airway cells. Infection and immunity. 2009;77(10):4597-608.

219. Pearson MM, Laurence CA, Guinn SE, Hansen EJ. Biofilm formation by Moraxella catarrhalis in vitro: roles of the UspA1 adhesin and the Hag hemagglutinin. Infection and immunity. 2006;74(3):1588-96.

220. Carlone GM, Thomas ML, Rumschlag HS, Sottnek FO. Rapid microprocedure for isolating detergent-insoluble outer membrane proteins from Haemophilus species. J Clin Microbiol. 1986;24(3):330-2.

221. Shaffer TL, Balder R, Buskirk SW, Hogan RJ, Lafontaine ER. Use of the Chinchilla model to evaluate the vaccinogenic potential of the Moraxella catarrhalis filamentous hemagglutinin-like proteins MhaB1 and MhaB2. PloS one. 2013;8(7):e67881.

222. Burtnick MN, Woods DE. Isolation of polymyxin B-susceptible mutants of Burkholderia pseudomallei and molecular characterization of genetic loci involved in polymyxin B resistance. Antimicrobial agents and chemotherapy. 1999;43(11):2648-56.

223. Lafontaine ER, Wagner NJ, Hansen EJ. Expression of the *Moraxella catarrhalis* UspA1 protein undergoes phase variation and is regulated at the transcriptional level. J Bacteriol. 2001;183(5):1540-51.

224. Deshazer D. Virulence of clinical and environmental isolates of Burkholderia oklahomensis and Burkholderia thailandensis in hamsters and mice. FEMS Microbiol Lett. 2007;277(1):64-9.

225. Brett PJ, Deshazer D, Woods DE. Characterization of Burkholderia pseudomallei and Burkholderia pseudomallei-like strains. Epidemiol Infect. 1997;118(2):137-48.

226. Smith MD, Angus BJ, Wuthiekanun V, White NJ. Arabinose assimilation defines a nonvirulent biotype of Burkholderia pseudomallei. Infection and immunity. 1997;65(10):4319-21.

227. Ulett GC, Currie BJ, Clair TW, Mayo M, Ketheesan N, Labrooy J, et al. Burkholderia pseudomallei virulence: definition, stability and association with clonality. Microbes Infect. 2001;3(8):621-31.

228. Lafontaine ER, Cope LD, Aebi C, Latimer JL, McCracken GH, Jr., Hansen EJ. The UspA1 protein and a second type of UspA2 protein mediate adherence of *Moraxella catarrhalis* to human epithelial cells in vitro. Journal of bacteriology. 2000;182(5):1364-73.

229. Laarmann S, Cutter D, Juehne T, Barenkamp SJ, St Geme JW. The Haemophilus influenzae Hia autotransporter harbours two adhesive pockets that reside in the passenger domain and recognize the same host cell receptor. Mol Microbiol. 2002;46(3):731-43.

230. Pearson MM, Hansen EJ. Identification of Gene Products Involved in Biofilm Production by Moraxella catarrhalis ETSU-9 In Vitro. Infection and immunity. 2007;75(9):4316-25.

231. Parthasarathy N, DeShazer D, England M, Waag DM. Polysaccharide microarray technology for the detection of Burkholderia pseudomallei and Burkholderia mallei antibodies. Diagn Microbiol Infect Dis. 2006;56(3):329-32.

232. Romero CM, DeShazer D, Feldblyum T, Ravel J, Woods D, Kim HS, et al. Genome sequence alterations detected upon passage of Burkholderia mallei ATCC 23344 in culture and in mammalian hosts. BMC genomics. 2006;7:228.

233. Tuanyok A, Kim HS, Nierman WC, Yu Y, Dunbar J, Moore RA, et al. Genome-wide expression analysis of iron regulation in Burkholderia pseudomallei and Burkholderia mallei using DNA microarrays. FEMS Microbiol Lett. 2005;252(2):327-35.

234. Ooi WF, Ong C, Nandi T, Kreisberg JF, Chua HH, Sun G, et al. The condition-dependent transcriptional landscape of Burkholderia pseudomallei. PLoS genetics. 2013;9(9):e1003795.

235. Burtnick MN, Brett PJ. Burkholderia mallei and Burkholderia pseudomallei cluster 1 type VI secretion system gene expression is negatively regulated by iron and zinc. PloS one. 2013;8(10):e76767.

236. Schell MA, Ulrich RL, Ribot WJ, Brueggemann EE, Hines HB, Chen D, et al. Type VI secretion is a major virulence determinant in Burkholderia mallei. Mol Microbiol. 2007;64(6):1466-85.

237. Tiyawisutsri R, Holden MT, Tumapa S, Rengpipat S, Clarke SR, Foster SJ, et al. Burkholderia Hep_Hap autotransporter (BuHA) proteins elicit a strong antibody response during experimental glanders but not human melioidosis. BMC microbiology. 2007;7:19.

238. Varga JJ, Vigil A, DeShazer D, Waag DM, Felgner P, Goldberg JB. Distinct human antibody response to the biological warfare agent Burkholderia mallei. Virulence. 2012;3(6):510-4.

239. Fernandes PJ, Guo Q, Waag DM, Donnenberg MS. The type IV pilin of Burkholderia mallei is highly immunogenic but fails to protect against lethal aerosol challenge in a murine model. Infection and immunity. 2007;75(6):3027-32.

240. Melville S, Craig L. Type IV pili in Gram-positive bacteria. Microbiology and molecular biology reviews : MMBR. 2013;77(3):323-41.

241. Lazar Adler NR, Dean RE, Saint RJ, Stevens MP, Prior JL, Atkins TP, et al. Identification of a Predicted Trimeric Autotransporter Adhesin Required for Biofilm Formation of Burkholderia pseudomallei. PloS one. 2013;8(11):e79461.

242. Wang L, Zhai B, Lin X. The link between morphotype transition and virulence in Cryptococcus neoformans. PLoS Pathog. 2012;8(6):e1002765.

243. Yang X, Thornburg T, Suo Z, Jun S, Robison A, Li J, et al. Flagella overexpression attenuates Salmonella pathogenesis. PLoS One. 2012;7(10):e46828.

244. Cao L, Lim T, Jun S, Thornburg T, Avci R, Yang X. Vulnerabilities in Yersinia pestis caf operon are unveiled by a Salmonella vector. PloS one. 2012;7(4):e36283.

245. Pascual DW, Suo Z, Cao L, Avci R, Yang X. Attenuating gene expression (AGE) for vaccine development. Virulence. 2013;4(5):384-90.

246. Simon R, Priefer U, Puhler A. A broad host range mobilisation system for in vivo genetic engineering: transposon mutagenesis in gram-negative bacteria. Bio/Technology. 1983;1:784-91.

247. Skorupski K, Taylor RK. Positive selection vectors for allelic exchange. Gene. 1996;169(1):47-52.

248. Ruiz-Perez F, Henderson IR, Nataro JP. Interaction of FkpA, a peptidyl-prolyl cis/trans isomerase with EspP autotransporter protein. Gut microbes. 2010;1(5):339-44.

249. Timpe JM, Holm MM, Vanlerberg SL, Basrur V, Lafontaine ER. Identification of a Moraxella catarrhalis outer membrane protein exhibiting both adhesin and lipolytic activities. Infection and immunity. 2003;71(8):4341-50.

250. J S, Russell D. Molecular Cloning: A Laboratory Manual. 3rd ed: Cold Spring Harbor Laboratory Press; 2001.

251. Simon R, Priefer U, Pühler A. A broad host range mobilization system for in vivo genetic engineering: transposon mutagenesis in gram negative bacteria. Nature Biotechnology. 1983;1(9):784-91.

252. Burtnick MN, Bolton AJ, Brett PJ, Watanabe D, Woods DE. Identification of the acid phosphatase (acpA) gene homologues in pathogenic and non-pathogenic Burkholderia spp. facilitates TnphoA mutagenesis. Microbiology. 2001;147(1):111-20.

253. Wilhelm S, Tommassen J, Jaeger K-E. A novel lipolytic enzyme located in the outer membrane of Pseudomonas aeruginosa. Journal of bacteriology. 1999;181(22):6977-86.

254. Lafontaine ER, Balder R, Michel F, Hogan RJ. Characterization of an autotransporter adhesin protein shared by Burkholderia mallei and Burkholderia pseudomallei. BMC microbiology. 2014;14(1):92.

255. Akoh CC, Lee G-C, Liaw Y-C, Huang T-H, Shaw J-F. GDSL family of serine esterases/lipases. Progress in lipid research. 2004;43(6):534-52.

256. Wilhelm S, Rosenau F, Kolmar H, Jaeger KE. Autotransporters with GDSL passenger domains: molecular physiology and biotechnological applications. Chembiochem. 2011;12(10):1476-85.

257. Torres AG, Perna NT, Burland V, Ruknudin A, Blattner FR, Kaper JB. Characterization of Cah, a calcium-binding and heat-extractable autotransporter protein of enterohaemorrhagic Escherichia coli. Molecular microbiology. 2002;45(4):951-66.

258. Benz I, Schmidt MA. Isolation and serologic characterization of AIDA-I, the adhesin mediating the diffuse adherence phenotype of the diarrhea-associated Escherichia coli strain 2787 (O126: H27). Infection and immunity. 1992;60(1):13-8.

259. Meng G, Spahich N, Kenjale R, Waksman G, St Geme JW. Crystal structure of the Haemophilus influenzae Hap adhesin reveals an intercellular oligomerization mechanism for bacterial aggregation. The EMBO journal. 2011;30(18):3864-74.

260. May KL, Grabowicz M, Polyak SW, Morona R. Self-association of the Shigella flexneri IcsA autotransporter protein. Microbiology. 2012;158(Pt 7):1874-83.

261. Mikula KM, Leo JC, Łyskowski A, Kedracka-Krok S, Pirog A, Goldman A. The translocation domain in trimeric autotransporter adhesins is necessary and sufficient for trimerization and autotransportation. Journal of bacteriology. 2012;194(4):827-38.

262. Echenique-Rivera H, Brunelli B, Scarselli M, Taddei AR, Pizza M, Aricò B, et al. A naturally occurring single-residue mutation in the translocator domain of Neisseria meningitidis NhhA affects trimerization, surface localization, and adhesive capabilities. Infection and immunity. 2011;79(11):4308-21.

263. Ulrich RL, Amemiya K, Waag DM, Roy CJ, DeShazer D. Aerogenic vaccination with a Burkholderia mallei auxotroph protects against aerosol-initiated glanders in mice. Vaccine. 2005;23(16):1986-92.

264. Zhu H, Liu M, Sumby P, Lei B. The secreted esterase of group a streptococcus is important for invasive skin infection and dissemination in mice. Infection and immunity. 2009;77(12):5225-32.

265. Liu M, Zhu H, Li J, Garcia CC, Feng W, Kirpotina LN, et al. Group A Streptococcus secreted esterase hydrolyzes platelet-activating factor to impede neutrophil recruitment and facilitate innate immune evasion. 2012.

266. Banerji S, Aurass P, Flieger A. The manifold phospholipases A of Legionella pneumophila–identification, export, regulation, and their link to bacterial virulence. International Journal of Medical Microbiology. 2008;298(3):169-81.

267. Banerji S, Bewersdorff M, Hermes B, Cianciotto NP, Flieger A. Characterization of the major secreted zinc metalloprotease-dependent glycerophospholipid: cholesterol acyltransferase, PlaC, of Legionella pneumophila. Infection and immunity. 2005;73(5):2899-909.

268. Evans RJ, Li Z, Hughes WS, Djordjevic JT, Nielsen K, May RC. Cryptococcal Phospholipase B1 Is Required for Intracellular Proliferation and Control of Titan Cell Morphology during Macrophage Infection. Infection and immunity. 2015;83(4):1296-304.

269. Adler NRL, Stevens MP, Dean RE, Saint RJ, Pankhania D, Prior JL, et al. Systematic Mutagenesis of Genes Encoding Predicted Autotransported Proteins of Burkholderia pseudomallei Identifies Factors Mediating Virulence in Mice, Net Intracellular Replication and a Novel Protein Conferring Serum Resistance. PloS one. 2015;10(4).

270. Mahan MJ, Heithoff DM, Sinsheimer RL, Low DA. Assesment of bacterial pathogenesis by analysis of gene expression in the host. Annual review of genetics. 2000;34(1):139-64.

271. Low DA, Weyand NJ, Mahan MJ. Roles of DNA adenine methylation in regulating bacterial gene expression and virulence. Infection and immunity. 2001;69(12):7197-204.

272. Mott T, Estes D, Torres A. Recent progress in the development of vaccines for glanders and melioidosis, chapter 4. Feodorova, VA, Motin, VL eds. 2011:93-110.

273. Hatcher CL, Muruato LA, Torres AG. Recent Advances in Burkholderia mallei and B. pseudomallei Research. Current tropical medicine reports. 2015;2(2):62-9.

274. Bandara AB. A wzt Mutant Burkholderia mallei Is Attenuated and Partially Protects CD1 Mice against Glanders. Advances in Infectious Diseases. 2012;2(03):53.

275. Cyranoski D. Marmoset model takes centre stage. Nature. 2009;459(7246):492.

276. Sequencing TMG, Consortium A. The common marmoset genome provides insight into primate biology and evolution. Nature Genetics. 2014;46(8):850-7.

277. Tomioka I, Maeda T, Shimada H, Kawai K, Okada Y, Igarashi H, et al. Generating induced pluripotent stem cells from common marmoset (Callithrix jacchus) fetal liver cells using defined factors, including Lin28. Genes to Cells. 2010;15(9):959-69.

278. Okano H, Hikishima K, Iriki A, Sasaki E, editors. The common marmoset as a novel animal model system for biomedical and neuroscience research applications. Seminars in Fetal and Neonatal Medicine; 2012: Elsevier.

279. Sasaki E, Suemizu H, Shimada A, Hanazawa K, Oiwa R, Kamioka M, et al. Generation of transgenic non-human primates with germline transmission. Nature. 2009;459(7246):523-7.

280. Schatten G, Mitalipov S. Developmental biology: transgenic primate offspring. Nature. 2009;459(7246):515-6.

281. Comanducci M, Bambini S, Brunelli B, Adu-Bobie J, Aricò B, Capecchi B, et al. NadA, a novel vaccine candidate of Neisseria meningitidis. The Journal of experimental medicine. 2002;195(11):1445-54.